CENTRO DE INVESTIGACIÓN Y DE ESTUDIOS AVANZADOS DEL INSTITUTO POLITÉCNICO NACIONAL

UNIDAD ZACATENCO

DEPARTAMENTO DE INGENIERÍA ELÉCTRICA

SECCIÓN DE ELECTRÓNICA DEL ESTADO SÓLIDO

Exploración y optimización de materiales nc-SiOxCy para desplazamiento de energía descendente y su posible aplicación a celdas solares

TESIS

Que presenta

MANMOHAN JAIN

Para obtener el grado de

DOCTOR EN CIENCIAS

En la especialidad de

INGENIERÍA ELÉCTRICA

Directores de tesis**:**

Dr. Yasuhiro Matsumoto Kuwabara

Dr. Ateet Dutt

Ciudad de México **Mayo, 2023**

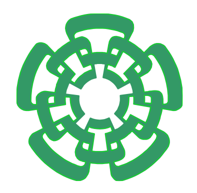

CENTER FOR RESEARCH AND ADVANCED STUDIES OF THE NATIONAL POLYTECHNIC INSTITUTE

ZACATENCO UNIT

DEPARTMENT OF ELECTRICAL ENGINEERING

SECTION OF SOLID STATE ELECTRONICS

The exploration and optimization of nc-SiO_xC_y-based materials for energy downshifting and their possible application to solar cells

THESIS

Presented by

MANMOHAN JAIN

To obtain the grade of

DOCTOR IN SCIENCE

Specialty in

ELECTRICAL ENGINEERING

Thesis Directors**:**

Dr. Yasuhiro Matsumoto Kuwabara

Dr. Ateet Dutt

Mexico City **May, 2023**

Resumen

La demanda de energía limpia incrementa debido al crecimiento de la población, el índice de contaminación y la rápida urbanización. No obstante, la eficiencia máxima teórica de la celda solar de c-Si es de alrededor del 30%, lo que es una limitación en su uso y puede mejorarse mediante el efecto de conversión por desplazamiento de energía descendente de fotoluminiscencia (PLDS).

En este trabajo se propone el estudio de las películas delgadas de SiO_xC_y depositadas como películas delgadas PLDS para celdas solares de c-Si. Se utilizó la técnica de depósito químico en fase de vapor catalítico-orgánico (O-Cat CVD). Para preparar estas películas delgadas de SiO_xC_y se emplearon precursores organometálicos, es decir, monometilsilano [MMS; (CH_3-SiH_3)], vinil silano [VS; (H_2C=$CHSiH_3$)] y ortosilicato de tetraetilo [TEOS; ($Si(OC_2H_5)_4$)], respectivamente. Se utilizaron dos sistemas O-Cat-CVD diferentes para los precursores gaseosos y líquidos por separado. En uno de los sistemas, se usaron precursores gaseosos de MMS y Vinil Silano para depositar películas delgadas de SiO_xC_y bajo una atmósfera reactiva de oxígeno (O_2) e hidrógeno (H_2), así mismo se usó filamento de tantalio (Ta) como catalizador en este sistema. En otro sistema O-Cat-CVD, se usó el precursor líquido TEOS para depositar películas delgadas de SiO_xC_y bajo una atmósfera inerte de argón (Ar) y tungsteno (W) como catalizador. Se analizó el efecto del flujo de argón para comprender las propiedades de las películas delgadas de SiO_xC_y depositadas con el precursor TEOS, mientras que también se investigó el efecto de la duración del depósito para todos los precursores sobre las propiedades luminiscentes de las películas obtenidas. Además, también se estudiaron las películas delgadas de SiO_xC_y depositadas como películas delgadas PLDS para celdas solares de c-Si.

Se utilizaron diferentes técnicas de caracterización para analizar las propiedades de las películas delgadas de SiO_xC_y. Aquí, se realizaron técnicas de caracterización de espectroscopía de fotoelectrones de rayos X (XPS) y de infrarrojo por transformada de Fourier (FTIR) para confirmar la presencia de enlaces relacionados con SiOC en películas delgadas. Las propiedades ópticas se estudiaron mediante técnicas de Elipsometría y fotoluminiscencia (PL). Aquí, la intensa y amplia emisión de PL se detectó en el espectro visible donde se utilizaron técnicas de excitación de fotoluminiscencia (PLE),

fotoluminiscencia resuelta en el tiempo (TRPL) y microscopía electrónica de transmisión de alta resolución (HRTEM) para confirmar el origen de la emisión de PL. Estas técnicas confirmaron que el origen de la emisión de PL podría deberse tanto a diferentes mecanismos de defectos, como por la presencia de nanocristales en la matriz de películas delgadas. Finalmente, también se estudió el efecto PLDS de estas películas delgadas fotoluminiscentes de SiO_xC_y en celdas solares de c-Si mediante caracterización de corriente-voltaje (I-V) y eficiencia cuántica externa (EQE) donde se obtuvieron mejores propiedades de celdas solares debido a la mejora encontrada en los espectros de EQE en región UV-azul. Esta tesis será una base para diseñar dispositivos optoelectrónicos basados en silicio con un precursor seguro y de bajo costo, incluso para mejorar la eficiencia de las celdas solares de Si cristalino por el efecto PLDS.

Palabras clave: O-Cat-CVD, SiO_xC_y, Fotoluminiscencia, PLDS, Celdas solares

Abstract

The demand for clean energy is increasing due to the growth of population, pollution index, and rapid urbanization. Nonetheless, the theoretical maximum efficiency of c-Si solar cell is about 30%, being a limitation in its use and it can be improved by Photo-Luminescence Down Shift (PLDS) effect.

This work proposes the study of the deposited SiO_xC_y thin films as PLDS thin films for c-Si solar cells. Organic Catalytic Chemical Vapor Deposition (O-Cat CVD) technique was used to prepare these SiO_xC_y thin films by employing organometallic precursors i.e. Monomethyl Silane [MMS; (CH_3-SiH_3)], Vinyl Silane [VS; (H_2C=$CHSiH_3$)] and Tetra-ethyl Orthosilicate [TEOS; ($Si(OC_2H_5)_4$)], respectively. Two different O-Cat-CVD systems were used for depositing the gaseous and liquid precursors separately. In one of the system, MMS and Vinyl Silane gaseous precursors were used to deposit SiO_xC_y thin films under a reactant atmosphere of oxygen (O_2) and hydrogen (H_2), likewise tantalum (T_a) filament was used as a catalyst in this system. In another O-Cat-CVD system, TEOS liquid precursor was used to deposit SiO_xC_y thin films under an inert atmosphere of argon (Ar) and tungsten (W) was used as a catalyst. The effect of argon flow was discussed to understand the properties of SiO_xC_y thin films deposited by using TEOS precursor while the effect of deposition duration was also investigated for all the precursors on the luminescent properties of the deposited films. Besides, the deposited SiO_xC_y thin films as PLDS thin films for c-Si solar cells were also studied.

Different characterization techniques were used to analyze the properties of SiO_xC_y thin films. Here, Fourier Transform InfraRed (FTIR) and X-ray Photoelectron Spectroscopy (XPS) characterization techniques were performed to confirm the presence of SiOC related bonding in thin films. The optical properties were studied by Ellipsometry and Photo-Luminescence (PL) techniques. Here, the intense and wide PL emission was detected in the visible spectrum where Photo-Luminescence Excitation (PLE), Time-Resolved Photo-Luminescence (TRPL), and High-Resolution Transmission Electron Microscopy (HRTEM) techniques were used to confirm the origin of PL emission. These techniques confirmed that the origin of PL emission could be either due to different defect mechanisms or due to the presence of nanocrystals in the matrix of thin films. Finally, the

PLDS effect of these photoluminescent SiO_xC_y thin films on c-Si solar cells were also studied by using current-voltage (I-V) characterization and External Quantum Efficiency (EQE) where improved solar cell properties were obtained due to better EQE spectra in UV-blue region. This thesis will be a base to design silicon based optoelectronic devices with a safe and low-cost precursor, including the improvement of the efficiency of crystalline Si solar cells by PLDS effect.

Keywords: O-Cat-CVD, SiO_xC_y, Photo-Luminescence, PLDS, Solar cells

Dedicated To

“My Beloved Family”

Acknowledgement

First, I would like to express my gratitude to my thesis director Dr. Yasuhiro Matsumoto for providing me an opportunity to work with his research team and for his continuous support, guidance, and motivation throughout my research. I am immensely appreciative of his profound knowledge, availability, and patience. It was a great experience and an overall growth of my personality. I also wanted to thank generously to Dr. Ateet Dutt who is my co-director of thesis and without the wise counsel and able guidance of him, it would have been impossible to complete my present work.

I also want to express my thankfulness to my thesis committee members: Dr. M. Alfredo Reyes Barranca, Dr. G. Romero-Paredes, Dr. Mauricio Ortega López from Solid State Electronic Section (SEES), Department of Electrical Engineering, CINVESTAV-IPN, and Dr. María de Lourdes Albor Aguilera from Escuela Superior de Física y Matemáticas (ESFM)-IPN, Mexico City for their valuable suggestions, help, encouragement and time to make my thesis perfect in all aspects. I would like to give special thanks to Dr. Guillermo Santana-Rodríguez, Dra. Sandra Rodil from IIM-UNAM and Dr. A. Méndez-Blas from Instituto de Física, Benemérita Universidad Autónoma de Puebla (BUAP) for their collaboration in the research work. Valuable technical support provided by Dr. Mario Francisco Avila Meza, Miguel A. Luna, José de Jesús Meza Serrano, Josué E. Romero-Ibarra and L. Huerta-Arcos. I also want to thank Dr. A. Avila, Dr. G. Romero-Paredes from SEES-CINVESTAV for FTIR and ellipsometry characterizations, respectively.

My sincere thanks to Dr. Arturo Maldonado Alvarez, Dr. Iouri Koudriavtsev, Dr. Arturo Escobosa Echavarria, Dr. Arturo Morales and other professors from the SEES for their help in professional work. I wish to thank the SEES secretaries, Monica Davar Ocegueda, Yesenia Cervantes Aguirre, Beatriz Urrutia Bohorquez, for their continuous support in many things.

I would like to thank the funding support for this project by the National Council of Science and Technology (CONACYT) Nos. 967775, and 299703 and Centro de Investigación y de Estudios Avanzados del Instituto Politécnico Nacional (CINVESTAV-IPN) for providing a place to do my research work. Additionally, the funding support from

PAPIIT IA 101321 and IA 100123 projects also played an important role to complete my present work.

I would also like to acknowledge Juan Ramón Ramos-Serrano, Andrés Galdamez and Maricela Meneses Meneses for their encouragement, support and suggestions in this research work. I would like to thank the Biblioteca-CINVESTAV for providing resources to improve my knowledge. I wish to express my acknowledgement to people from the Department of Becas y Estímulos. I want to express special acknowledgement to Katia Gabriela Ocampo Reyna and Laura Agama for helping to make immigration documents. I am also grateful to my Indian and Mexican friends for their support, time, and encouragement during this academic journey.

Last but not least, I am very grateful to my family members and my spiritual and philosophical gurus for their endless love, faith, support, encouragement and guidance during these years. Thank you all for believing in me and supporting me to fulfill my dreams.

Table of Contents

Chapter 1 Introduction 1

1.1. Background 1

1.2. Reasons of Recombination loss 3

1.3. Photo-Luminescence 4

1.3.1. Intrinsic Luminescence 5

1.3.2. Extrinsic Luminescence 7

1.4. Downshifting Process 7

1.5. Silicon material and Limitations 8

1.6. Luminescence in silicon-based materials 10

1.7. Quantum confinement effect 10

1.8. Defect related mechanisms 14

1.8.1. Oxygen-Deficiency Center (ODC) 15

1.8.2. Non-Bridging Oxygen Hole Center (NBOHC) 16

1.8.3. Self-Trapped Exciton (STE) 17

1.8.4. Hydrogen related defects 18

1.8.5. Carbon related defects 18

1.9. Silicon Oxycarbide (SiO_xC_y) 19

1.10. Objectives and structure of the thesis 20

References 22

Chapter 2 Experimental and Characterization Techniques 30

2.1. Introduction 30

2.2. History of synthesis techniques of silicon oxycarbide (SiO_xC_y) 30

2.3. Organic Catalytic Chemical Vapor Deposition (O-Cat-CVD) 33

2.3.1. Structure of O-Cat-CVD 34

2.3.2. Growth mechanism of thin films 35

2.3.3. Advantages of O-Cat-CVD 36
2.4. Metal-organic compounds as an alternative precursor 36
2.5. Material characterization techniques 38
2.5.1. Fourier Transform Infrared Spectroscopy (FTIR) 39
2.5.2. X-Ray Photoelectron Spectroscopy (XPS) 41
2.5.3. High-Resolution Transmission Electron Microscopy (HR-TEM) 42
2.5.4. Photo-Luminescence (PL) Spectroscopy 43
2.5.5. Ellipsometry 45
2.5.6. Current-Voltage measurement 46
2.5.7. External Quantum Efficiency instrument 47
2.6. General Discussion 48
References 49
Chapter 3 SiO_xC_y thin films deposited with MMS and Vinyl silane 57
3.1. Experimental Details 57
3.2. Results and discussions 57
3.2.1. SiO_xC_y thin films deposited by monomethyl silane 58
3.2.1.1. Fourier Transform Infrared (FTIR) Spectroscopy 58
3.2.1.2. X-Ray Photoelectron Spectroscopy (XPS) 60
3.2.1.3. Ellipsometry 61
3.2.1.4. Photo-Luminescence Spectroscopy 63
3.2.2. SiO_xC_y thin films deposited by vinyl silane 64
3.2.2.1. Fourier Transform Infrared (FTIR) Spectroscopy 64
3.2.2.2. Ellipsometry 65
3.2.2.3. Photo-Luminescence Spectroscopy 66
3.3. General Discussion 69
References 70
Chapter 4 SiO_xC_y thin films deposited with TEOS 76

4.1. Experimental Details 76

4.2. Results and discussions 76

4.2.1. Effect of the argon flow on SiO_xC_y thin films 77

4.2.1.1. Fourier Transform Infrared (FTIR) Spectroscopy 77

4.2.1.2. X-Ray Photoelectron Spectroscopy (XPS) 78

4.2.1.3. Ellipsometry 79

4.2.1.4. Photo-Luminescence Spectroscopy 80

4.2.2. Effect of the deposition time on SiO_xC_y thin films 82

4.2.2.1. Fourier Transform Infrared (FTIR) Spectroscopy 82

4.2.2.2. X-Ray Photoelectron Spectroscopy (XPS) 84

4.2.2.3. Ellipsometry 85

4.2.2.4. Photo-Luminescence Spectroscopy 86

4.2.2.5 High-Resolution Transmission Electron Microscopy (HR-TEM) 89

4.2.3. Effect of the SiO_xC_y thin films on solar cells 90

4.2.3.1. UV-Vis Spectroscopy 91

4.2.3.2. Current density-Voltage (J-V) measurement 92

4.2.3.3. External Quantum Efficiency (EQE) measurement 94

4.3. General Discussion 95

Reference 96

Chapter 5 Conclusions and Future Scopes 102

Future works 103

Appendix 104

A. Publications 104

B. Conference Activities 105

List of Figures

Fig. 1.1 Loss processes in a single-junction solar cell, (a) lattice thermalisation loss, (b) transmission loss, (c) recombination loss, (d) junction loss and (e) contact voltage loss 1
Fig. 1.2 Spectral conversion design for PV applications... 2
Fig. 1.3 Internal quantum efficiency (IQE) curve of the solar cell corresponding to three different front surface recombination velocities.. 3
Fig. 1.4 Photo-Luminescence Process... 4
Fig. 1.5 Luminescent down-shifting process to increase solar cell active range and efficiency 7
Fig. 1.6 Band structure of GaAs and Si material... 9
Fig. 1.7 Function of the electron and holes as wave particle for the Si and nc-Si. 11
Fig. 1.8 Schematic illustration of the density of states for confined materials at different dimensionalities of Space i.e. D = 1,2,3 12
Fig. 1.9 Schematic illustration of PL transition due to deep and shallow level defects 14
Fig. 1.10 Schematic diagram of oxygen deficiency center (ODCs) defects....................... 16
Fig. 1.11 Schematic diagram of Non-bridging oxygen hole center (NBOHC) defect. 17
Fig. 1.12 Schematic diagram of self-trapped exciton (STE) defect. 17

Fig. 2.1 O-Cat-CVD systems present in Electrical Engineering Department of CINVESTAV. 34
Fig. 2.2 Schematic illustration of O-Cat-CVD deposition chamber. 35
Fig. 2.3 Schematic diagrams of the molecules of (a) Monomethyl Silane (MMS), (b) Vinyl Silane and (c) Tetraethyl Orthosilicate (TEOS). 38
Fig. 2.4 Flow chart of used characterization techniques. 39
Fig. 2.5 (a) Photo of FTIR spectroscopy (Nicolet 560) in IIM-UNAM, and (b) Schematic block diagram of FTIR spectroscopy. 40
Fig. 2.6 Illustration of X-ray Photoelectron Spectroscopy (XPS) instrument.................... 41
Fig. 2.7 (a) Photo of HR-TEM (JEOL-JEM-2010) in IIM-UNAM, and (b) Schematic block diagram of HR-TEM. 43
Fig. 2.8 (a-b) Photo of Photo-Luminescence (PL) spectroscopy placed in IIM-UNAM, and (c) Schematic block diagram of PL spectroscopy. 44

Fig. 2.9 (a) Photo of ellipsometry spectroscopy placed in SEES-CINVESTAV, and (b) Schematic block diagram of ellipsometry spectroscopy. 46
Fig. 2.10 (a) Photo of current-voltage (I-V) measurement instrument (ABET Technologies) placed at IIM-UNAM, and (b) Schematic diagram of an I-V measurement instrument (Copyright ABET TECHNOLOGIES, INC. 2021). 47
Fig. 2.11 (a) Photo of the external quantum efficiency (EQE) measurement instrument (Oriel® Instruments QEPVSI-b) placed at IIM-UNAM, and (b) Schematic block diagram of EQE measurement instrument. 48

Fig. 3.1 FTIR spectra of deposited samples at various deposition duration by using MMS 58
Fig. 3.2 XPS spectra of a) SiO_xC_y, b) Si 2p, c) C 1s, and d) O 1s for 30 min deposited sample by using MMS. 60
Fig. 3.3 Refractive index and thickness of deposited samples at various deposition times using MMS 62
Fig. 3.4 PL spectra of deposited samples at room temperature for various deposition times by using MMS 63
Fig. 3.5 FTIR spectra of deposited samples at various deposition duration by using vinyl silane. 64
Fig. 3.6 Refractive index and thickness of deposited samples at various deposition times by using vinyl silane. 65
Fig. 3.7 PL spectra of deposited samples at at room temperature for various deposition times by using vinyl silane. 66
Fig. 3.8 PLE spectra of as deposited thin films by using vinyl silane. 67
Fig. 3.9 PL lifetime decay measurements (TRPL) for a 30 min. deposited sample by using vinyl silane. 68

Fig. 4.1 FTIR spectra of the as-deposited samples at various argon flows by using TEOS 77
Fig. 4.2 a) XPS Spectrum b) Si 2p XPS fitted spectrum for the deposited sample at 20 sccm argon flow by using TEOS 78
Fig. 4.3 Thickness and refractive index of as-deposited samples at various argon flow by using TEOS 80

Fig. 4.4 PL spectra of samples obtained at at room temperature for different argon flows by using TEOS 81
Fig. 4.5 FTIR spectra of deposited samples at various deposition times by using TEOS... 82
Fig. 4.6 XPS Spectrum b) Si 2p XPS for 30 min. deposited sample with TEOS precurso. 84
Fig. 4.7 Refractive index and thickness of deposited samples at various deposition times by using TEOS 85
Fig. 4.8 PL spectra of deposited samples at at room temperature for various deposition times by using TEOS 86
Fig. 4.9 PLE spectra of as-deposited thin films by using TEOS. 87
Fig. 4.10 PL lifetime decay measurements (TRPL) for 30 min. deposited sample by using TEOS. 88
Fig. 4.11 HRTEM images of SiO_xC_y films obtained at 30 min deposition by using TEOS 89
Fig. 4.12 UV-Vis transmittance spectra at various deposition times with TEOS precursor-based SiO_xC_y thin films. 91
Fig. 4.13 J-V characteristics of solar cells at various deposition times with TEOS precursor based SiO_xC_y thin films. 93
Fig. 4.14 EQE characteristics of solar cells at various deposition duration of SiO_xC_y thin films 94

List of Tables

Table 1.1 The relationship of dimensionality of the low-dimensional semiconductors with the kinetic energy (dispersion) and the corresponding and effective density of states at the conduction band 13

Table 2.1 SiO_xC_y matrix: methods of preparation, precursors, Photo-Luminescence (PL) emission band, and related mechanism of PL emission 31
Table 2.2 Autoignition temperatures for different gases 37

Table 3.1 FTIR infrared absorption bands with their respective wavenumbers 59
Table 3.2 The relative content of the phases calculated by the XPS fitted results. 60
Table 3.3 Refractive index and thickness of samples by ellipsometry. 62
Table 3.4 Refractive index and thickness of samples by ellipsometry. 65

Table 4.1 The relative content of the different bonding phases of si 2p spectra calculated by the XPS fitted results 79
Table 4.2 Refractive index and thickness of samples by ellipsometry. 80
Table 4.3 The relative content of the different bonding phases of si 2p spectra calculated by the XPS fitted results 84
Table 4.4 Refractive index and thickness of samples by ellipsometry 85
Table 4.5 The effect of Si and SiC nanoparticles size on PL peak energy by using eq. (4.2) and (4.3) 90
Table 4.6 Characteristics of monochromatic solar cells with and without the presence of deposited SiO_xC_y thin films. 92

CHAPTER 1
INTRODUCTION

1.1. Background

The generation of electricity from coal, nuclear, and other non-renewable power plants is one of the main causes of air pollution which can be overcome by using renewable energy. Now, the demand for energy is increasing day by day due to the growth of the world's population and rapid urbanization. Silicon solar cells can play an important role to achieve this goal but the theortical efficiency of silicon solar cells is limited to 30% for the band gap of 1.12 eV according to the Shockley-Quisser's model [1].

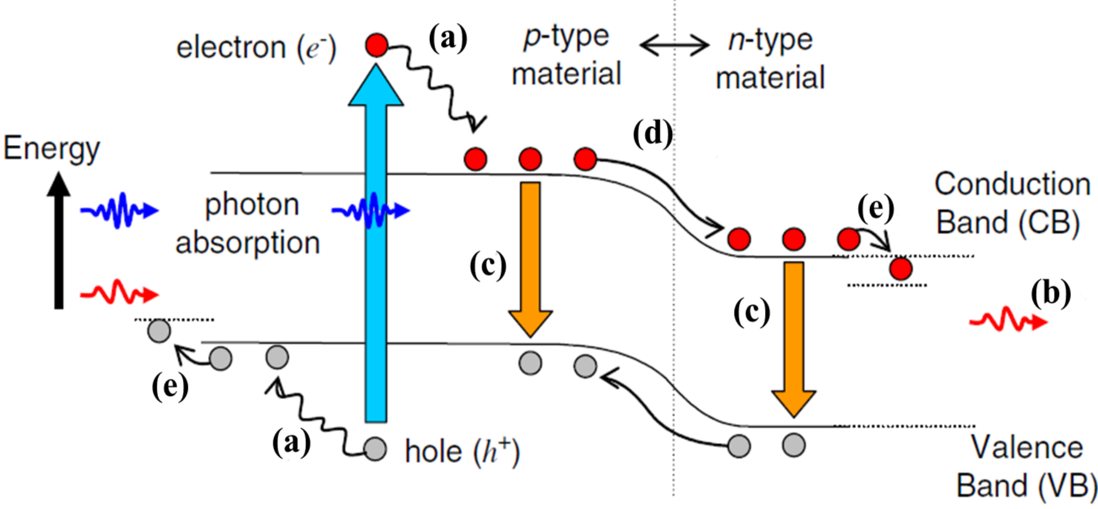

Fig. 1.1 Loss processes in a single-junction solar cell, (a) lattice thermalisation loss, (b) transmission loss, (c) recombination loss, (d) junction loss and (e) contact voltage loss [2].

This limitation may be overcome with the concept of third-generation silicon solar cell and in this way, the efficiency could be improved up to 37% [3] by using the modification in the spectrum at one sun. Fig. 1.1 shows the types of losses which occur in a single-junction solar cell. Here, thermalization [Fig. 1.1 (a)], transmission [Fig. 1.1 (b)], and recombination losses [Fig. 1.1 (c)] are termed as spectral mismatch losses [2], [4]. Although, there is also junction loss [Fig. 1.1 (d)] and contact voltage loss [Fig. 1.1 (e)] available in the solar cells but it assumes that these losses are unavoidable losses from the

device [2]. Besides, the thermalization loss occurs when a photon has higher energy than the bandgap of the material and when this photon is absorbed by the material then it generates an electron-hole pair while the excess energy is dissipated in the form of heat. This kind of loss is known as thermalization loss. On the other hand, in the case of transmission loss, a photon with energy less than the required band gap is not absorbed by the semiconductor and these kinds of photons do not make any contribution for the generation of electron hole pair. The mentioned loss is known as transmission loss. 70% of the total energy losses is present due to these two types of losses [2]. While the third type of loss, the recombination loss, occurrs due to the fast recombination of electron-hole pairs close to the surface. This type of loss mainly affects the high-energy photons (short wavelength) because these photons are absorbed in the surface region which reduces the spectral response [2]–[4].

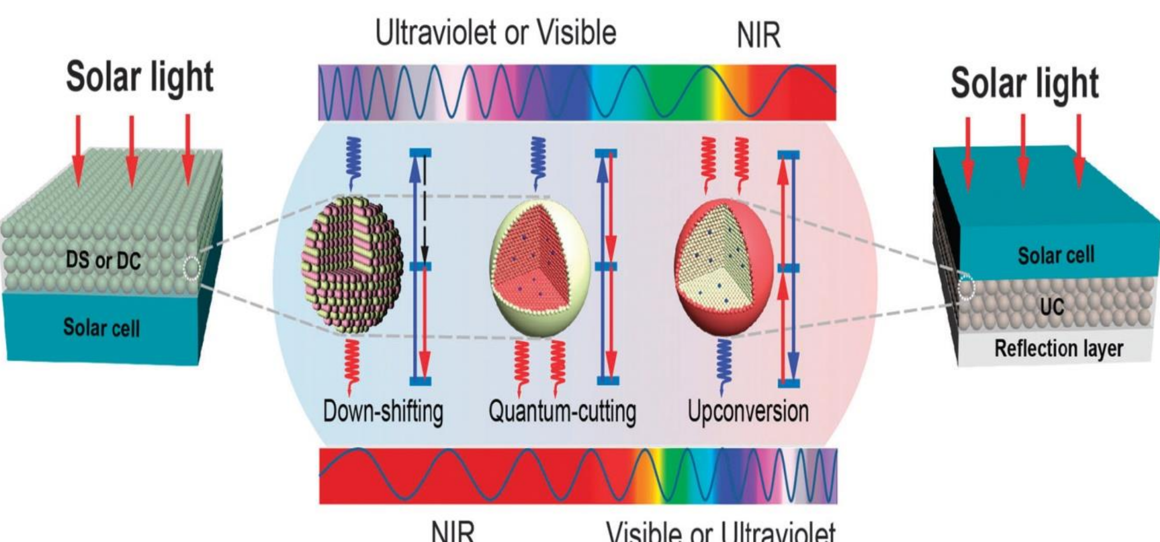

Fig. 1.2 Spectral conversion design for PV applications [5].

The previously discussed losses i.e. thermalization loss, transmission loss, and recombination loss can be overcome by the methods of down-conversion, up-conversion, and Photo-Luminescence, respectively as shown in Fig. 1.2 which may improve the efficiency of silicon solar cells [2]–[4].

As shown in Fig. 1.2, the upconversion method is used to reduce the transmission loss of the solar cell and a upconversion layer should be deposited in the rear part of the solar cell. In this method, two or more photons of less energy transform into a photon of higher

energy which may contribute to create an electron-hole pair and consequently, improve the efficiency of the solar cell. On the other hand, a down-converted layer and down-shifted layers are deposited on the front part of the solar cell, as shown on the left side of Fig. 1.2. In the case of down conversion, a photon of high energy splits into two photons of the same energy of the band gap of the material and increase the efficiency of the solar cell. This method is also known as quantum cutting. Furthermore, in the case of downshifting, a UV energy photon converts into a visible energy photon by the mechanism of Photo-Luminescence, and this visible energy or shifted photon contributes to improve the efficiency of the solar cell [5]. The main aim of this thesis is to shift these high energy UV photons to low energy visible photons by the method of PL downshifting which is more described in the next sections.

1.2. Reasons of Recombination loss

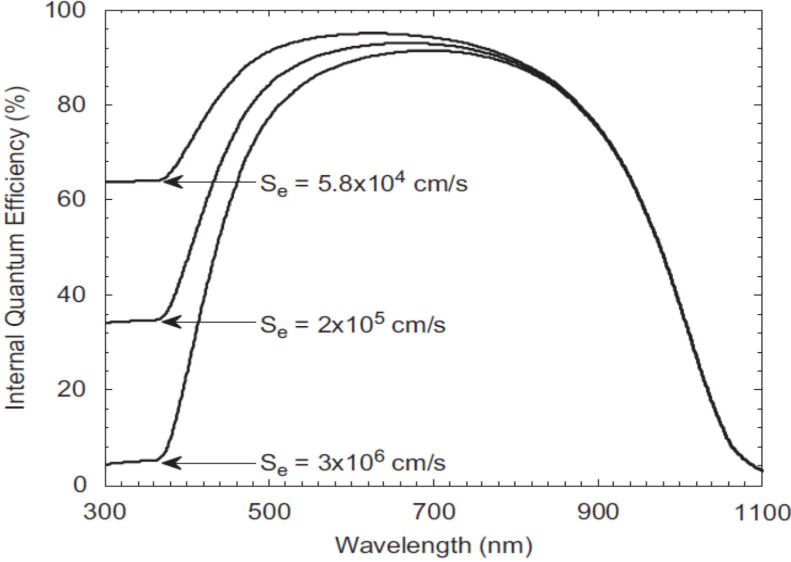

Fig. 1.3 Internal quantum efficiency (IQE) curve of the solar cell corresponding to three different front surface recombination velocities [6].

As we have discussed previously, a recombination loss occurs due to the high recombination rate of high-energy photons of UV region on the surface of the solar cell. Here, in Fig. 1.3, it is observed that the internal quantum efficiency curve is giving a poor UV response when the surface recombination velocity is increasing. The main reasons for this bad UV response are as follows [6]:

- The possibilities of the recombination of the generated carriers via surface states defects increase due to the shallow absorption depth of ultra-violet (UV) photons which consequently reduces the UV response.
- Increased reflection of UV photons due to higher refractive index (RI) of silicon in this region also reduces the UV response.
- Higher RI also cause the high dispersivity which creats difficulties to optimize the anti-reflection (AR) coatings.

This kind of loss might overcome by the downshifting process mechanism by using the Photo-Luminescence process which is described in the next section.

1.3. Photo-Luminescence

The use of luminescent devices such as LEDs, displays and lasers, etc., have become a necessary part of our daily life. Normally, light can be generated by using an energy source by two methods, i.e., incandescence and luminescence. Light generated from the incandescence process is also known as hot light because it is generated by heating some material (e.g. tungsten or tantalum wire) to an appropriate high temperature so that material can glow [7].

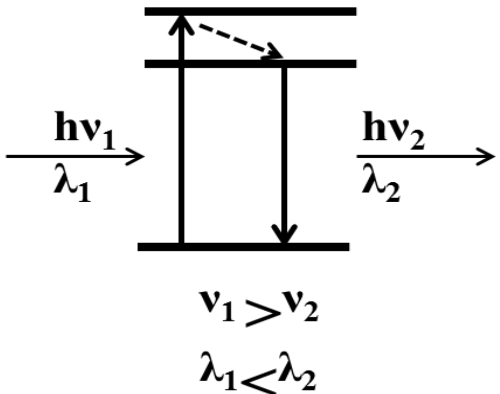

Fig. 1.4 Photo-Luminescence Process.

On the other hand, the light generated from the luminescence process is also known as "cold light" because the generation of light takes place at normal temperature and the emission of blackbody radiation is not included in it. The word luminescence was used for the first time by a German physicist, Eilhardt Wiedemann in 1888 and the Latin words "lumen" means "light" and "escentia" means "the process of" so it means the process of

giving of light [8]. The materials with this phenomenon are known as luminescent materials.

This luminescence process involves three steps as shown in Fig. 1.4:

(1) The excitation of an electron from the valence band to a higher vibrational level of the conduction band,

(2) Non-radiative relaxation of this excited electron from higher vibrational energy to the lower vibrational energy level in the conduction band through the internal conversion process,

(3) Subsequent emission of photons i.e. light after the recombination of an excited electron with the hole in the valence band.

In the case of Photo-Luminescence (PL), an electron is excited by absorbing a photon and this PL can be further classified into two parts based on its duration of light emission, i.e., into fluorescence and phosphorescence, respectively. Fluorescence is a temperature-independent process where the duration of emission remains less than 10^{-8} seconds and it takes place simultaneously with the absorption of radiation and it stops immediately after the removal of excitation. On the other hand, phosphorescence is a temperature-dependent process, and the duration of emission remains more than 10^{-8} seconds and phosphorescence emission can be continued for some time even after the removal of excitation. Both processes have their own advantages and significance in science and technology according to their use. The Luminescence of a semiconductor can also be classified as either intrinsic or extrinsic luminescence in terms of the nature of the electronic transitions producing it [9].

1.3.1. Intrinsic Luminescence

When luminescence occurs within a pure material or crystal, then this kind of luminescence refers to intrinsic luminescence. It can be classified into three categories as described below.

a) Band-to-Band Luminescence

This luminescence usually occurs in direct bandgap materials such as III-V compounds where an electron of the conduction band recombines with a hole of the valence band by a direct band-to-band transition. Very pure materials can also show this luminescence at high temperatures. Moreover, from the perspective of luminescence applications, light emission through band-to-band transition takes place in semiconductor lasers and very bright type light-emitting diodes [9].

b) Exciton Luminescence

An exciton consists of a bounded electron-hole pair when an excited electron interacts with a hole through the Coulomb forces. Therefore, an exciton no longer represents two independent quasi-particles. So, when a luminescence occurs due to the movement of an exciton through the crystal, then it is known as exciton luminescence [10].

Luminescence may occur due to two kinds of excitons i.e. Wannier (or Wannier-Mott) exciton and the Frenkel exciton. Normally, the presence of luminescence due to Wannier exciton can be found in III–V and II–VI inorganic semiconductors where an electron of the conduction band and a hole of the valence band are bounded together by the Coulomb force. It is noteworthy that the stability of Wannier excitons is found only at low temperatures where its binding energy is higher than thermal energy. However, band-to-band luminescence appears at high temperatures because excitons are not so stable at high thermal energy. On the other hand, the luminescence due to Frenkel exciton can be found normally in organic molecular crystals and inorganic complex salts where the expanse of the electron and hole wavefunctions is smaller than the lattice constant [7], [9].

c) Cross-Luminescence

This kind of luminescence occurs when an electron in the valence band recombines with a hole created in the outermost core band. Cross-luminescence is usually detected in double halides, alkaline-earth halides, and alkali materials [5]. Normally, cross luminescence takes place only when the energy difference between the outermost core or the minima of the conduction band and the maxima of valence is smaller than the bandgap energy of the material i.e. $E_{c\text{-}v} < E_g$. Moreover, a fast decay time, of the order of nanoseconds, is an

important characteristic of cross-luminescence, which makes scintillators a good example of cross-luminescence transitions.

1.3.2. Extrinsic Luminescence

When impurities or defects are intentionally incorporated in a semiconductor or ionic crystal, then this can be classified as extrinsic luminescence. These intentionally incorporated impurities are known as activators and these kinds of luminescent materials are known as phosphors. It can be categorized into two types, i.e., unlocalized and localized, respectively. An unlocalized extrinsic luminescence occurs when the free electrons in the conduction band and holes in the valence band of the host lattice contributes to the luminescence process, while the excitation and emission process of the luminescence is confined within a localized luminescent center.

1.4. Downshifting Process

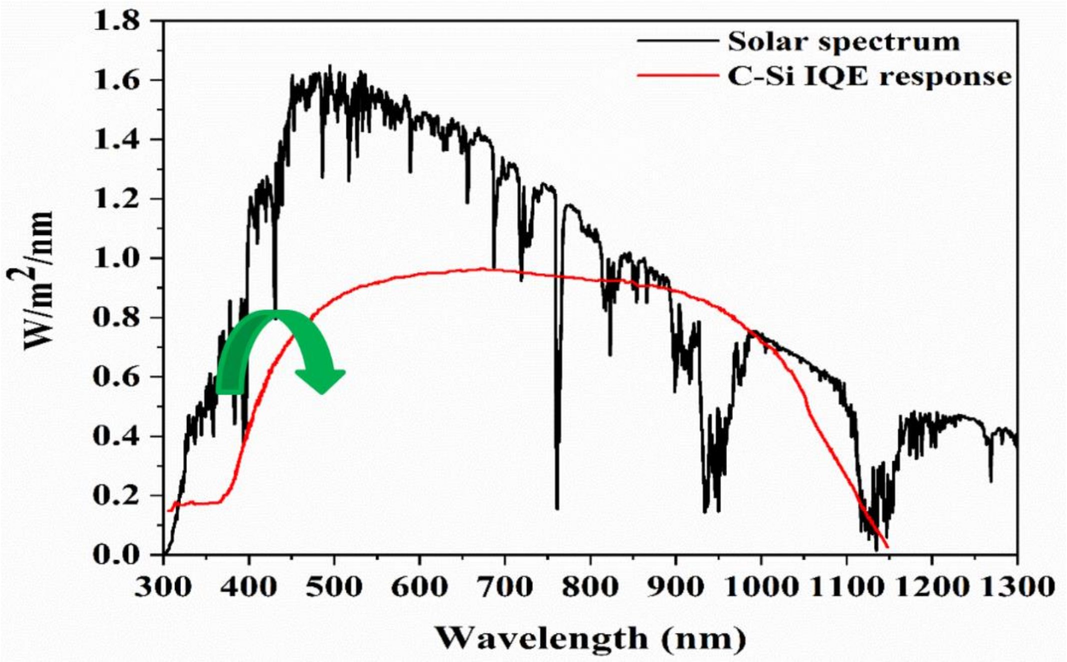

Fig. 1.5 Luminescent down-shifting process to increase solar cell active range and efficiency [13].

Hovel et al. [11] proposed the down-shifting method of UV photons to longer wavelength by using the Photo-Luminescence process, in order to increase the efficiency of solar cells with poor UV response, as shown in Fig. 1.4. Down-shifting process allows to generate

only one photon by each incoming photon. For the down-shift conversion approach, the quantum efficiency remains less than one, in which non-radiative losses can be prevented [12]. It works by increasing the current of the solar cell by elevating the number of photons absorbed while the voltage remains the same. The down-shift process only shifts the UV photons into the solar spectrum, where light absorption properties are better as shown in Fig. 1.5. This process does not modify the intrinsic structure of the solar cell. Therefore, the conversion efficiency of the solar cell would get improved due to increase in the current of solar cell. Two types of approaches are very general for down-shifting, i.e., [6]:

a) An organic photoluminescent down-shifting (PLDS) layer on the front face of a solar cell reduces cost and device complexity.
b) Thermally or PECVD-grown thin films like SiC or SiO_xC_y layers passivate surface defects to decrease the front surface recombination velocity which consequently improve the efficiency of solar cell by PLDS process.

So here, the main focus of this thesis is to explore the second type of approach for downshifting by thermally grown SiO_xC_y layers, but before understanding the properties and nature of the SiO_xC_y matrix, it is necessary to understand the limitations of silicon as a photoluminescent (PL) material and the possible reasons of the origin of PL in silicon which is discussed in the next parts of this chapter.

1.5. Silicon material and Limitations

As we know that a bigger portion of the earth’s crust is constituted with silicon (27.2 wt%) after the presence of oxygen (45.5 wt%). Silicon word is derived from the latin word silex or silicis which means "flint" and it is discovered by the Swedish chemist Jöns Jacob Berzelius in 1824 [14]. Although it is difficult to find pure Si in nature, but it is currently possible to obtain with a high degree of purity and crystallinity at relatively low costs due to the production at the industrial level. Silicon dominates the electronic industry due to its intrinsic properties, proven reliability, ease of fabrication, and low-cost volume production, but it faces the technological challenge to develop the optoelectronic devices such as LEDs, etc., due to its indirect bandgap structure.

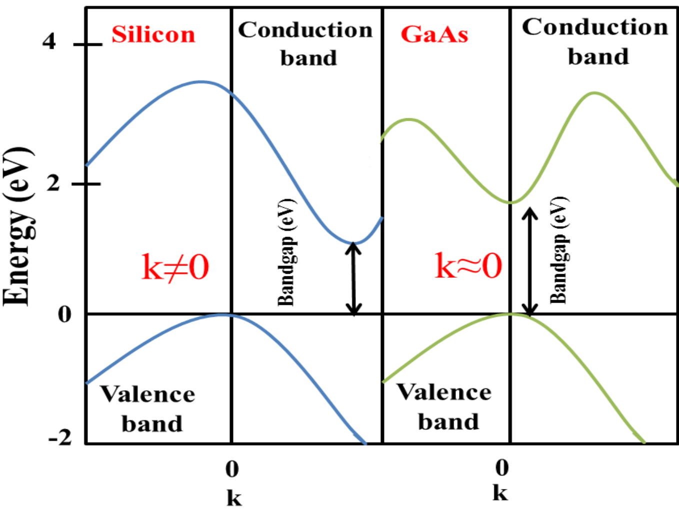

Fig. 1.6 Band structure of GaAs and Si material.

In Fig. 1.6, an energy (E) vs momentum (k) graph is shown with the band structures of GaAs and Si materials which have the direct and indirect bandgap, respectively. Here, it is observable that the maxima of the valence band is aligned with the minima of the conduction band in the case of GaAs material. This phenomenon shows that the vector momentum (k) is equal to zero due to which a photon can easily emit in the case of direct bandgap materials. On the other hand, the maxima of the valence band is not aligned with the minima of the conduction band in the case of indirect bandgap material, e.g., silicon. Due to this reason, vector momentum (k) is not equal to zero and it is very rare to emit a photon in this case, while it emits a phonon to conserve the momentum and the radiative recombination of electron–hole pairs in the indirect material, is a second-order process. Hence, it is very difficult to obtain a photoluminescent device with a bulk silicon material.

Fig. 1.6 illustrates that if there is a recombination in a direct gap semiconductor, the probability of a photon being emitted is high, whereas in indirect gap materials, the probability of photon emission is very low. For example, in the case of GaAs, the probability of emitting a photon, when there is recombination, is close to 50%, while for silicon the probability is of the order of 0.0001%. This signifies that in order to emit a photon in silicon, a million electron-hole pairs are needed to recombine and therefore the radiative recombination of electron–hole pairs in the indirect material is taking place with lesser probability and slower rate than in the direct band material [15].

Many of these ideas changed with the discovery of visible light emission in porous silicon by L.T. Canham in the 1990s [16] and the presence of radiative defects [17] which we will study in the next section.

1.6. Luminescence in silicon-based materials

The discovery of strong luminescence from silicon-based materials at room temperature have attracted a lot of attention in recent years. Some potential silicon-based optoelectronic applications such as LEDs, Blue lasers, solar cells, sensors, etc., can be obtained by using these photoluminescent materials [18]–[21]. The first demonstration of visible emission by porous silicon was reported in the starting of the 1990s by the research group of L. T. Canham where the origin of Photo-Luminescence was discussed due to the Quantum Confinement Effect (QCE) using the silicon nanoparticles [16]. In the same year, another research group discussed the origin of Photo-Luminescence in Si due to radiative defects, i.e., nonbridging oxygen hole centers [17] and afterward many other kinds of defect-related mechanisms were reported discussing the origin of PL in Silicon [10], [22]–[24]. So here, the mechanism of QCE and some important defect mechanisms are going to be discussed in detail.

1.7. Quantum confinement effect

Quantum Confinement Effect (QCE) is the most popular term in the field of nanoscience and nanotechnology and firstly, this concept was proposed by Herbert Kroemer and by Zhores Alferov and R. F. Kazarinov in 1963 [25], [26]. This effect takes place when one of the dimensions of any bulk material is confined. The length size for the regime of quantum confinement may vary according to the semiconductor materials, where the spatial extent of the electronic wave function is comparable with the particle size. Electrons experience the presence of particle boundaries due to the effect of the quantum size or geometrical limitations and adjust their energy according to the changes in particle size [27]. QCE can occur when at least one of the particle dimensions of the bulk material is equal to or less than the Bohr exciton radius, where the minimum required diameter is different for each material, e.g., in the case of silicon, this effect can be achieved when the crystal size is

below or equal to 4.3 nm [28], [29]. Hence, photoluminescence is dependent on the size of nanoparticles according to this phenomenon.

In quantum mechanics, it is claimed that some physical variables of an electron, i.e., position and momentum, cannot be determined accurately simultaneously. This idea was postulated by Werner Karl Heisenberg in 1927 and it is known as the "principle of uncertainty" [30] which can be described by the given expression in equation (1.1):

$$\Delta p \Delta x \geq \frac{h}{4\pi} \quad (1.1)$$

Here, *Δp* denotes the uncertainty of the moment of the particle (moment is equal to mass by speed), *Δx* denotes the uncertainty of the position of the particle and *h* is the Planck's constant ($h = 6.63 \times 10^{-34}$ Js).

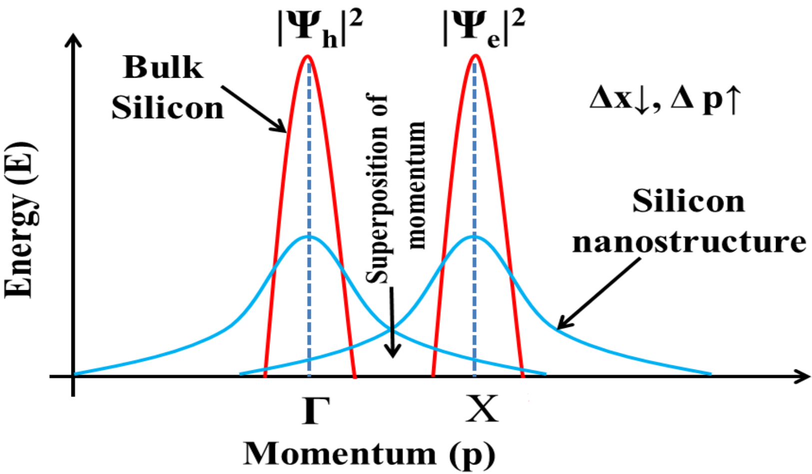

Fig. 1.7 Function of the electron and holes as wave particle for the Si and nc-Si.

If an electron is confined within a very small volume, according to this principle, e.g., a silicon nanocrystal, then its position can be estimated with great precision. However, this implies that now its momentum will be uncertain, as well. As we can see in Fig. 1.7, if *Δx* is very small, then the value of *Δp* will become larger and this uncertainty causes a widening in the wave functions associated with the momentum of electrons and holes, which produces an overlap between them. This area of superposition of momentum is known as quasi-direct recombination, which means that now it is possible to have recombination without the assistance of a phonon, which significantly increases the probability of emitting a photon [31].

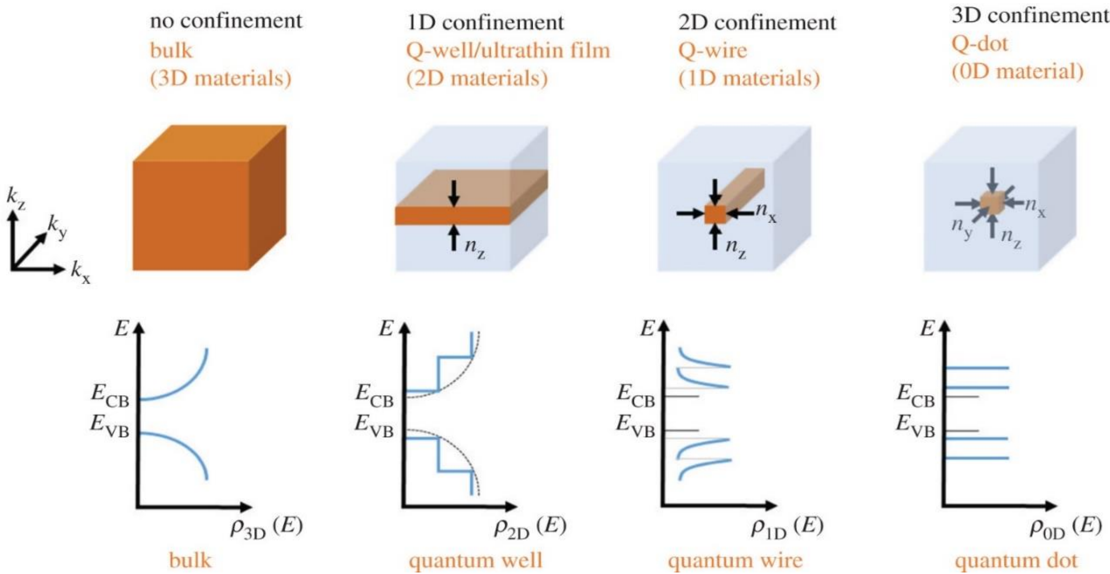

Fig. 1.8 Schematic illustration of the density of states for confined materials at different dimensionalities of Space i.e. D = 1,2,3 [29].

Here, the quantum confined structures can be distinguished according to the confinement of their dimensions, as shown in Fig. 1.8. When a material is confined only in one dimension, then this two-dimensional material is known as quantum well or ultrathin film. If any material is confined in two dimensions, then this one-dimensional material is known as quantum wire, while a zero-dimensional structure, that is confined in all the dimensions, is known as a quantum dot. A quantum dot or zero-dimensional structure has very well-defined and quantized energy levels where a simple effective-mass approximation model can help to determine the QCE of the nanostructure.

The density of states of a confined material are shown in Fig. 1.8 and the relationship of corresponding and effective density of states for the conduction band and the kinetic energy with the degrees of freedom of the material, are discussed in Table 1.1. Here, it is observable that the reduction in the degree of freedom of dimensions leads the density of states into discrete energy levels instead of the continuous energy band of bulk silicon, due to confinement in one or more directions by potential barriers [27], [29]. The discrete structure of energy states leads to a discrete absorption spectrum which influences the transition probability. Moreover, a discretization of the energy bands of the material causes an apparent increase in the band gap, which produces a shift in the emission lengths towards the blue-violet colors.

Table 1.1 The relationship of dimensionality of the low-dimensional semiconductors with the kinetic energy (dispersion) and the corresponding and effective density of states at the conduction band [29].

Degrees of freedom	Kinetic energy (dispersion)	Density of states (close to the conduction band)	Effective density of states (at the conduction band)
3D (bulk)	$E = \frac{\hbar^2}{2m^*}(K_x^2 + K_y^2 + K_z^2)$	$\rho_{3D} = \frac{1}{2\pi^2}\left(\frac{2m^*}{\hbar^2}\right)^{\frac{3}{2}}(E - E_c)^{1/2}$	$N_C^{3D} = \frac{1}{\sqrt{2}}\left[\frac{m^*kT}{\pi\hbar^2}\right]^{3/2}$
2D (film)	$E = \frac{\hbar^2}{2m^*}(K_x^2 + K_y^2)$	$\rho_{2D} = \sum_{i=1}^{n}\frac{m^*}{\pi\hbar^2}H(E - E_c)$	$N_C^{2D} = \frac{m^*kT}{\pi\hbar^2}$
1D (wire)	$E = \frac{\hbar^2}{2m^*}(K_x^2)$	$\rho_{1D} = \frac{1}{\pi m^*\hbar}\left(\frac{m^*}{2(E - E_c)}\right)^{\frac{1}{2}}$	$N_C^{1D} = \sqrt{\frac{m^*kT}{2\pi\hbar^2}}$
0D (dot)	#	$\rho_{0D} = 2\delta(E - E_c)$	$N_C^{0D} = 2$

Note- #The dispersion has not been defined for zero-dimensional structure because there is no periodicity in any direction.

Moreover, different models have been applied to estimate the changes in emission length when changing the diameter of the nanocrystals. However, it is a complex process to calculate the bandgap energy for silicon nanostructures in a host matrix. Several models and approximations such as Tight-Binding Scheme, Empirical Pseudopotential Approach (EPA), and Effective Mass Approximation (EMA) models are considered for this where the EMA model is the most used. Here, Ledoux et. al., have given one of the most popular theoretical expressions which is discussed below in equation (1.2) [32]:

$$E = 0.925 + \frac{3.73}{d^{1.39}} + \frac{0.881}{d} \quad \ldots\ldots\ldots\ldots\ldots\ldots\ldots (1.2)$$

Here, peak photon energy (in eV) and nanoparticle diameter (in nm) are represented by *E* and *d*, respectively. Another relation proposed by Delerue et. al., is also very prominent, which is given as equation (1.3), where E_g is the bandgap of bulk silicon, and *d* is the average diameter of the nanocrystals [33]:

$$E_{pl} = E_g + \frac{3.73}{d^{1.39}} \quad \ldots\ldots\ldots\ldots\ldots\ldots\ldots\ldots\ldots\ldots (1.3)$$

Thus, the key outcomes of QCE on the nanostructures are i) broadening of wave factors, which provide a quasi-direct recombination center, like the ones present within a material with direct bandgap, i.e., there is no need for phonon to conserve the momentum. ii) It also results in increasing of the bandgap.

1.8. Defect related mechanisms

The position of each atom is well defined in an ideal crystal lattice and if any deviations occur in this lattice structure, then this phenomenon is known as defects or imperfections in the material. Electronic energy states may be introduced due to these defects in the bandgap of semiconductors, which can be categorized in two types: shallow levels and deep levels as shown in Fig. 1.9.

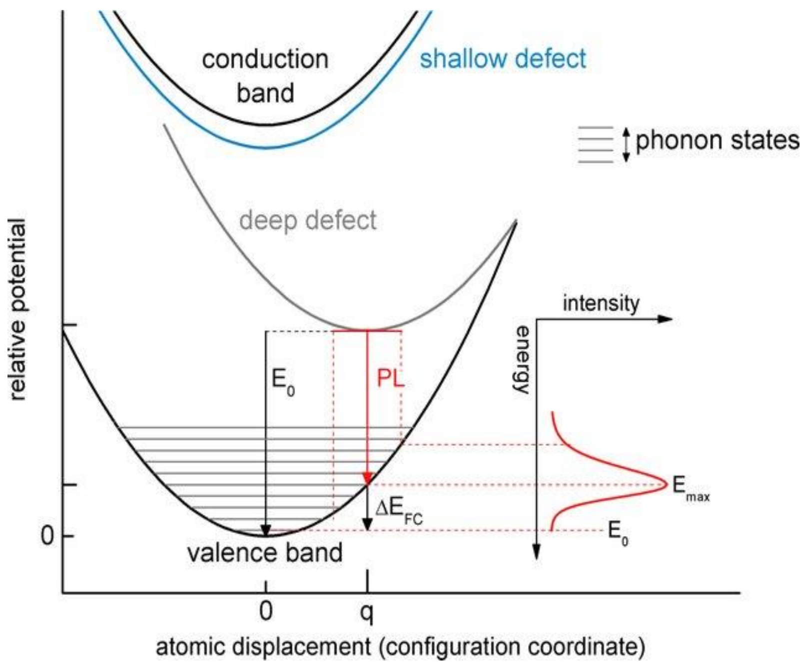

Fig. 1.9 Schematic illustration of PL transition due to deep and shallow level defects *[34].*

Shallow levels in semiconductors play an important role and commonly, they are located at ~0.1 eV from the valence or the conduction band-edges. Thus, thermal ionization takes place in these levels at room temperature and the effective mass theory is used to describe the ionization energy of a shallow level, where it also behaves as hydrogen-like levels [35]. For instance, a shallow donor looks like a hydrogen atom which consists of an electron bounded with a positive nucleus. A shallow level is created by impurity elements in the

outermost shell of the element, which is used as a dopant, and the size of these impurity atoms are usually the same as the size of the host atom. These shallow levels easily get ionized because they have very low activation energy which provides free carriers to create a p-type or n-type semiconductor [34].

If the energy levels are located deeper in the forbidden gap, i.e., beyond 0.1 eV from the band-edges of valence or conduction band, then this level is commonly mentioned as a deep level and defects related to this level are often known as "generation centers", "recombination center", or "traps". Inherent crystal defects or the introduction of impurities can be the reasons for the formation of deep levels. The deep level cannot be described by the effective mass theory, which is a major difference between deep and shallow levels. Furthermore, the ionization energy of deep levels is higher so they generate very less free charge carriers, due to which the conduction mechanism of deep levels is not too significant in comparison to shallow levels. However, deep levels can be important controling some other important properties of semiconductors, e.g., they can be exploited as a recombination center in fast-switching devices [36], [37]. Deep levels may behave as recombination centers when they are near to mid-band gap, and it can be handled as constructive or destructive phenomenon, according to their utilization, e.g., it provides a path for the generation of electron-hole pairs across the bandgap, which can affect the performance of devices such as LEDs.

Therefore, the presence of defects can cause changes in the structural, optical, and electrical properties. Many factors can be the reason for these defects, such as manufacturing processes, mechanical stress, changes in temperature, irradiation, and the presence of impurities. Different defects such as oxygen deficiency centers, non-bridging oxygen hole centers (NBOHC), self-trapped exciton and hydrogen-related defects, etc., could be the cause of emission bands at spectra. Some of them are discussed in the following sections.

1.8.1. Oxygen-Deficiency Center (ODC)

Oxygen-deficiency centers (ODC) are one of the most common defect-related mechanisms in oxides. It usually behaves as radiative centers in luminescence processes, where a

visible emission occurs when a conduction band electron recombines with an oxygen vacancy [38], [39]. Normally, two types of ODC models are described in literature, i.e., neutral oxygen vacancy (NOV) and two-fold coordinated silicon which are also termed as ODC (I) and ODC (II), respectively. Fig. 1.10 shows a schematic diagram of both kinds of ODCs where a ≡Si-Si≡ bond is formed for ODC (I) while ODC (II) is denoted as =Si•• where silicon is bounded with two oxygens and two free bonds. Photo-Luminescence and cathodoluminescence spectroscopy can help to observe and distinguish these defects. Typically, the PL occurs at 2.7 eV for ODC (I) with a decay time of 10 ms, while PL occurs at 4.4 eV for ODC (II) with a decay time of 4 ns [10].

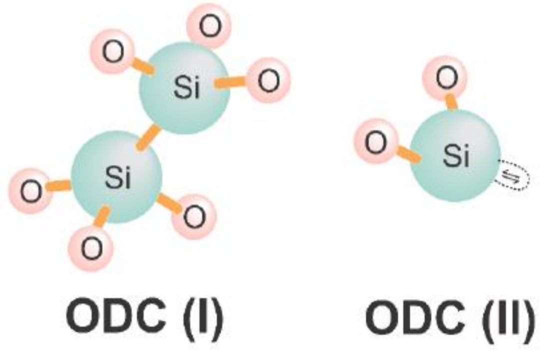

Fig. 1.10 Schematic diagram of oxygen deficiency center (ODCs) defects.

1.8.2. Non-Bridging Oxygen Hole Center (NBOHC)

NBOHC is an intrinsic defect that is electrically neutral and paramagnetic by nature. It is denoted by a free bond in oxygen (≡Si-O •) as shown in Fig. 1.11. It is commonly characterized by using optical spectroscopies such as Photo-Luminescence or cathodoluminescence and by more complex techniques such as Electron Paramagnetic Resonance spectroscopy (EPR). A luminescent band at 1.9 eV or 650 nm of the visible spectra is a unique characteristic of this defect center. It can also be recognized by its Full-Width Half Maximum (FWHM) of 0.17 eV with a time decay constant of 20 μs [40]. Some authors propose that the formation of this defect is related to the rupture and release of hydrogen from a silanol group [41].

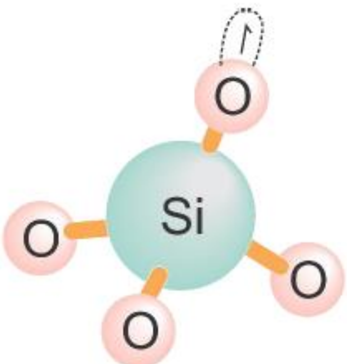

Fig. 1.11 Schematic diagram of Non-bridging oxygen hole center (NBOHC) defect.

1.8.3. Self-Trapped Exciton (STE)

This is a short-living or transient defect, that can be created by energy transfer between the combination of the electronic excitation energy such as electron-hole pairs and electron-phonon interaction. So, when a luminescence occurs due to the self-trapping of excitons through the crystal, e.g., the trapping of electrons by self-trapped holes, then it is known as exciton luminescence [10]. Fig. 1.12 illustrates a model of the structure of this defect. This type of defect is quite common in dielectric materials. This defect can be recognized by using the EPR technique and generally, the photoluminescent emission from 2-3 eV or 620-420 nm has been attributed to this defect [42]. Two models are very common to understand STE, in which the first model is explained by the removal of an oxygen atom to a peroxy bridge position, while another model can be explained by the transient absorption at 5.2 eV using a threefold coordinated silicon [43]–[45]. Usually, the idea of all models is based on the rupture of the silicon-oxygen bond (Si−O) and create an oxygen-oxygen bond (−O−O−) [10].

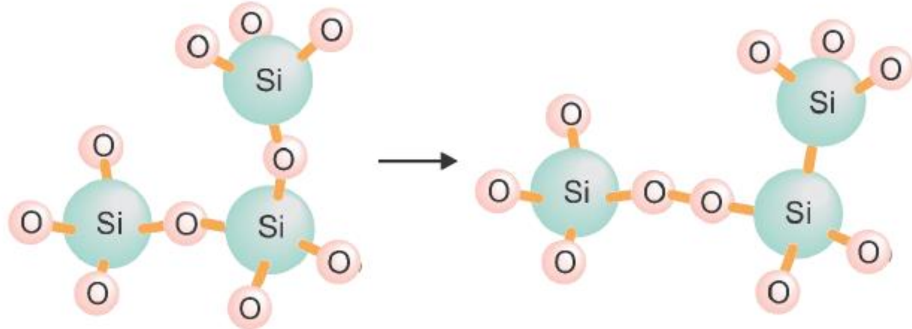

Fig. 1.12 Schematic diagram of self-trapped exciton (STE) defect.

1.8.4. Hydrogen related defects

The incorporation of Hydrogen related defects is usually intentionally or unintentionally found into SiO_2 layers in the form of steam, which may passivate the oxygen or silicon dangling bonds [46]. This defect is considered an intrinsic defect because it's very commonly found in SiO_2. This defect is normally found in the form of ≡Si-H and ≡Si-OH on the surface of the material, due to which nanoparticles are assumed to aggregate into web-like microstructures and micron-sized composited (globules) [47]. The involvement of hydrogen-related defect in the PL emission can't be doubted since it appears as a localized center and PL emission at 2.3 eV is considered due to this defect [48]. Thermally grown silica is one of the main reasons for the formation of ≡Si-H and ≡Si-O• species and the energy levels of these species have been calculated by tight-binding calculations [49].

1.8.5. Carbon related defects

It is a point defect that is very commonly found in mono-crystalline Si wafers grown by the Czochralski technique (Cz-Si) in the form of substitutional carbon (Cs) impurities. The nature of Cs is electrically inert and immobile. On the other hand, an interstitial carbon (Ci) is produced by the reaction of substitutional carbon (Cs) and self-interstitial Si through the Watkins exchange mechanism [50], [51]. It is a prominent defect center that is electronically active and highly mobile and has a doublet electronic ground state. Ci also makes different kinds of complexes with other centers such as CiOi, CiCs, etc., which are electrically active and stable at very high temperatures [52]. It is noteworthy that CiCs complexes normally occur in carbon-rich Si while CiOi complexes occur in oxygen-rich Si [53], [54]. Here, it is notable that a local strain occurs in the lattice due to the introduction of carbon because of its smaller size in comparison to Si [50]. Carbon-related defects, i.e., CiCs, which are also known as G centers, are used to enhance the performance of Si optical emitters [55]. Some other carbon related defects such as Si_2—C=C—Si_2 and Si_2—C—O, [$(C_2)_{Si}$] and Si—(CO)—Si have been suggested in SiO_2, SiC and SiC/SiO_2 interface, respectively [56]–[59]. The maximum PL emission is observed at 405–550 nm with a PL lifetime of less than 10 ns [39], [60].

1.9. Silicon Oxycarbide (SiO_xC_y)

Silicon oxycarbide (SiO_xC_y) material has attracted a lot of attention in the last few decades due to its optoelectronic properties [61]–[65]. Although it was synthesized for the first time by R. B. Ellis in 1951 by incorporating carbon into porous silica [66], the photoluminescent study of this material was started since 1990s, after the first successful demonstration of the Photo-Luminescence from porous silicon [16]. Silicon oxycarbide (SiO_xC_y) structure is represented by bounded silicon with oxygen and carbon. The hybrid nature of this material shows the characteristics of organic and inorganic functional groups [67], [68]. Notably, the inorganic component shows mechanical strength, thermal stability, and chemical properties, while the organic components of the material show the properties like hydrophobicity, plasticity, and solubility [68]–[70]. The composition of multi-elements, i.e., SiC and SiO_2, etc., strongly affect the film properties of the SiO_xC_y matrix, which helps to tailor its properties by controlling the deposition parameters [70]–[72]. Due to the aforementioned explanations, the SiO_xC_y thin film shows superior properties than other Si-related matrices such as SiN, SiC and SiO_2, etc. [61]–[63], [73]–[77]. Although various applications have been explored by distinct research groups such as piezoresistive sensors [78], [79], anode material for storage batteries [80]–[82], gas barrier coating for PET bottles [83], [84], and biomedical application, etc., [85]–[87], the PL study on SiO_xC_y thin films has also received much attention in recent years due to its wide range of intensive emission in visible spectra [61]–[65].

In this work, the silicon oxycarbide (SiO_xC_y) matrix has been deposited by the use of alkylsilane or organometallic compound precursors, i.e., monomethyl silane [MMS; (CH_3-SiH_3)], Vinyl Silane [VS; ($H_2C{=}CHSiH_3$)] and tetra-ethyl orthosilicate [TEOS; ($Si(OC_2H_5)_4$)], which corresponded to gaseous and liquid sources, respectively. These alkylsilane or organometallic precursors provide a better and safer substitute precursor than silane because silane can auto-ignite spontaneously in contact with air beacuse of its pyrophoric nature and it also has the lowest auto-ignition temperature in comparison to other materials [88], [89]. From the molecular formula of MMS,VS, and TEOS, it can be observable that the ratio of the carbon content for each silicon atom is 1:1 and 2:1 in MMS and VS, respectively, while it is 8:1 for TEOS material and the probability of having a

dissociation of the entire molecule, is high in MMS and VS while it is very low in TEOS because of its big molecular structure.

1.10. Objectives and structure of the thesis

This thesis work aims to explore and optimize the luminescent properties of SiO_xC_y thin film by using silicon-based organometallic materials, which may further explore possible solar cell applications by using the PL down shifting (PLDS) conversion method.

The principal objective of this work is:

- To explore the optimization of SiO_xC_y-based materials for the down-shift conversion and their possible application to solar cells.

The general objectives of this work are:

- To develop SiO_xC_y thin films by using Monomethyl Silane (MMS), Vinyl Silane and Tetraethylorthosilicate (TEOS) in Organic Catalytic (O-Cat) CVD.
- To optimize the different parameters of O-Cat CVD, i.e., deposition time, filament temperature, the flow of gases, etc., to understand the properties of the thin film.
- To investigate the origin of the PL emission.
- To observe the downshifting effect of photoluminescent SiO_xC_y thin film on solar cells by using EQE and I-V characteristics.

This thesis work is divided into 5 main chapters and a final chapter in which the conclusions are presented.

Chapter 1: An introduction regarding the spectral losses in silicon solar cells are discussed in this chapter, which is accompanied by the downshifting process with the expectations to improve the efficiency of the solar cell. Also, different types of PL mechanisms are discussed to understand the light emission in silicon-based materials.

Chapter 2: The deposition technique, i.e., Organic Catalytic (O-Cat) CVD is discussed along with the different characterization techniques that have been used to understand the properties of the obtained thin film.

Chapters 3: This chapter describes the results obtained by the use of alkylsilane or organometallic compound precursors, i.e., monomethyl silane, and Vinyl Silane and a general discussion is made of the possible emission mechanisms for the films obtained with the used precursors based on the results obtained.

Chapter 4: This chapter describes the results obtained by using tetra-ethyl orthosilicate precursor and the Downshifting effect of SiO_xC_y films on solar cells deposited by TEOS precursor, where a general discussion is made of the possible emission mechanisms for the films obtained with all the used precursors based on the results obtained and the effectiveness of SiO_xC_y films deposited by TEOS to understand the Downshifting effect in the solar cell.

Chapter 5: Finally, the conclusions obtained during the development of this work are presented with suggestions for future work.

References

[1] W. Shockley and H. J. Queisser, "Detailed Balance Limit of Efficiency of p-n Junction Solar Cells," *J. Appl. Phys.*, vol. 32, no. 3, pp. 510–519, 1961, doi: 10.1063/1.1736034.

[2] B. S. Richards, "Enhancing the performance of silicon solar cells via the application of passive luminescence conversion layers," *Sol. Energy Mater. Sol. Cells*, vol. 90, pp. 2329–2337, 2006, doi: 10.1016/j.solmat.2006.03.035.

[3] T. Trupke, P. Würfel, and M. A. Green, "Up-and down-conversion as new means to improve solar cell efficiencies," in *3rd World Conference on Photovoltaic Energy Conversion*, 2003, pp. 67–70.

[4] B. S. Richards, "Luminescent layers for enhanced silicon solar cell performance : Down-conversion," *Sol. Energy Mater. Sol. Cells*, vol. 90, pp. 1189–1207, 2006, doi: 10.1016/j.solmat.2005.07.001.

[5] X. Huang, S. Han, W. Huang, and X. Liu, "Enhancing solar cell efficiency: The search for luminescent materials as spectral converters," *Chem. Soc. Rev.*, vol. 42, no. 1, pp. 173–201, 2013, doi: 10.1039/c2cs35288e.

[6] C. P. Thomas, A. B. Wedding, and S. O. Martin, "Theoretical enhancement of solar cell efficiency by the application of an ideal 'down-shifting' thin film," *Sol. Energy Mater. Sol. Cells*, vol. 98, pp. 455–464, 2012, doi: 10.1016/j.solmat.2011.11.027.

[7] K. V. R. Murthy and H. S. Virk, "Luminescence phenomena: An introduction," *Defect Diffus. Forum*, vol. 347, pp. 1–34, 2014, doi: 10.4028/www.scientific.net/DDF.347.1.

[8] E. Wiedemann, "Ueber Fluorescenz und Phosphorescenz I. Abhandlung," *Ann. Phys.*, vol. 270, no. 7, pp. 446–463, Jan. 1888, doi: https://doi.org/10.1002/andp.18882700703.

[9] S. Shionoya, "Photoluminescence," in *Luminescence of Solids*, D. R. Vij, Ed. Boston, MA: Springer US, 1998, pp. 95–133.

[10] R. Salh, "Defect Related Luminescence in Silicon Dioxide Network: A Review," *Intechopen*, pp. 135–172, 2011, doi: http://dx.doi.org/10.5772/57353.

[11] H. J. Hovel, R. T. Hodgson, and J. M. Woodall, "The effect of fluorescent wavelength shifting on solar cell spectral response," *Sol. Energy Mater.*, vol. 2, pp. 19–29, 1979.

[12] C. Strümple *et al.*, “Modifying the solar spectrum to enhance silicon solar cell efficiency — An overview of available materials,” *Sol. Energy Mater. Sol. Cells*, vol. 91, pp. 238–249, 2007, doi: 10.1016/j.solmat.2006.09.003.

[13] H. A. Ahmed, J. Walshe, M. Kennedy, T. Confrey, J. Doran, and S. J. Mccormack, “Enhancement in solar cell efficiency by luminescent down-shifting layers,” *Adv. Energy Res.*, vol. 1, no. 2, pp. 117–126, 2013.

[14] N. N. GREENWOOD and A. EARNSHAW, Eds., “Silicon,” in *Chemistry of the Elements (Second Edition)*, Butterworth-Heinemann, 1997, pp. 328–366.

[15] A. Li, “Interaction of Nanoparticles with Radiation,” in *Astrophysics of Dust, ASP Conference Series*, 2003, vol. 309, pp. 417–452, [Online]. Available: http://arxiv.org/abs/astro-ph/0311066.

[16] L. T. Canham, “Silicon quantum wire array fabrication by electrochemical and chemical dissolution of wafers,” *Appl. Phys. Lett.*, vol. 57, no. 10, pp. 1046–1048, 1990, doi: 10.1063/1.103561.

[17] S. Munekuni *et al.*, “Various types of nonbridging oxygen hole center in high-purity silica glass,” *J. Appl. Phys.*, vol. 68, no. 3, pp. 1212–1217, 1990, doi: 10.1063/1.346719.

[18] C.-C. Tu, J. H. Hoo, K. F. Böhringer, L. Y. Lin, and G. Cao, “Red-emitting silicon quantum dot phosphors in warm white LEDs with excellent color rendering,” *Opt. Express*, vol. 22, no. S2, p. A276, 2014, doi: 10.1364/oe.22.00a276.

[19] G. R. Lin, C. J. Lin, and K. C. Yu, “Time-resolved photoluminescence and capacitance-voltage analysis of the neutral vacancy defect in silicon implanted SiO_2 on silicon substrate,” *J. Appl. Phys.*, vol. 96, no. 5, pp. 3025–3027, 2004, doi: 10.1063/1.1775041.

[20] R. Lopez-Delgado *et al.*, “Solar cell efficiency improvement employing down-shifting silicon quantum dots,” *Microsyst. Technol.*, vol. 24, pp. 495–502, 2018, doi: 10.1007/s00542-017-3405-x.

[21] Y. Jin, W. Duan, F. Wo, and J. Wu, “Two-Dimensional Fluorescent Strategy Based on Porous Silicon Quantum Dots for Metal-Ion Detection and Recognition,” *ACS Appl. Nano Mater.*, vol. 2, no. 10, pp. 6110–6115, 2019, doi: 10.1021/acsanm.9b01647.

[22] L. Skuja, “Optically active oxygen-deficiency-related centers in amorphous silicon dioxide,” *J. Non. Cryst. Solids*, vol. 239, no. 1–3, pp. 16–48, 1998, doi: 10.1016/s0022-3093(98)00720-0.

[23] Z. Lin *et al.*, "Defect emission and optical gain in SiC_xO_y:H films," *ACS Appl. Mater. Interfaces*, vol. 9, no. 27, pp. 22725–22731, 2017.

[24] M. Sendova-Vassileva, N. Tzenov, D. Dimova-Malinovska, T. Marinova, and V. Krastev, "Visible luminescence from C-containing silicon oxide films," *Thin Solid Films*, vol. 276, no. 1–2, pp. 318–322, 1996, doi: 10.1016/0040-6090(95)08107-0.

[25] Z. I. Alferov and R. F. Kazarinov, "Authors Certificate 28448 (U.S.S.R)." 1963.

[26] H. Kroemer, "A proposed class of hetero-junction injection lasers," in *Proceedings of the IEEE*, 1963, vol. 51, no. 12, pp. 1782–1783.

[27] D. A. B. Miller *et al.*, "Band-edge electroabsorption in quantum well structures: The quantum-confined stark effect," *Phys. Rev. Lett.*, vol. 53, no. 22, pp. 2173–2176, 1984, doi: 10.1103/PhysRevLett.53.2173.

[28] N. Bohr, "I . On the constitution of atoms and molecules," *London, Edinburgh, Dublin Philos. Mag. J. Sci.*, vol. 26, no. 151, pp. 1–25, 1913.

[29] T. Edvinsson, "Optical quantum confinement and photocatalytic properties in two-, one- and zerodimensional nanostructures," *R. Soc. Open Sci.*, vol. 5, no. 9, 2018, doi: 10.1098/rsos.180387.

[30] W. Heisenberg, "Über den anschaulichen Inhalt der quantentheoretischen Kinematik und Mechanik," *Zeitschrift für Phys.*, vol. 43, no. 3–4, pp. 172–198, 1927, doi: 10.1007/BF01397280.

[31] B. Sain and D. Das, "Tunable photoluminescence from nc-Si/a-SiN_x:H quantum dot thin films prepared by ICP-CVD," *Phys. Chem. Chem. Phys.*, vol. 15, no. 11, pp. 3881–3888, 2013, doi: 10.1039/c3cp43875a.

[32] G. Ledoux *et al.*, "Photoluminescence properties of silicon nanocrystals as a function of their size," *Phys. Rev. B*, vol. 62, no. 23, pp. 15942–15951, 2000, doi: https://doi.org/10.1103/PhysRevB.62.15942.

[33] C. Delerue, G. Allan, and M. Lannoo, "Theoretical aspects of the luminescence of porous silicon," *Phys. Rev. B*, vol. 48, no. 15, pp. 11024–11036, Oct. 1993, doi: 10.1103/PhysRevB.48.11024.

[34] C. Spindler *et al.*, "Electronic defects in Cu(In,Ga)Se_2: Towards a comprehensive model," *Phys. Rev. Mater.*, vol. 3, no. 090302, pp. 1–20, 2019, doi: 10.1103/PhysRevMaterials.3.090302.

[35] G. L. Miller, D. V. Lang, and L. C. Kimerling, "CAPACITANCE TRANSIENT SPECTROSCOPY," *Annu. Rev. Mater. Sci.*, vol. 7, pp. 377–448, 1977, doi: https://doi.org/10.1146/annurev.ms.07.080177.002113.

[36] A. Hallén and M. Bakowski, "Combined proton and electron irradiation for improved GTO thyristors," *Solid State Electron.*, vol. 32, no. 11, pp. 1033–1037, 1989, doi: 10.1016/0038-1101(89)90167-6.

[37] F. D. Auret and P. N. K. Deenapanray, "Deep level transient spectroscopy of defects in high-energy light-particle irradiated Si," *Crit. Rev. Solid State Mater. Sci.*, vol. 29, no. 1, pp. 1–44, 2004, doi: 10.1080/10408430490442458.

[38] F. Gu, S. F. Wang, M. K. Lu, G. J. Zhou, D. Xu, and D. R. Yuan, "Photoluminescence Properties of SnO_2 Nanoparticles Synthesized by Sol-Gel Method," *J. Phys. Chem. B*, vol. 108, no. 24, pp. 8119–8123, 2004, doi: https://doi.org/10.1021/jp036741e.

[39] C. Zhang and J. Lin, "Defect-related luminescent materials: synthesis, emission properties and applications," *chem. sol. rev.*, vol. 41, pp. 7938–7961, 2012, doi: 10.1039/c2cs35215j.

[40] G. Ledoux *et al.*, "Photoluminescence properties of silicon nanocrystals as a function of their size," *Phys. Rev. B*, vol. 62, no. 23, pp. 15942–15951, Dec. 2000, doi: 10.1103/PhysRevB.62.15942.

[41] M. Stapelbroek, D. L. Griscom, E. J. Friebele, and G. H. Sigel, "Oxygen-associated trapped-hole centers in high-purity fused silicas," *J. Non. Cryst. Solids*, vol. 32, no. 1–3, pp. 313–326, 1979, doi: 10.1016/0022-3093(79)90079-6.

[42] C. Itoh, K. Tanimura, and N. Itoh, "Optical studies of self-trapped excitons in SiO_2," vol. 4693, 1988.

[43] A. N. Trukhin, "Luminescence of a self-trapped exciton in GeO_2 crystal," *Solid State Commun.*, vol. 85, no. 8, pp. 723–728, 1993, doi: 10.1016/0038-1098(93)90579-C.

[44] A. N. Trukhin, "Excitons in SiO_2: a review," *J. Non. Cryst. Solids*, vol. 149, no. 1–2, pp. 32–45, 1992, doi: 10.1016/0022-3093(92)90052-L.

[45] K. S. Song and R. T. Williams, *Self-Trapped Excitons*, vol. 105, no. 9. 1993.

[46] E. Cartier, J. H. Stathis, and D. A. Buchanan, "Passivation and depassivation of silicon dangling bonds at the Si/SiO_2 interface by atomic hydrogen," *Appl. Phys. Lett.*, vol. 63, no. 11, pp. 1510–1512, 1993, doi: 10.1063/1.110758.

[47] M. S. El-Shall, S. Li, and T. Turkki, "Synthesis and Photoluminescence of Weblike Agglomeration of Silica Nanoparticles," *J. Phys. Chem.*, vol. 99, no. 51, pp. 17805–17809, 1995, doi: https://doi.org/10.1021/j100051a001.

[48] Y. D. Glinka, S. Lin, and Y. Chen, "The photoluminescence from hydrogen-related

species in composites of SiO_2 nanoparticles," *Appl. Phys. Lett.*, vol. 75, no. 6, pp. 778–780, 1999, doi: 10.1063/1.124510.

[49] J. Robertson, "Electronic Structure of Defects in Amorphous SiO_2," in *The Physics and Technology of Amorphous SiO_2*, R. A. B. Devine, Ed. Boston, MA: Springer US, 1988, pp. 91–101.

[50] H. Wang, A. Chroneos, C. A. Londos, E. N. Sgourou, and U. Schwingenschlögl, "Carbon related defects in irradiated silicon revisited," *Sci. Rep.*, vol. 4, no. 4909, pp. 1–9, 2014, doi: 10.1038/srep04909.

[51] G. D. Watkins, "Defects in irradiated silicon: EPR and electron-nuclear double resonance of interstitial boron," *Phys. Rev. B*, vol. 12, no. 12, pp. 5824–5839, 1975.

[52] P. Leary, R. Jones, and S. Öberg, "Interaction of hydrogen with substitutional and interstitial carbon defects in silicon," *Phys. Rev. B - Condens. Matter Mater. Phys.*, vol. 57, no. 7, pp. 3887–3899, 1998, doi: 10.1103/PhysRevB.57.3887.

[53] C. A. Londos, "Effect of oxygen on the migration of the carbon interstitial defect in silicon," *Phys. Rev. B*, vol. 37, no. 8, pp. 4175–4179, 1988, doi: https://doi.org/10.1103/PhysRevB.37.4175.

[54] K. P. O'Donnell, K. M. Lee, and G. D. Watkins, "Origin of the 0.97 eV luminescence in irradiated silicon," *Phys. B+C*, vol. 116, no. 1–3, pp. 258–263, 1983, doi: 10.1016/0378-4363(83)90256-5.

[55] E. Rotem, J. M. Shainline, and J. M. Xu, "Enhanced photoluminescence from nanopatterned carbon-rich silicon grown by solid-phase epitaxy," *Appl. Phys. Lett.*, vol. 91, no. 051127, pp. 1–3, 2007, doi: 10.1063/1.2766843.

[56] T. Kobayashi and Y. I. Matsushita, "Structure and energetics of carbon defects in SiC (0001)/SiO_2 systems at realistic temperatures: Defects in SiC, SiO_2, and at their interface," *J. Appl. Phys.*, vol. 126, no. 145302, pp. 1–8, 2019.

[57] N. Tajima *et al.*, "First-principles study on C=C defects near SiC/SiO_2 interface: Defect passivation by double-bond saturation," *Jpn. J. Appl. Phys.*, vol. 57, no. 04FR09, pp. 1–4, 2018, doi: 10.7567/JJAP.57.04FR09.

[58] F. Devynck, A. Alkauskas, P. Broqvist, and A. Pasquarello, "Charge transition levels of carbon-, oxygen-, and hydrogen-related defects at the SiC/SiO_2 interface through hybrid functionals," *Phys. Rev. B*, vol. 84, no. 23, pp. 1–18, 2011, doi: 10.1103/PhysRevB.84.235320.

[59] S. Wang *et al.*, "Bonding at the SiC-SiO_2 interface and the effects of nitrogen and hydrogen," *Phys. Rev. Lett.*, vol. 98, no. 026101, pp. 1–4, 2007, doi:

10.1103/PhysRevLett.98.026101.

[60] C. Lin, C. Zhang, and J. Lin, “Phase Transformation and Photoluminescence Properties of Nanocrystalline ZrO_2 Powders Prepared via the Pechini-type Sol−Gel Process,” *J. Phys. Chem. C*, vol. 111, no. 8, pp. 3300–3307, 2007.

[61] A. V. Vasin *et al.*, “The effect of deposition processing on structural and luminescent properties of a-SiOC:H thin films fabricated by RF-magnetron sputtering,” *J. Lumin.*, vol. 191, pp. 102–106, 2017, doi: 10.1016/j.jlumin.2016.10.029.

[62] Y. Matsumoto *et al.*, “Luminescence study of Si/SiC Nano-particles embedded in SiO_xC_y matrix deposited using O-Cat-CVD,” *Phys. E Low-dimensional Syst. Nanostructures*, vol. 111, no. March, pp. 179–184, 2019, doi: 10.1016/j.physe.2019.03.024.

[63] M. Jain, J. R. Ramos-Serrano, A. Dutt, and Y. Matsumoto, “Photoluminescence properties of thin-film SiO_xC_y deposited by O-Cat CVD technique using MMS and TEOS,” in *2020 17th International Conference on Electrical Engineering, Computing Science and Automatic Control (CCE). Mexico City, Mexico. November 11-13*, 2020, pp. 1–6, doi: 10.1109/cce50788.2020.9299113.

[64] V. Nikas *et al.*, “The origin of white luminescence from silicon oxycarbide thin films,” *Appl. Phys. Lett.*, vol. 061906, no. 104, pp. 1–5, 2014.

[65] A. Coyopol *et al.*, “Strong white light emission from SiC_xO_y films grown by HFCVD technique,” *Opt. Mater. (Amst).*, vol. 99, no. 109551, pp. 1–7, 2020, doi: 10.1016/j.optmat.2019.109551.

[66] R. B. Ellis, “Method of making electrically conducting glass and articles made therefrom,” United States Patent No.2556616, 1951.

[67] K. C. Liu, H. L. Cheng, J. R. Tsai, Y. L. Chiang, Y. C. Hsieh, and D. J. Jan, “Investigation of SiO_xC_y film as the encapsulation layer for full transparent OLED using hollow cathode discharge plasma at room temperature,” *Thin Solid Films*, vol. 518, no. 22, pp. 6195–6198, 2010, doi: 10.1016/j.tsf.2010.01.052.

[68] Y. Iwase, T. Fuchigami, Y. Horie, Y. Daiko, S. Honda, and Y. Iwamoto, “Formation and thermal behaviors of ternary silicon oxycarbides derived from silsesquioxane derivatives,” *Materials (Basel).*, vol. 12, no. 10, 2019, doi: 10.3390/MA12101721.

[69] S. H. Mir, L. A. Nagahara, T. Thundat, P. Mokarian-Tabari, H. Furukawa, and A. Khosla, “Review—Organic-Inorganic Hybrid Functional Materials: An Integrated Platform for Applied Technologies,” *J. Electrochem. Soc.*, vol. 165, no. 8, pp.

B3137–B3156, 2018, doi: 10.1149/2.0191808jes.

[70] U. Díaz and A. Corma, "Organic-Inorganic Hybrid Materials: Multi-functional Solids for Multi-step Reaction processes," *Chem. - A Eur. J.*, vol. 24, no. 16, pp. 3944–3958, 2018, doi: 10.1002/chem.201704185.

[71] J. Zhou, X. Zheng, Z. Shi, B. Zhao, F. Liu, and Y. Li, "Structure and photoluminescent properties of SiCO thin-films doped with Al prepared by dual magnetron sputtering," *Int. J. Mod. Phys. B*, vol. 25, no. 16, pp. 2149–2156, 2011, doi: 10.1142/S0217979211100278.

[72] S. L. Shevchuk and Y. P. Maishev, "Silicon oxycarbide thin films deposited from viniltrimethoxysilane ion beams," *Thin Solid Films*, vol. 492, no. 1–2, pp. 114–117, 2005, doi: 10.1016/j.tsf.2005.06.086.

[73] G. R. Lin, Y. H. Pai, C. T. Lin, and C. C. Chen, "Comparison on the electroluminescence of Si-rich SiN_x and SiO_x based light-emitting diodes," *Appl. Phys. Lett.*, vol. 96, no. 263514, 2010, doi: 10.1063/1.3459144.

[74] A. Dutt, Y. Matsumoto, S. Godavarthi, G. Santana-Rodríguez, J. Santoyo-Salazar, and A. Escobosa, "White bright luminescence at room temperature from TEOS-based thin films via catalytic chemical vapor deposition," *Mater. Lett.*, vol. 131, pp. 295–297, 2014, doi: 10.1016/j.matlet.2014.05.206.

[75] J. R. Ramos-Serrano, Y. Matsumoto, A. Méndez-Blas, A. Dutt, C. Morales, and A. I. Oliva, "Luminescent silicon oxycarbide thin films obtained with monomethyl-silane by hot-wire chemical vapor deposition," *J. Alloys Compd.*, vol. 780, pp. 341–346, 2019, doi: 10.1016/j.jallcom.2018.11.353.

[76] B. H. Kim, C. H. Cho, T. W. Kim, N. M. Park, G. Y. Sung, and S. J. Park, "Photo-Luminescence of silicon quantum dots in silicon nitride grown by NH_3 and SiH_4," *Appl. Phys. Lett.*, vol. 86, no. 9, pp. 1–3, 2005, doi: 10.1063/1.1872211.

[77] M. Jain, J. R. Ramos-Serrano, A. Dutt, and Y. Matsumoto, "The influence of deposition time on the photoluminescent properties of SiO_xC_y thin films obtained by Cat-CVD from monomethyl silane precursor," *Mater. Lett.*, vol. 291, p. 129547, 2021, doi: 10.1016/j.matlet.2021.129547.

[78] F. Roth, C. Schmerbauch, E. Ionescu, N. Nicoloso, O. Guillon, and R. Riedel, "High-temperature piezoresistive C / SiOC sensors," *J. Sensors Sens. Syst.*, vol. 4, no. 1, pp. 133–136, 2015, doi: 10.5194/jsss-4-133-2015.

[79] R. Riedel, L. Toma, E. Janssen, J. Nuffer, T. Melz, and H. Hanselka, "Piezoresistive effect in SiOC ceramics for integrated pressure sensors," *J. Am. Ceram. Soc.*, vol.

93, no. 4, pp. 920–924, 2010, doi: 10.1111/j.1551-2916.2009.03496.x.

[80] V. S. Pradeep, M. Graczyk-zajac, R. Riedel, and G. D. Sorarù, “New Insights in to the Lithium Storage Mechanism in Polymer Derived SiOC Anode Materials,” *Electrochim. Acta*, vol. 119, pp. 78–85, 2014, doi: 10.1016/j.electacta.2013.12.037.

[81] C. Chandra and J. Kim, “Silicon oxycarbide produced from silicone oil for high-performance anode material in sodium ion batteries,” *Chem. Eng. J.*, vol. 338, no. December 2017, pp. 126–136, 2018, doi: 10.1016/j.cej.2018.01.032.

[82] J. Huang *et al.*, “An interfacial crosslinking strategy to fabricate an ultrathin two-dimensional composite of silicon oxycarbide-enwrapped silicon nanoparticles for high-performance lithium storage,” *J. Mater. Chem. A*, vol. 7, no. 40, pp. 22950–22957, 2019, doi: 10.1039/c9ta07738c.

[83] M. Nakaya, K. Kodama, S. Yasuhara, and A. Hotta, “Novel Gas Barrier SiOC Coating to PET Bottles through a Hot Wire CVD Method,” *J. Polym.*, vol. 2016, no. 4657193, pp. 1–7, 2016, doi: https://doi.org/10.1155/2016/4657193.

[84] M. Nakaya, S. Yasuhara, T. Maeda, and A. Hotta, “Impact of hot wire and material gas species on the Cat-CVD coating of gas barrier SiOC thin films onto PET bottles,” *Surf. Coat. Technol.*, vol. 344, no. February, pp. 21–29, 2018, doi: 10.1016/j.surfcoat.2018.02.101.

[85] M. Arango-Ospina, F. Xie, I. Gonzalo-juan, R. Riedel, E. Ionescu, and A. R. Boccaccini, “Review : Silicon oxycarbide based materials for biomedical applications,” *Appl. Mater. Today*, vol. 18, p. 100482, 2020, doi: 10.1016/j.apmt.2019.100482.

[86] A. Tamayo, R. Ruiz-Caro, A. Mazo, M. D. Veiga-Ochoa, and J. Rubio, “Chemical oxidation of silicon oxycarbide ceramics for advanced drug delivery systems,” *J. Mater. Sci.*, vol. 51, no. 3, pp. 1382–1391, 2016, doi: 10.1007/s10853-015-9457-3.

[87] P. Lagonegro *et al.*, “A cytotoxicity study of silicon oxycarbide nanowires as cell scaffold for biomedical applications,” *Mater. Sci. Eng. C*, vol. 73, pp. 465–471, 2017, doi: 10.1016/j.msec.2016.12.096.

[88] L. G. Britton, “Combustion hazards of silane and its chlorides,” *Plant/operations Prog.*, vol. 9, no. 1, pp. 16–38, 1990, doi: 10.1002/prsb.720090107.

[89] F. Tamanini, J. L. Chaffee, and R. L. Jambor, “Reactivity and Ignition Characteristics of Silane/Air Mixtures,” *Process Saf. Prog.*, vol. 17, no. 4, pp. 243–258, 1998, doi: 10.1002/prs.680170405.

CHAPTER 2
EXPERIMENTAL AND CHARACTERIZATION TECHNIQUES

2.1. Introduction

This chapter describes the experimental and characterization techniques used for reaching the objectives of the thesis as defined in the previous chapter. Primarily the chapter has been divided into two major sections.

The focus of the first section of this chapter is to understand the details of deposition technique and precursor used in our laboratory, i.e., Organic Catalytic Chemical Vapor Deposition (O-Cat-CVD) technique and organometallic precursors, respectively. Here, the growth mechanism of thin films will be discussed. On the other hand, the focus of the second section of this chapter is to understand the various characterization techniques used for the analysis of the SiO_xC_y thin films.

2.2. History of synthesis techniques of silicon oxycarbide (SiO_xC_y)

Before the description of the deposition technique and the precursor used in our laboratory, it will be worth mentioning about the history of the synthesis of SiO_xC_y thin films. The first synthesis of silicon oxycarbide (SiO_xC_y) was performed by R. B. Ellis in 1951, where the author incorporated carbon into porous silica [1]. Although different studies took place related to mechanical and chemical properties of SiO_xC_y after its first synthesis by using oxidation, sol-gel, etc., techniques [2]–[9], the study of the Photo-Luminescence on SiO_xC_y matrix started after 1990s, when L. T. Canham proposed the Photo-Luminescence from porous silicon [10]. S. Hayashi et al., prepared a composite film of SiO_2 and carbon by using rf co-sputtering technique in 1993 [11], [12] and discussed the role of carbon cluster for PL. Many other research groups have also used the same rf co-sputtering technique for obtaining PL properties from SiO_xC_y matrix [13]–[18] where they have used the targets of

SiC, SiO_2 or Carbon to obtain the SiO_xC_y thin film. Likewise, B. Garrido et al., used ion implantation to incorporate Si and C in amorphous SiO_2 [19]–[21]. Furthermore, different types of chemical vapor deposition (CVD) techniques such as Hot-Wire CVD (HWCVD) [22]–[28], Plasma-Enhanced CVD (PECVD) [29], [30], Thermal CVD (TCVD) [31]–[33] were also used to synthesize SiO_xC_y thin films to obtain PL properties. Silane was used as the main precursor in the PECVD technique [29], [30], while different types of organo-metallic materials, such as tetra-ethyl orthosilicat(TEOS), monomethyl silane (MMS), and 2,4,6-trimethyl-2,4,6-trisila-heptane ($C_7H_{22}Si_3$) were used in HWCVD and TCVD techniques, respectively, [22]–[28], [31]–[33]. Besides, white luminescence was also observed in the sol-gel derived thin film [34]. It is worth mentioning that the pyrolysis technique was extensively used for the other application of SiO_xC_y matrix, such as in biomedical applications [35], anode material for storage batteries [36], [37], and piezoresistive sensors [38], [39], etc.

Table 2.1 SiO_xC_y matrix: methods of preparation, precursors, Photo-Luminescence (PL) emission band, and related mechanism of PL emission.

Synthesis Method	Precursors	PL (eV)	Properties	Reference
RF Sputtering	SiO_2 + C plates	2.20	Carbon clusters (~2nm) comparable or smaller than C_{60}	[11], [12]
Magnetron co-sputtering	Suprasil + Graphite chips	1.80 - 2.20	C-related defects, a-Si:O:C regions, and carbon clusters in a-SiO_2:C	[15]
Ion- implantation	$SiO_2 + Si^+ + C^+$	1.40 - 1.60, 2.00 - 2.20 and 2.70	Formation of silicon nano-crystals (1.4-1.6 eV), carbon amorphous clusters (2.0-2.2 eV), and SiC clustering (2.7 eV)	[19]–[21]
Ion- implantation	$SiO_2 + Si^+ + C^+$	1.90, 2.50, and 2.70	Formation of Si nanocrystals (1.9 eV), SiC and/or a complex of Si, O, and C (2.5 and 2.7 eV)	[40]
Ion- implantation	$SiO_2 + C^+$	2.53	Amorphous carbon clusters	[41]
Ion- implantation	$SiO_2 + Si^+ + C^+$	2.10 and 2.70	Amorphous carbon clusters (2.1 eV) and $Si_yC_{1-y}O_x$ complexes ($x < 2$) (2.7 eV)	[42]
RF co-sputtering	SiO_2 + C plates	2.27, 2.54	C-rich clusters (2.27 eV) and SiC nanocrystals luminescence centers (2.54 eV)	[14]
RF co-sputtering	SiO_2 + SiC	2.70	Defects in SiO_2 at the SiC/SiO_2	[13]

			interface: Twofold coordinated silicon defect (i.e., O–Si–C–O– and –O–Si–O–) and Neutral oxygen vacancy (NOV) defect	
ECR PECVD	$SiH_4 + O_2 + CH_4$	2.46	Carbon-incorporated Si nanoclusters	[29]
Thermal carbonization/oxidation of porous silicon	Porous Si + (N_2/C_2H_2) + wet argon	2.50	Carbon bonding state and Carbon-based clusters in a silicon oxide matrix	[43]–[47]
Pyrolysis process by sol–gel method	SiO_2 + triethoxysilane and methyldiethoxysilane	2.00 and 2.21	The presence of a low amount of free C and SiC (2.21 eV) and presence of Si, C and SiC in the film (2 eV)	[34]
Atmospheric pressure VHF microplasma jet	TEOS-Ar	2.70	NOV defects	[48]
Thermal chemical vapor deposition (TCVD)	2,4,6-trimethyl-2,4,6-trisila-heptane ($C_7H_{22}Si_3$) + O_2	2.13	Carbon related oxygen defect centers (CODCs) and electronic transitions of Si-C/Si-O-C bond	[31], [32]
RF-magnetron sputtering technique	$SiC + O_2 + Ar$	2.64, 3.22 and 3.78.	The oxygen deficiency centers (3.78 eV), Si-O_x related defects (3.22 eV) and surface defects of 6H SiC nano-crystal particles (2.64 eV)	[17], [18]
Catalyst-assisted process	$SiO_2 + CH_4$	2.34 and 3.26	Oxygen deficiency center (ODC) in SiO_2 shell (3.26 eV) and Quantum confinement effect (QCE) in β-SiC nanowires (2.34 eV)	[49], [50]
VHF-PECVD	$SiH_4 + CH_4 + O_2$	1.68, 2.13 and 2.70	Si-related NOV Defect (2.7 eV), Si-C related defect state (2.13 eV) and silicon dangling bond (DB) defects (1.68 eV)	[51]–[53]
Molten salt mediated carbothermal reduction (CR) route	Silica fume and sucrose	2.93	Quantum size effect due to SiC NWs	[54]
Hot –wire CVD (HWCVD)	Monomethyl-silane (MMS) + O_2	2.21, 2.70 and 2.95	Combination of different defects and quantum confinement effects in the SiOC matrix	[23], [26], [28]
Cat-CVD	TEOS + Ar	2.48, 2.21, 2.70 and	Formation of Si and SiC-based nano-crystals (2.48 and 2.21 eV)	[22], [24]–[26]

		2.95 -3.26	and Defects with H and C related bonds and ODC defects (3.26-2.95 and 2.7 eV)	
Hot filament chemical vapor deposition technique (HFCVD)	Ethanol + SiO_2 + H_2	2.70 - 2.80	Si related defects such NOVs and ODCs	[27]
RF-magnetron sputtering	Si or SiC target + O_2 + CH_4 + Ar	2.50	Formation of light-emitting centers in SiOx and amorphous carbon nanoclusters	[16], [55]
Cat-CVD	Mesoporous silica pellets and TEOS	2.95-3.26	Quantum confinement effects due to Si-C/Si–O–C bonding groups	[56]
Chemical treatment	Fumed silica + Tetramethoxysilane [$Si(OCH_3)_4$]	2.50	Carbon precipitates (nanodots)	[57]

2.3. Organic Catalytic Chemical Vapor Deposition (O-Cat-CVD)

Organic Catalytic Chemical Vapor Deposition (O-Cat-CVD) is a CVD technique which is also known as Hot-Wire CVD technique [58]. This instrument was ingeniously designed in the SEES, Electrical Engineering Department, CINVESTAV and successfully established since 2001.

The first use of the catalytic process in the CVD technique was mentioned in 1970 by S. Yamazaki et. al. [59]. In this work, a catalyst was inserted in a conventional Thermal CVD apparatus to improve the quality of silicon nitride film at low deposition temperature, however, results were not promising enough in comparison to simple TCVD process. Later in 1979, the fabrication of hydrogenated amorphous silicon (a-Si:H) films was reported by Wiesmann et. al., from silane gas and by using Tungsten (W) wires or carbon (C) rods at higher temperature [60]. However, the quality of the films was not good enough because of the deposition at low pressure. The research was stagnated in this field after these discouraging results, until the demonstration of high-quality hydrofluorinated amorphous silicon (a-Si:F:H) films using silicon tetrafluoride (SiF_4) and hydrogen (H_2) as gas precursors from the group of H. Matsumura [61], [62]. This was the first time when they claimed this process as Catalytic CVD (Cat-CVD) because they found the catalytic nature by the reaction of hydrogen with heated tungsten filament [62]. These results encouraged

the researchers in this field once again and high-quality amorphous silicon (a-Si) was obtained by Doyle et. al. [63], with few slight changes in the deposition conditions from those of Matsumura and this process was termed as Evaporative Surface Decomposition (ESD) by them. In 1991, Mahan et. al., formally introduced the term "Hot Wire Chemical Vapor Deposition" (HWCVD) [64], where better film quality of a- Si were studied from HWCVD in comparison to the films obtained from PECVD. This research group's work led a lot of growth in the field of HWCVD research in comparison to the work of the past two decades. Later, T. Hata et. al., used metal-organic precursors in this Cat-CVD and termed it as Organic Catalytic CVD in 2007 [58].

2.3.1. Structure of O-Cat-CVD

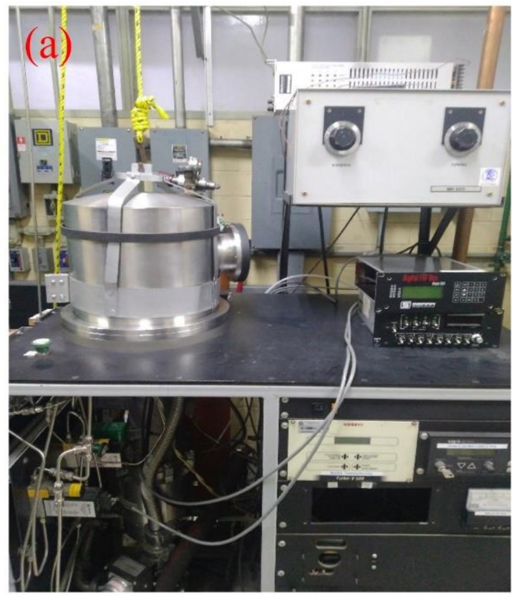

Fig. 2.1 O-Cat-CVD systems present in Electrical Engineering Department of CINVESTAV.

In this thesis work, two different Organic Catalytic Chemical Vapor Deposition (O-Cat-CVD) systems were used to deposit SiO_xC_y thin films; these systems are shown in Fig. 2.1. These both systems mainly are constituted by a reaction chamber with a window, vacuum pumps, i.e., turbo-molecular and mechanical pumps. Control systems for mass flow and filament temperature are also presented. Here, one of the systems is used for gaseous precursors such as monomethyl Silane (MMS) (Sigma Aldrich-462993- purity 99.9%) and Vinyl Silane (Gelest-7291-09-0) where Oxygen (O_2), and Hydrogen (H_2) were also used as reactant gases (Fig. 2-1a). While the other system (Fig. 2-1b), was used for liquid

precursors such as Tetraethyl orthosilcate (TEOS) (Sigma-Aldrich, reagent grade, 98%) where argon gas was used as a carrier gas. Filaments of tantalum (T_a) wire with a diameter of 0.5 mm and tungsten (W) wire with a diameter of 0.75 mm are used for the catalytic process for gaseous and liquid precursor systems, respectively. The distance from the substrate to the catalyst filament is 5 cm for both systems and the temperature of the filament is measured by using the infrared (IR) detector (Chino model IR-AHS) through the window of the corresponding chamber during the deposition period.

2.3.2. Growth mechanism of thin films

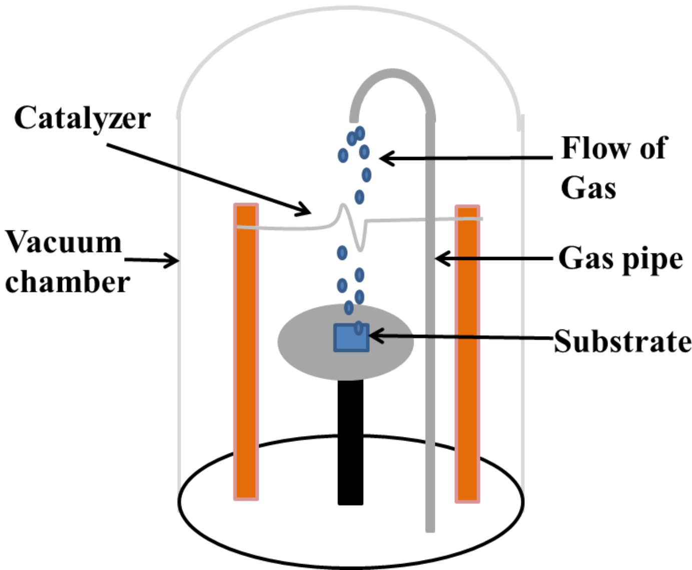

Fig. 2.2 Schematic illustration of O-Cat-CVD deposition chamber.

Typically, the process of O-Cat-CVD is quite simple and straightforward. The precursor is introduced into the vacuum chamber. In our case, TEOS liquid precursor and MMS and Vinyl Silane gas precursors were used in the chamber. Here, an incandescent filament (i.e. tungsten or tantalum) is resistively heated up to higher temperatures (around at 1600ºC-2000ºC). This high temperature of the hot filament catalytically affects the molecules of the precursor materials and dissociates them. Subsequently, mainly reactive radicals are released from the surface of filament and some of these reactive radicals can reach the substrate directly after their release from the filament without any collisions. On the other hand, some of the other radicals may give rise to secondary gas phase reactions between the filament and substrate, where they may react with other generated radicals or parent molecules due to the collisions. Finally, there will be a nucleation and adsorption of these

radicals on the surface of the substrate, with which the deposition of the films is generated where the radicals resulting from the collisions may affect the properties of the growing film. There are different parameters on which the quality and properties of the material depend, such as: precursor gases, gas flows, filament temperature, substrate temperature, substrate-filament distance, chamber pressure and deposition times. A schematic diagram of the system is presented in Fig. 2.2.

2.3.3. Advantages of O-Cat-CVD

The O-Cat-CVD configuration has proven more advantages over other CVD configurations. First of all in this technique, only molecules (radicals) and neutral atoms are presented in the gas phase, due to which the surface of the films doesn't suffer from the charge-induced damage or plasma damage, in comparison to PECVD [65]. This advantage is effective for depositing passivation films in compound semiconductors or organic devices. The deposition of thin films with high deposition rate without deteriorating their quality is also another advantage over PECVD method. Further advantage is the ease of increasing the deposition area by simply increasing the area covered by the filament, making this technique easily adjustable on an industrial scale [66]. Additionally, as it is a cold-wall system, low substrate temperature can be easily used in this method. Meanwhile, the radiation from the heated filament doesn't affect the substrate temperature when there is a distance above 1 cm between filament and substate. Subsequently, this technique makes possible to deposit the thin films practically on any type of substrates and making it ideal for the development of technologies on flexible substrates [67]. Finally, the low cost of O-Cat-CVD system and the possibility to use gaseous, liquid and even solid precursors with this technique allows obtaining a wide range of materials [22], [28], [58], [61].

2.4. Metal-organic compounds as an alternative precursor

Silane is one of the most used precursors used to obtain silicon related materials since the beginning of the semiconductor industry from 1960s. But lately, a lot of research groups started to look for an alternative to silane-gas, because of the occurrence of numerous accidents in the past. As it is well known that silane is a pyrophoric gas and due to its

lower auto ignition temperature (<18 °C), it can ignite spontaneously in contact with air [68], [69]. The following Table 2.2 shows the autoignition temperatures for different gases.

It is known that in the last two decades, the number of victims and damages in accidents related to silane gas is greater than those related to all other gases used in the electronics industry together, such as arsine, phosphine, hydrogen, etc. This raises the need to search for alternative precursors allowing the development of silicon-based technologies and reducing risks significantly.

Table 2.2 Autoignition temperatures for different gases.

Gas	Auto ignition Temperature (°C)
Silane	<18
Disilane	-70
Dichlorosilane	136
Monomethylsilane (MMS)	160
Tetraethyl orthosilicate (TEOS)	260
Hydrogen	400
Methane	537

Alkylsilane compounds are safer precursor sources than silane.

Dichlorosilane and trichlorosilane were one of the first precursors which were used as an alternative to Silane to produce silicon-based films because of their high autoignition temperatures (100°C) [70]. These precursors contain the chlorine which may favor the formation of nanocrystals [71] but it also forms the HCl as a byproduct which is highly corrosive and represents a potential damage to the deposited film, as well as in the deposition system [72].

Furthermore, metal-organic compounds are also arising as another alternative of silane gas, which allows to obtain a wide variety of functional carbon-based materials, such as carbides-metals, carbon-doped metal oxides, metal nitrides doped with carbon and so on. These types of metals can be classified as organic-inorganic hybrid materials. It is noteworthy that mechanical strength, thermal stability, and chemical properties depend on the inorganic component of the material, while hydrophobicity, plasticity, and solubility

properties depend on the organic components of the material [73]–[75]. Due to these attractive properties, metal-organic compounds such as monomethyl silane [MMS; (CH_3-SiH_3)], Vinyl Silane [VS; ($H_2C{=}CHSiH_3$)] and tetra-ethyl orthosilicate [TEOS; ($Si(OC_2H_5)_4$)], are presented as noteworthy alternatives for obtaining silicon/carbon based materials. Fig. 2.3 presents the molecular structure of these precursors.

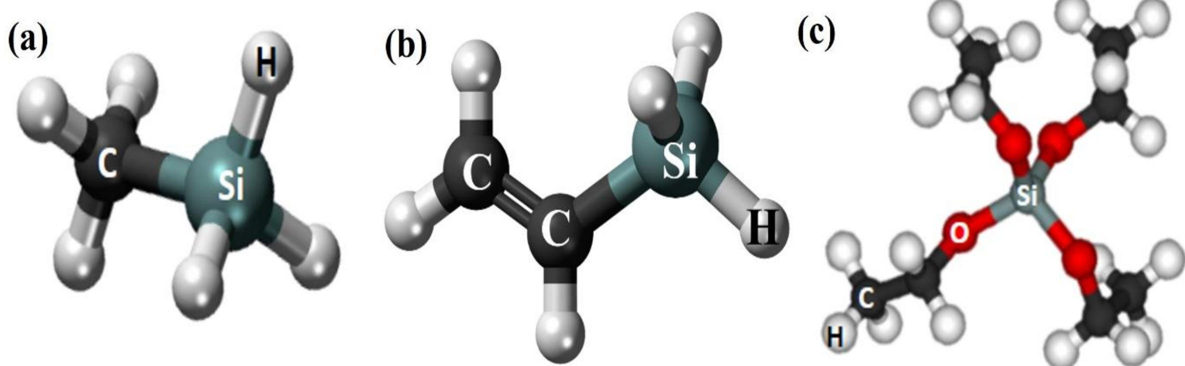

Fig. 2.3 Schematic diagrams of the molecules of (a) Monomethyl Silane (MMS), (b) Vinyl Silane and (c) Tetraethyl Orthosilicate (TEOS).

From Fig. 2.3, it is shown that the molecular structure of MMS and vinyl silane are smaller than TEOS, so it is easy to dissociate the complete molecule of MMS and vinyl silane during the deposition at higher temperatures. On the other hand in regard with the molecule of TEOS, the silicon atom is inherently bounded with four oxygen atoms, while ethyl radicals are attached with these oxygen atoms due to which these ethyl radicals dissociates initially from the TEOS molecule [76], [77]. These dissociation processes of different molecules allow us to get the different kind of SiO_xC_y thin films which may help us to obtain a good comparative thin film for our application.

2.5. Material characterization techniques

In this section, some of the experimental techniques are explained briefly which were used to understand the properties of the deposited thin films. It comprises structural, morphological and optical characterization techniques. Here, Fourier Transform Infrared Spectroscopy (FTIR) and X-ray Photoelectron Spectroscopy (XPS) were used to visualize the elemental properties, while Transmission Electron Microscopy at High Resolution (HR-TEM) were used to understand the morphological properties of the thin film. Additionally, Photo-Luminescence (PL) spectroscopy, Time Resolved Photo-

Luminescence (TRPL) spectroscopy and ellipsometry were also used to understand the optical properties of deposited thin films. Moreover, current-voltage (I-V) characterization and external quantum efficiency (EQE) characterization was also performed to understand the characteristics of solar cells with and without the deposition of SiO_xC_y thin films.

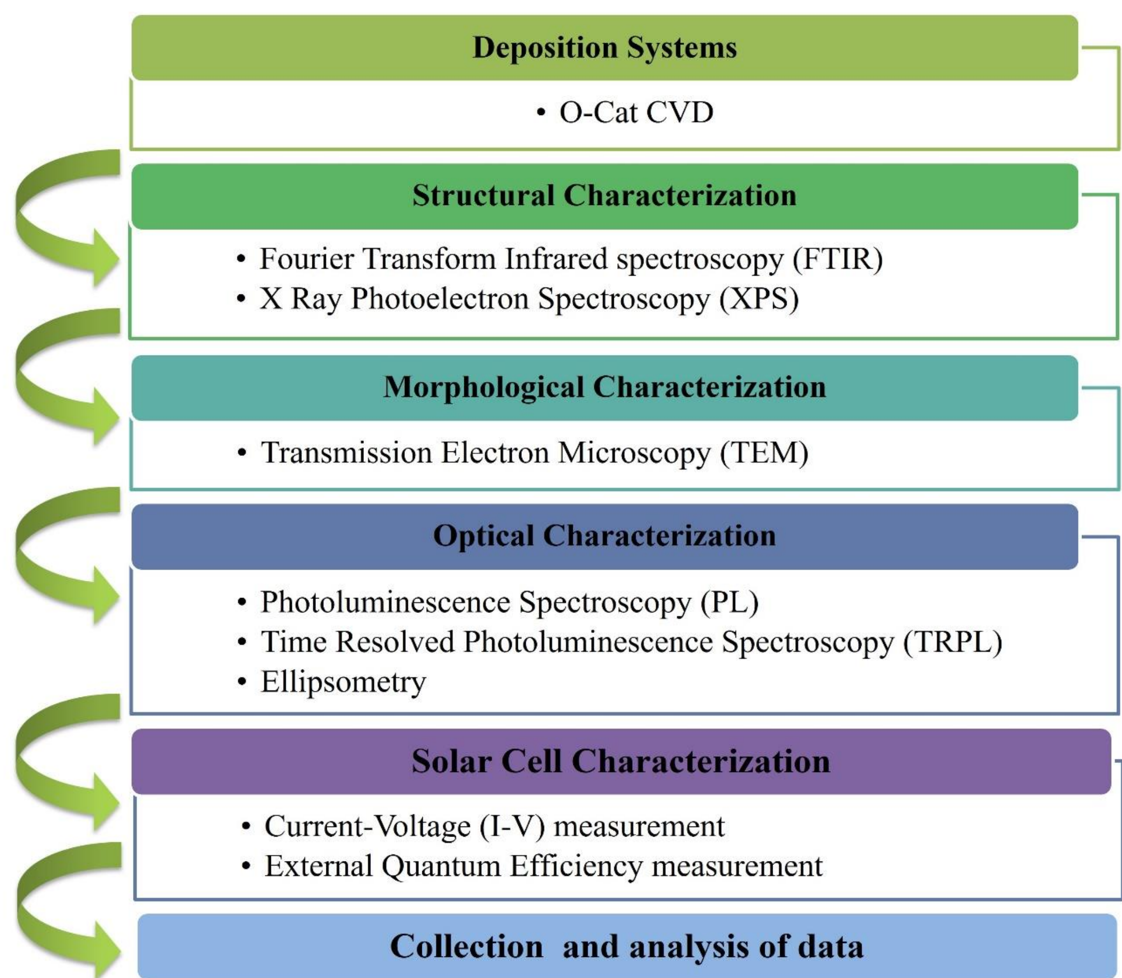

Fig. 2.4 Flow chart of used characterization techniques.

2.5.1. Fourier Transform Infrared Spectroscopy (FTIR)

Fourier Transform Infrared Spectroscopy (FTIR) is a well-recognized non-destructive method to understand the different bonding states of many materials and it overcome the limitations of dispersive instruments. The infrared spectrum represents the fingerprint of a sample because two different compounds do not give rise to the same absorption spectrum. It provides the information about the absorption peaks corresponding to the vibration frequencies of the atoms that make up a molecule which helps in the positive identification

of each different material. The intensity of the peak of any bonding in the spectrum directly corresponds to the presence of that bonding in the material. Here, Fig. 2.5 (a) shows the FTIR instrument (Nicolet 560) which was used for the analysis of bonding and is placed at IIM-UNAM, Mexico while Fig. 2.5 (b) shows a schematic block diagram of FTIR to understand the working principle.

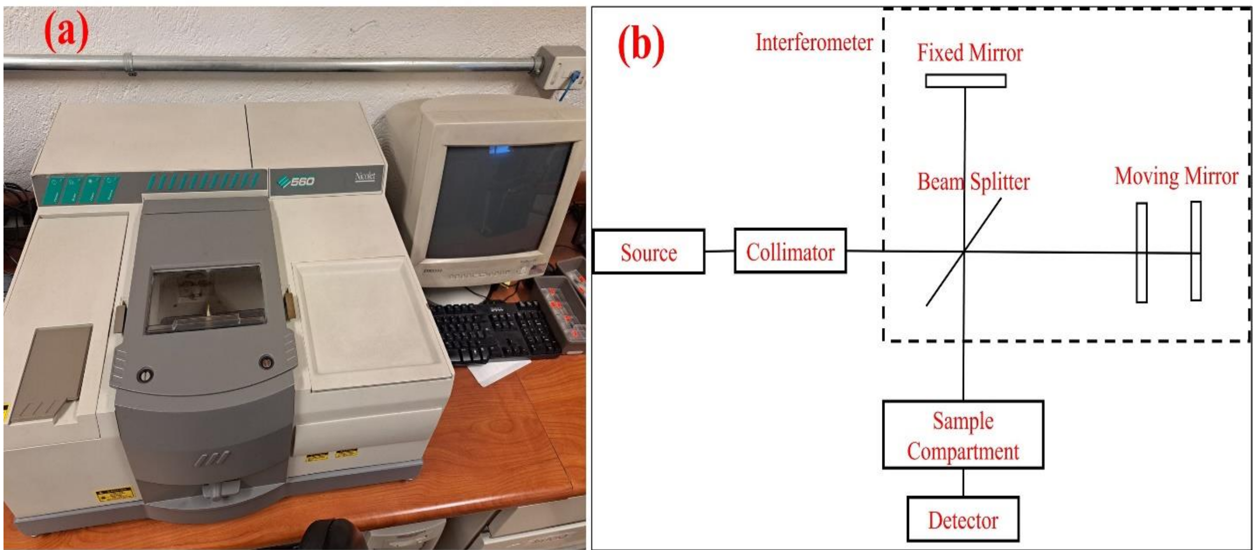

Fig. 2.5 (a) Photo of FTIR spectroscopy (Nicolet 560) in IIM-UNAM, and (b) Schematic block diagram of FTIR spectroscopy.

The FTIR instrument contains an infrared (IR) source and the generated beam pass through the collimator which supports IR beams to obtain the uniform directionality. Now, this output from the collimator passes through the interferometer which comprises a beam splitter, a fixed mirror and a moving mirror. A beam splitter is arranged at 45° to the incident beam direction and the fixed mirror is situated in the perpendicular direction of it and the moving mirror is placed in the direction of the beam. When the beam goes out from the collimator, it goes through the beam splitter; then this beam is partitioned into two beams in which one beam reflects towards the flat mirror while the other is directed to the moving mirror which move this mirror with a very short distance. This arrangement of components allows getting the precise values of frequencies reading the different positions of moving mirror. This range of frequencies now passes through the sample compartment and then they are perceived by the detector. Now, a time varying signal is produced by the detector which corresponds to the transmittance of the sample for distinct frequencies and Fourier transformation is used to convert these time signals into a frequency output.

2.5.2. X-Ray Photoelectron Spectroscopy (XPS)

X-ray Photoelectron Spectroscopy (XPS) is a surface analysis technique which was developed by Dr. Kai Siegbahn in mid-1960 and he was also awarded with a Nobel Prize in 1981. XPS was also termed as Electron Spectroscopy for Chemical Analysis (ESCA) because it is used to study the chemical composition of surfaces. This technique is based on the principle of photo-electric effect. In this effect, a photon of high energy (X-ray in this case) is absorbed by an electron of the atom and gets ejected. The kinetic energy of this ejected electron can give enough information for atom identification.

In this work, a XPS microprobe PHI 5000 VersaProbe II spectrometer was used with a monochromatic Al X-ray source and an excitation line at 1486.6 eV. This instrument is placed at IIM-UNAM. XPS data was analyzed by using Spectral Data Processor (SDP) v4.1 (32-bit version) software, where the peak-fit of the data was obtained by Shirley-type baseline. The use of this instrument was funded by CONACyT project no. 299703. A schematic block diagram of XPS instrument is shown in Fig. 2.6.

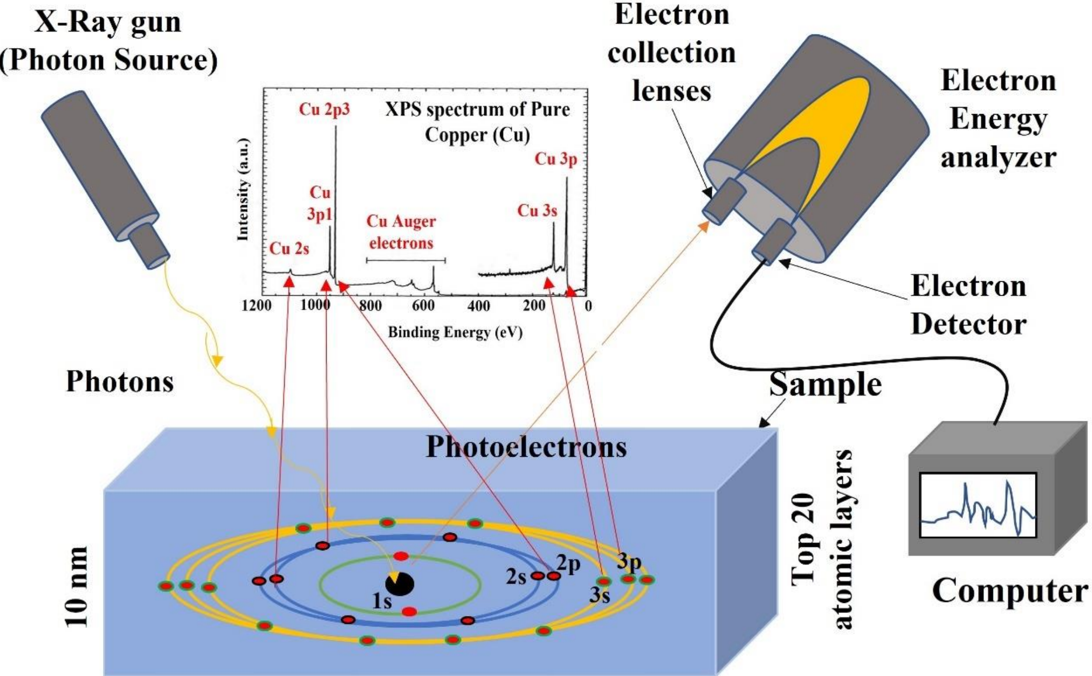

Fig. 2.6 Illustration of X-ray Photoelectron Spectroscopy (XPS) instrument.

Normally, an XPS instrument has a source of photons or a X-ray gun with a target of aluminum (Al) or Magnesium (Mg) and a suitable filter. When these X-rays impact the

sample, then photoelectrons generate with a certain kinetic energy as explained by the photoelectric effect. Next, the electron energy analyzer identifies the electrons with different energy by employing the electrostatic and magnetic fields. Finally, a detector is used to detect these signals and provide the corresponding output.

2.5.3. High-Resolution Transmission Electron Microscopy (HR-TEM)

Transmission Electron Microscopy (TEM) is a very important technique to analyze the crystallographic structure, morphology, defects, particle size, etc., by using a beam of high energy electrons which transmits through an ultra-thin specimen. This high energy electron beam provides an image with a resolution at the atomic scale, where the analysis of a microstructure becomes easy. This technique overcomes the limitations of optical microscope which is regulated by the wavelength of light. This technique (TEM) uses electrons as the source, where these electrons are accelerated at several hundreds of keVs, due to which these electrons have a shorter wavelength than light. For instance, if an energy of 200 keV is used in a TEM, then the wavelength of electrons will be around 0.025 Å, which provides a thousand times better resolution than in case of the optical microscope. However, the inherent aberration in electromagnetic lenses also limits the resolution of TEM. This technique is widely used in physical and biological sciences as an analysis method, including the field of semiconductors, material science, virology, etc., where different operational modes such as bright field, dark field and lattice mode are used to get the image.

In our work, we have used HR-TEM (JEOL-JEM-2010) as shown in Fig. 2.7 (a) which is also situated at LUME of IIM-UNAM. An accelerated energy of 200 keV and a camera distance of 20 cm were used to obtain a bright field mode image of the deposited samples. In this work, samples were prepared by simply scraping on the surface of the thin film. Fig. 2.7 (b) shows the block diagram of the HR-TEM system used, which explains its working principle. Here, the accelerated beam of electrons is produced by an electron gun or cathode. The higher accelerated voltage provides higher power of resolution. Then, this beam of electrons passes through an anode and then the beam of electrons flow in an analogous way like a beam of light does in an optical microscope. Here, an electromagnetic field is generated by electronic coils in the lens-system. Firstly, the beam

is focused by the condenser lenses and passes through the sample. Here, the beam deflects partially and the degree of deflection varies according to the electron density of the sample. Next, the objective aperture lens collects these scattered electrons and an image is registered, which is enlarged by the projector lenses. Finally, an image can be visible on an imaging device, such as a fluorescent screen or a sensor such as a CCD camera.

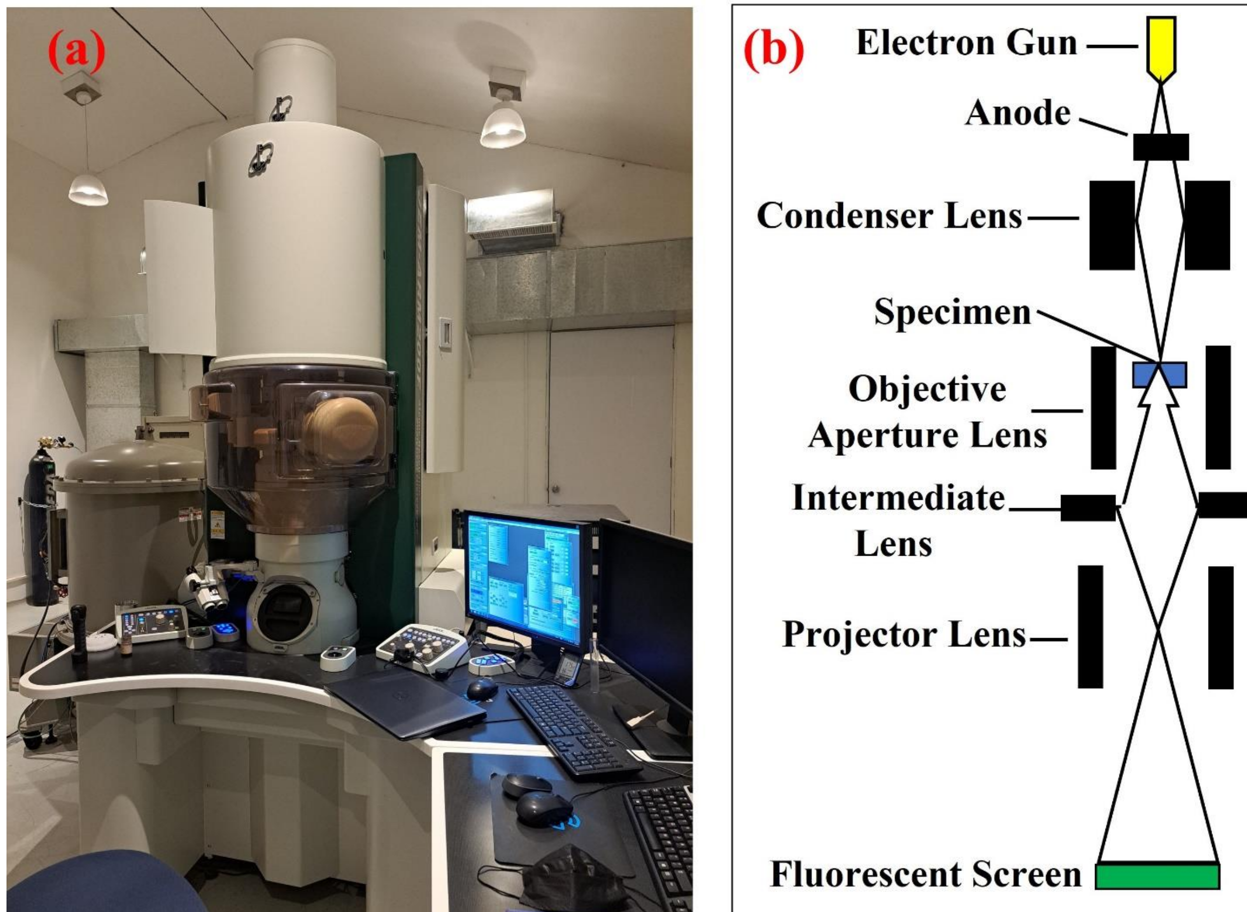

Fig. 2.7 (a) Photo of HR-TEM (JEOL-JEM-2010) in IIM-UNAM, and (b) Schematic block diagram of HR-TEM.

2.5.4. Photo-Luminescence (PL) Spectroscopy

Photo-Luminescence (PL) spectroscopy is one of the non-destructive, contactless and powerful optical techniques that allows investigation of the luminescence by using the source of photons. This technique provides the optical properties of any material where different excitation energies and intensities can be chosen to explore and investigate the material. The obtained emission spectrum and its intensity can be used to identify various important material properties such as impurity levels, roughness of the interface and

surface, etc. Additionally, the process of Photo-Luminescence is already explained in chapter 1 in detail including for direct and indirect materials.

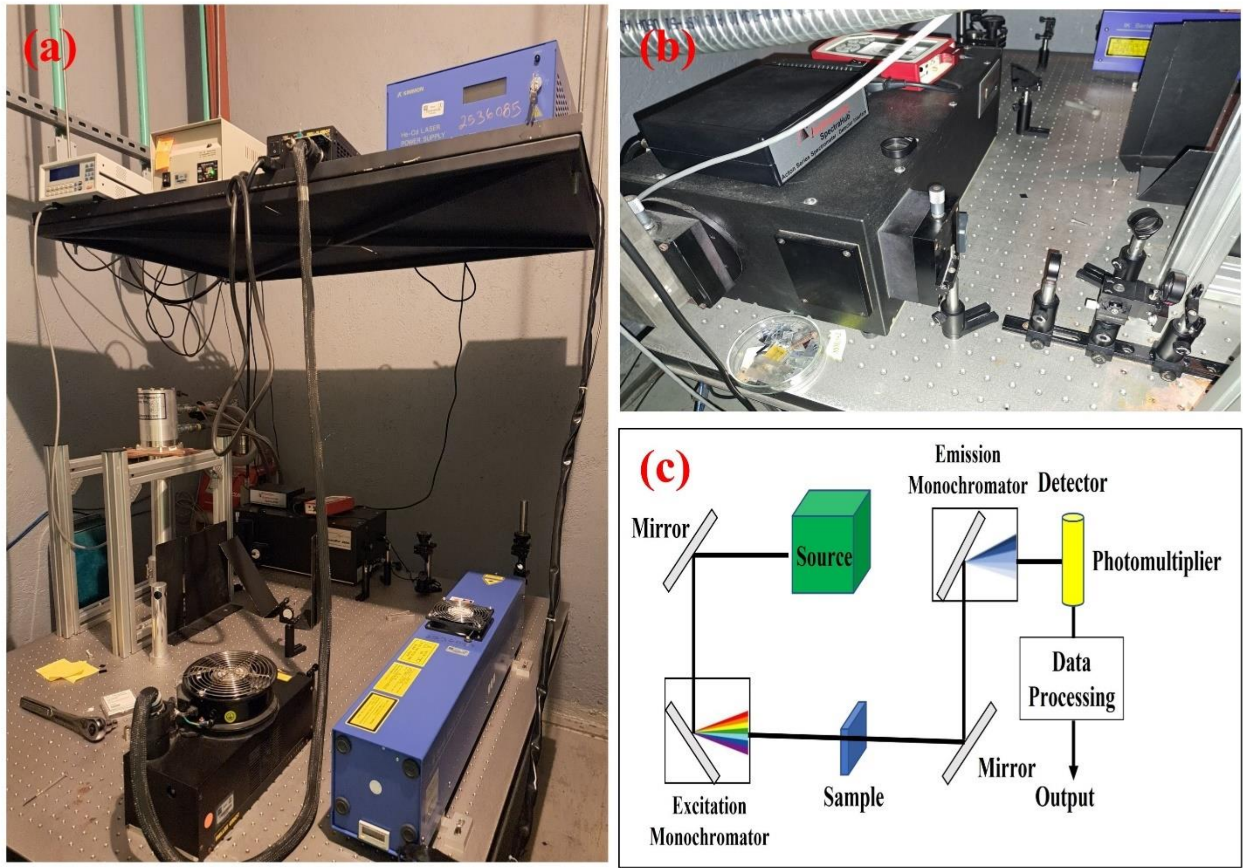

Fig. 2.8 (a-b) Photo of Photo-Luminescence (PL) spectroscopy placed in IIM-UNAM, and (c) Schematic block diagram of PL spectroscopy.

Photo-Luminescence Excitation Spectra (PLE) and Time-Resolved Photo-Luminescence (TRPL) spectra were analyzed by a Photo-Luminescence (HORIBA-Nanolog kit) equipment. Normally, these spectra are used to analyze additional information about the PL emission, e.g., the origin of PL emission. PLE spectra are almost obtained the same as PL is done, but there is a supplementary element altering the excitation wavelength of the laser. Fundamentally, a fixed excitation wavelength is used in PLE which is tuned to a wavelength just when the PL emission intensity is high. Hence, the obtained PLE spectra or signal provides an electronic energy structure which provides the ratio of emitted photon flux to the product of incident photon flux and tuned wavelength [78]. Moreover, TRPL is used to analyze the subsequent decay in Photo-Luminescence (PL) as a function of time by using a pulsed light source [79]. The fundamental limitation of this technique is its dependence on radiative events due to which materials of poor radiative quality, such as

indirect band gap semiconductors, can be difficult to investigate via typical PL spectroscopy.

In the present work, PL spectroscopy [Kimmon Koha (Co., Ltd., Centennial, CO, USA)] was used to obtain a PL emission spectrum by using a He-Cd laser at room temperature for all the deposited thin films as shown in Fig. 2.8 (a-b). The excitation wavelength of this laser is 325 nm and an output power of 20 mW. Fig. 2.8 (c) shows the block diagram of PL spectroscopy. Normally, a PL spectroscopy contains an Illuminator source, monochromators, gratings, slits, shutter, sample compartment and detectors.

Firstly, the monochromator selects the excitation wavelength which comes from the illuminator source. Then this beam hits the sample, and giving place to the PL to occur and emitting light. This emitted light is directed towards the emission monochromator, where a diffraction grating spreads the light in different wavelengths and directions towards the photodetector, which helps to measure the intensity of each wavelength of the scattered light.

2.5.5. Ellipsometry

Ellipsometry is a surface sensitive and non-destructive measurement technique which helps to investigate the thickness and optical properties of a material. Normally, the polarization of light changes after its reflection or transmission from/through a material and this spectroscopy measures this response of polarization of light. Ellipsometry uses the law where linearly polarized light at an oblique incidence over a surface, modifies the polarization state when it is reflected. So, the linearly polarized light becomes elliptically polarized due to which it is named as “ellipsometry”. In some circumstances, elliptically polarized light is applied as the incident light wave. The picture of the instrument situated at CINVESTAV and the block diagram of ellipsometry is shown in general in Fig. 2.9. This technique is not dependent on the absolute intensity, which makes it a more precise and reproducible technique. Although it is largely used to obtain the optical constants and film thickness, it also helps to study the other properties of the material such as roughness, crystallinity, doping concentration, etc.

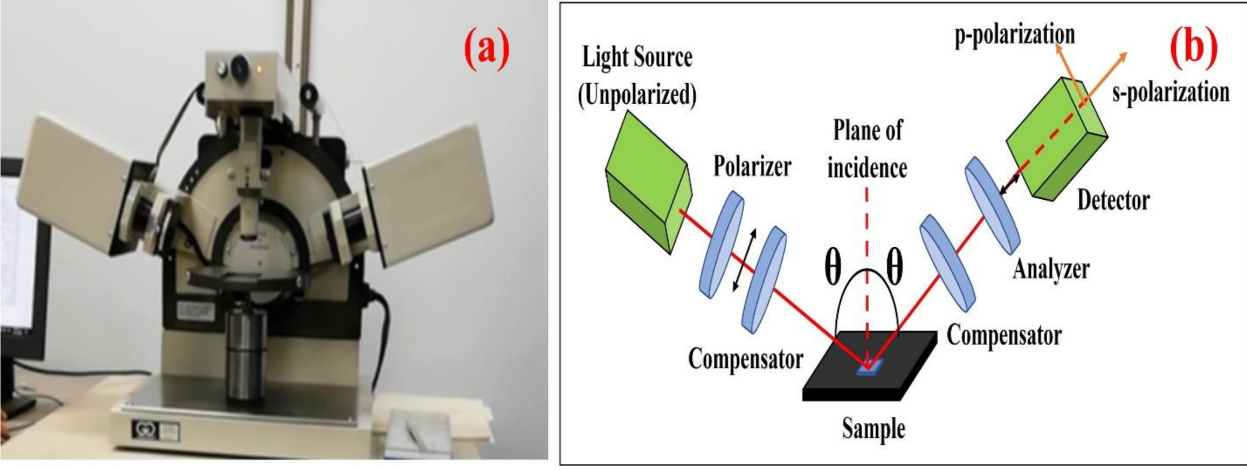

Fig. 2.9 (a) Photo of ellipsometry spectroscopy placed in SEES-CINVESTAV, and (b) Schematic block diagram of ellipsometry spectroscopy.

In the present work, an ellipsometer (Gaertner) was used with a constant wavelength of 632.8 nm and the reading of different angles of incidence from 45° to 80° was used with an interval of 5°. An unpolarized or circular light is emitted by the light source, which goes through a linear polarizer. It transforms the incoming light into linearly polarized light. Then, a compensator hinders the two perpendicular components of the electrical vector by distinct amounts thus rotating the polarization state of the wave. This focused beam hits the surface at a given angle of the material and a part of this light wave is reflected and another part is transmitted. After the reflection from the sample, the detector unit converts the reflected beam into voltage and determines its polarization state. Finally, the raw data is analyzed by using the WVASE32 software.

2.5.6. Current-Voltage measurement

Current-Voltage (I-V) measurement of solar cells was used to determine the electrical performance of the solar cell. Open-circuit voltage (V_{oc}), short-circuit current density (J_{sc}) and fill factors can be obtained by using I-V curves. A solar simulator of ABET Technologies (Sun 3000 class AAA) was used to measure the current-voltage (I-V) characteristics of solar cells as shown in Fig. 2.10 (a). This experimental setup includes a Keithley 2450 source measure unit and the Kickstart software helps to provide the corresponding I-V curve.

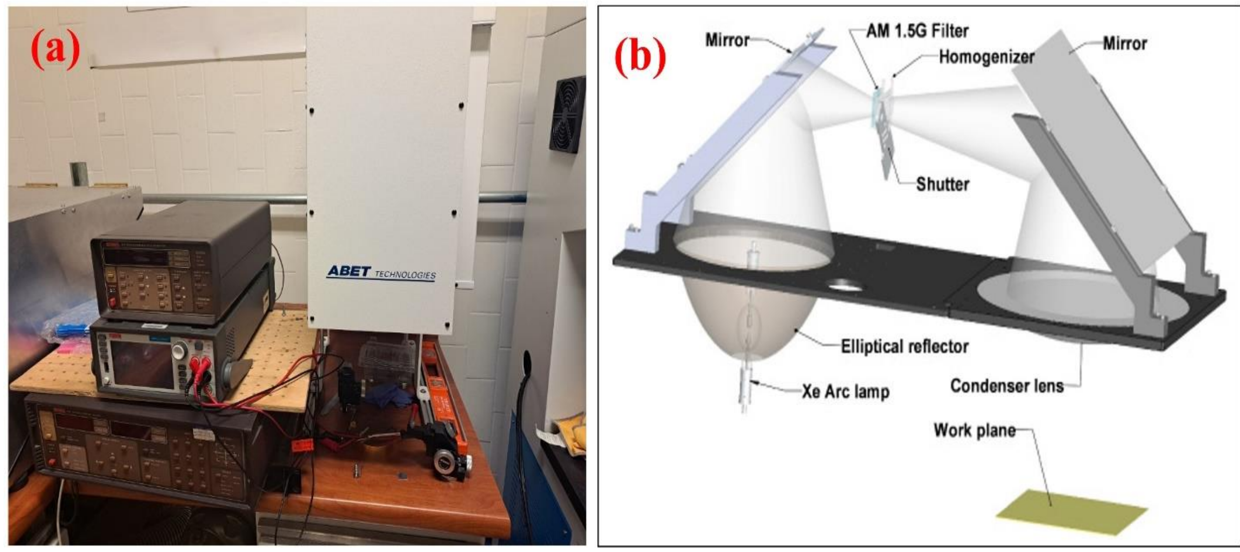

Fig. 2.10 (a) Photo of current-voltage (I-V) measurement instrument (ABET Technologies) placed at IIM-UNAM, and (b) Schematic diagram of an I-V measurement instrument (Copyright ABET TECHNOLOGIES, INC. 2021).

Fig. 2.10 (b) shows the schematic diagram of the I-V measurement instrument. This system contains a xenon (Xe) short arc lamp inside an elliptical reflector, which provides the power supply to the lamp. Next, the mirrors refocus the output of the lamp towards the optical homogenizer which comprises a pair of offset lens set arrays. Here, an AM 1.5G filter, and a spectrum shaping element, are positioned just before the homogenizer so that the same spectral shaping can be reproduced. After this, the condenser lens and homogenizer both create a uniform illumination and here, the intensity of irradiation usually remains 100 $mWcm^{-2}$.

2.5.7. External Quantum Efficiency instrument

The External Quantum Efficiency (EQE) measurement is one of the most important techniques to observe the solar cells' performance in a specific range of wavelengths. This technique is also recognized as Incident Photon to Charge Carrier Efficiency (IPCE) and it is described as the ratio of the number of charge carriers collected in the external circuit with the number of incident photons at a given wavelength [80]. An Oriel® Instruments QEPVSI-b System was used to obtain EQE measurements as shown in Fig. 2.11 (a) and Oriel's TracQ™ Basic software was used to analyze the EQE raw data.

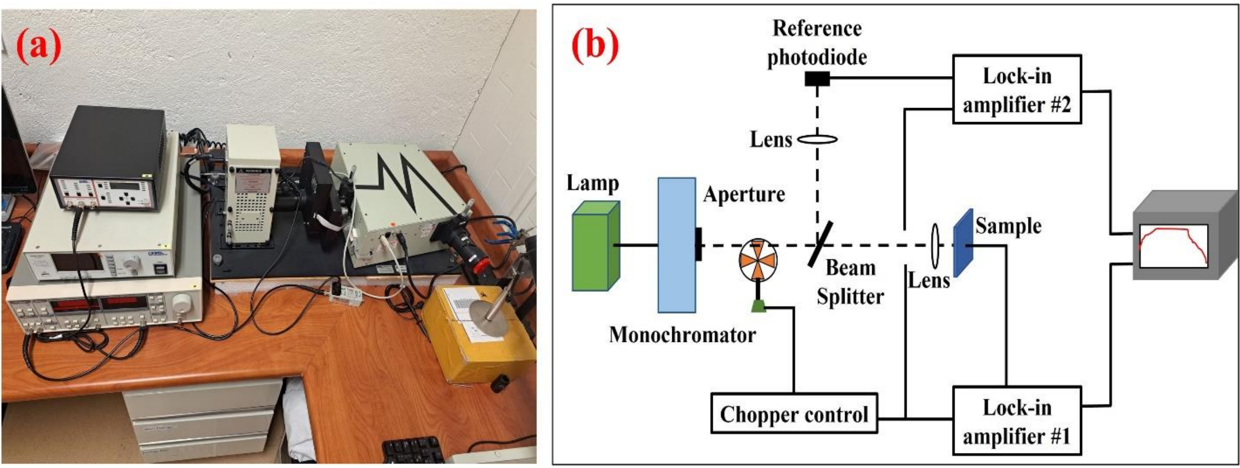

Fig. 2.11 (a) Photo of the external quantum efficiency (EQE) measurement instrument (Oriel® Instruments QEPVSI-b) placed at IIM-UNAM, and (b) Schematic block diagram of EQE measurement instrument.

Fig. 2.11 (b) shows the schematic block diagram of the EQE measurement instrument. This EQE setup consists of a Xenon Light Source with 300 W of power, which is paired with a monochromator to generate the scanning light. A chopper is used to block the ambient light, which can undesirably affect the output from the system while current and sensitive optical power measurements are achieved by using the lock-in amplifier.

2.6. General Discussion

In this chapter, a brief background and various deposition techniques of SiOC thin films were discussed in the first section. Later, experimental and characterization techniques used in this thesis work were also discussed. Here, two different HWCVD or O-Cat-CVD equipment were used to obtain SiO_xC_y thin films by using gaseous and liquid precursors. Different kinds of characterization techniques helped to understand the structural, morphological, and optical properties of deposited SiO_xC_y thin films. Besides, characterization techniques for solar cells i.e. I-V and EQE measurement were also discussed to understand the relevance of SiO_xC_y thin films deposited on solar cells.

References

[1] R. B. Ellis, "Method of making electrically conducting glass and articles made therefrom," United States Patent No.2556616, 1951.

[2] V. Belot, R. J. P. Corriu, D. Leclercq, P. H. Mutin, and A. Vioux, "Organosilicon gels containing silicon-silicon bonds, precursors to novel silicon oxycarbide compositions," *J. Non. Cryst. Solids*, vol. 144, no. C, pp. 287–297, 1992, doi: 10.1016/S0022-3093(05)80412-0.

[3] R. H. Doremus and S. Prochazka, "Silicon oxycarbide glasses: Part I. Preparation and chemistry," *J. Mater. Res.*, vol. 6, no. 12, pp. 2716–2722, 1991, doi: 10.1557/JMR.1991.2716.

[4] F. Babonneau, K. Thorne, and J. D. Mackenzie, "Dimethyldiethoxysilane/Tetraethoxysilane Copolymers: Precursors for the Si–C–O System," *Chem. Mater.*, vol. 1, no. 5, pp. 554–558, 1989, doi: 10.1021/cm00005a017.

[5] F. K. Chi, "Carbon-Containing Monolithic Glasses via the Sol-Gel Process," in *Proceedings of the 7th Annual Conference on Composites and Advanced Ceramic Materials January 16-19, 1983, Holiday Inn of Cocoa Beach, Cocoa Beach, FL*, 1983, pp. 704–717.

[6] M. Yamane, S. Aso, and T. Sakaino, "Preparation of a gel from metal alkoxide and its properties as a precursor of oxide glass," *J. Mater. Sci.*, vol. 13, no. 4, pp. 865–870, 1978, doi: 10.1007/BF00570525.

[7] T. H. Elmer and H. E. Meissner, "Increase of Annealing Point of 96% SiO_2 Glass on Incorporation of Carbon," *J. Am. Ceram. Soc.*, vol. 59, no. 5–6, pp. 206–209, 1976, doi: 10.1111/j.1151-2916.1976.tb10934.x.

[8] P. J. Jorgensen, M. E. Wadsworth, and I. B. Cutler, "Oxidation of Silicon Carbide," *J. Am. Ceram. Soc.*, vol. 42, no. 12, pp. 613–616, 1959, doi: 10.1111/j.1151-2916.1959.tb13582.x.

[9] G. Ervin, "Oxidation Behavior of Silicon Carbide," *J. Am. Ceram. Soc.*, vol. 41, no. 9, pp. 347–352, 1958, doi: 10.1111/j.1151-2916.1958.tb12932.x.

[10] L. T. Canham, "Silicon quantum wire array fabrication by electrochemical and chemical dissolution of wafers," *Appl. Phys. Lett.*, vol. 57, no. 10, pp. 1046–1048, 1990, doi: 10.1063/1.103561.

[11] S. Hayashi, M. Kataoka, and K. Yamamoto, "Photoluminescence Spectra of Carbon Clusters Embedded in SiO_2," *Jpn. J. Appl. Phys.*, vol. 32, no. Pt. 2, No. 2B, pp. L274–L276, 1993.

[12] S. Hayashi, M. Kataoka, H. Koshida, and K. Yamamoto, "Optical Properties of Carbon Clusters Embedded in SiO_2 Films," *Surf. Rev. Lett.*, vol. 3, no. 1, pp. 1095–1100, 1996, [Online]. Available: https://doi.org/10.1142/S0218625X96001959.

[13] Y. P. Guo *et al.*, "Photoluminescence studies of SiC nanocrystals embedded in a SiO_2 matrix," *Chem. Phys. Lett.*, vol. 339, no. 5–6, pp. 319–322, 2001, doi: 10.1016/S0009-2614(01)00308-6.

[14] X. Liu, J. Zhang, Z. Yan, S. Ma, and Y. Wang, "Photoluminescence from SiC nanocrystals embedded in SiO_2," *Mater. Phys. Mech.*, vol. 4, pp. 85–88, 2001.

[15] M. Sendova-Vassileva, N. Tzenov, D. Dimova-Malinovska, T. Marinova, and V. Krastev, "Visible luminescence from C-containing silicon oxide films," *Thin Solid Films*, vol. 276, no. 1–2, pp. 318–322, 1996, doi: 10.1016/0040-6090(95)08107-0.

[16] A. V. Vasin *et al.*, "Light-emitting properties of amorphous Si:C:O:H layers fabricated by oxidation of carbon-rich a-Si:C:H films," *Solid State Sci.*, vol. 11, no. 10, pp. 1833–1837, 2009, doi: 10.1016/j.solidstatesciences.2009.05.030.

[17] J. Zhou, X. Zheng, Z. Shi, B. Zhao, F. Liu, and Y. Li, "Structure and photoluminescent properties of SiCO thin-films doped with Al prepared by dual magnetron sputtering," *Int. J. Mod. Phys. B*, vol. 25, no. 16, pp. 2149–2156, 2011, doi: 10.1142/S0217979211100278.

[18] Y. Peng, J. Zhou, X. Zheng, B. Zhao, and X. Tan, "Structure and photoluminescence properties of silicon oxycarbide thin films deposited by the rf reactive sputtering," *Int. J. Mod. Phys. B*, vol. 25, no. 22, pp. 2983–2990, 2011, doi: 10.1142/S0217979211100412.

[19] B. Garrido *et al.*, "Visible photoluminescence of SiO_2 implanted with carbon and silicon," *J. Nucl. Instrum. methods Phys. Res. B*, vol. 120, pp. 101–105, 1996.

[20] M. López *et al.*, "Blue, Yellow-Green and Red Simultaneuous Emission from SiO_2 Matrices Co-implanted with Si and C," *MRS Online Proc. Libr.*, vol. 486, pp. 237–242, 1998, [Online]. Available: https://doi.org/10.1557/PROC-486-237.

[21] A. P. Rodrguez *et al.*, "White luminescence from Si^+ and C^+ ion-implanted SiO_2 films White," *J. Appl. Phys.*, vol. 94, no. 1, pp. 254–262, 2003, doi: 10.1063/1.1578172.

[22] A. Dutt, Y. Matsumoto, S. Godavarthi, G. Santana-Rodríguez, J. Santoyo-Salazar,

and A. Escobosa, "White bright luminescence at room temperature from TEOS-based thin films via catalytic chemical vapor deposition," *Mater. Lett.*, vol. 131, pp. 295–297, 2014, doi: 10.1016/j.matlet.2014.05.206.

[23] J. R. Ramos-Serrano, Y. Matsumoto, A. Méndez-Blas, A. Dutt, C. Morales, and A. I. Oliva, "Luminescent silicon oxycarbide thin films obtained with monomethyl-silane by hot-wire chemical vapor deposition," *J. Alloys Compd.*, vol. 780, pp. 341–346, 2019, doi: 10.1016/j.jallcom.2018.11.353.

[24] J. R. Ramos-Serrano, Y. Matsumoto, and C. Morales, "Luminescent Silicon Oxycarbide Thin Films via Hot-wire CVD using Tetraethyl Orthosilicate: Role of the Chamber Pressure and Post-deposition Annealing," *2018 15th Int. Conf. Electr. Eng. Comput. Sci. Autom. Control. CCE 2018*, pp. 1–4, 2018, doi: 10.1109/ICEEE.2018.8533970.

[25] Y. Matsumoto *et al.*, "Luminescence study of Si/SiC Nano-particles embedded in SiO_xC_y matrix deposited using O-Cat-CVD," *Phys. E Low-dimensional Syst. Nanostructures*, vol. 111, no. March, pp. 179–184, 2019, doi: 10.1016/j.physe.2019.03.024.

[26] M. Jain, J. R. Ramos-Serrano, A. Dutt, and Y. Matsumoto, "Photoluminescence properties of thin-film SiO_xC_y deposited by O-Cat CVD technique using MMS and TEOS," in *2020 17th International Conference on Electrical Engineering, Computing Science and Automatic Control (CCE). Mexico City, Mexico. November 11-13*, 2020, pp. 1–6, doi: 10.1109/cce50788.2020.9299113.

[27] A. Coyopol *et al.*, "Strong white light emission from SiC_xO_y films grown by HFCVD technique," *Opt. Mater. (Amst).*, vol. 99, no. 109551, pp. 1–7, 2020, doi: 10.1016/j.optmat.2019.109551.

[28] M. Jain, J. R. Ramos-Serrano, A. Dutt, and Y. Matsumoto, "The influence of deposition time on the photoluminescent properties of SiO_xC_y thin films obtained by Cat-CVD from monomethyl silane precursor," *Mater. Lett.*, vol. 291, p. 129547, 2021, doi: 10.1016/j.matlet.2021.129547.

[29] S. Y. Seo, K. S. Cho, and J. H. Shin, "Intense blue-white luminescence from carbon-doped silicon-rich silicon oxide," *Appl. Phys. Lett.*, vol. 84, no. 5, pp. 717–719, 2004, doi: 10.1063/1.1645989.

[30] Z. Lin *et al.*, "Defect emission and optical gain in SiC_xO_y:H films," *ACS Appl. Mater. Interfaces*, vol. 9, no. 27, pp. 22725–22731, 2017.

[31] S. Gallis, V. Nikas, H. Suhag, M. Huang, and A. E. Kaloyeros, "White light

emission from amorphous silicon oxycarbide (a-SiC_xO_y) thin films: Role of composition and postdeposition annealing," *Appl. Phys. Lett.*, vol. 97, no. 8, pp. 1–4, 2010, doi: 10.1063/1.3482938.

[32] V. Nikas *et al.*, "The origin of white luminescence from silicon oxycarbide thin films," *Appl. Phys. Lett.*, vol. 061906, no. 104, pp. 1–5, 2014, doi: 10.1063/1.4865100.

[33] B. Ford, N. Tabassum, V. Nikas, and S. Gallis, "Strong photoluminescence enhancement of silicon oxycarbide through defect engineering," *Materials (Basel).*, vol. 10, no. 4, 2017, doi: 10.3390/ma10040446.

[34] A. Karakuscu, R. Guider, L. Pavesi, and G. D. Sorarù, "White luminescence from sol-gel-derived SiOC thin films," *J. Am. Ceram. Soc.*, vol. 92, no. 12, pp. 2969–2974, 2009, doi: 10.1111/j.1551-2916.2009.03343.x.

[35] A. Tamayo, R. Ruiz-Caro, A. Mazo, M. D. Veiga-Ochoa, and J. Rubio, "Chemical oxidation of silicon oxycarbide ceramics for advanced drug delivery systems," *J. Mater. Sci.*, vol. 51, no. 3, pp. 1382–1391, 2016, doi: 10.1007/s10853-015-9457-3.

[36] V. S. Pradeep, M. Graczyk-zajac, R. Riedel, and G. D. Sorarù, "New Insights in to the Lithium Storage Mechanism in Polymer Derived SiOC Anode Materials," *Electrochim. Acta*, vol. 119, pp. 78–85, 2014, doi: 10.1016/j.electacta.2013.12.037.

[37] C. Chandra and J. Kim, "Silicon oxycarbide produced from silicone oil for high-performance anode material in sodium ion batteries," *Chem. Eng. J.*, vol. 338, no. December 2017, pp. 126–136, 2018, doi: 10.1016/j.cej.2018.01.032.

[38] F. Roth, C. Schmerbauch, E. Ionescu, N. Nicoloso, O. Guillon, and R. Riedel, "High-temperature piezoresistive C / SiOC sensors," *J. Sensors Sens. Syst.*, vol. 4, no. 1, pp. 133–136, 2015, doi: 10.5194/jsss-4-133-2015.

[39] R. Riedel, L. Toma, E. Janssen, J. Nuffer, T. Melz, and H. Hanselka, "Piezoresistive effect in SiOC ceramics for integrated pressure sensors," *J. Am. Ceram. Soc.*, vol. 93, no. 4, pp. 920–924, 2010, doi: 10.1111/j.1551-2916.2009.03496.x.

[40] J. Zhao *et al.*, "Intense short-wavelength photoluminescence from thermal SiO_2 films co-implanted with Si and C ions," *Appl. Phys. Lett.*, vol. 73, no. 13, pp. 1838–1840, 1998, doi: 10.1063/1.122299.

[41] Y. H. Yu, S. P. Wong, and I. H. Wilson, "Visible Photoluminescence in Carbon-Implanted Thermal SiO_2 Films," vol. 531, pp. 531–534, 1998.

[42] L. Rebohle, T. Gebel, H. Fröb, H. Reuther, and W. Skorupa, "Ion beam processing for Si/C-rich thermally grown SiO_2 layers: Photoluminescence and microstructure,"

Appl. Surf. Sci., vol. 184, no. 1–4, pp. 156–160, 2001, doi: 10.1016/S0169-4332(01)00490-1.

[43] S. Muto, A. V. Vasin, Y. Ishikawa, N. Shibata, J. Salonen, and V. P. Lehto, "Nano-Order Structural Analysis of White Light-Emitting Silicon Oxide Prepared by Successive Thermal Carbonization/Oxidation of the Porous Silicon," *Mater. Sci. Forum*, vol. 561–565, pp. 1127–1130, 2007, doi: 10.4028/www.scientific.net/msf.561-565.1127.

[44] A. V. Vasin, Y. Ishikawa, N. Shibata, J. Salonen, and V. P. Lehto, "Strong white photoluminescence from carbon-incorporated silicon oxide fabricated by preferential oxidation of silicon in nano-structured Si:C layer," *Japanese J. Appl. Physics, Part 2 Lett.*, vol. 46, no. 17–19, pp. 464–467, 2007, doi: 10.1143/JJAP.46.L465.

[45] Y. Ishikawa *et al.*, "Color control of white photoluminescence from carbon-incorporated silicon oxide," *J. Appl. Phys.*, vol. 104, no. 8, pp. 1–7, 2008, doi: 10.1063/1.3003079.

[46] A. V. Vasin, V. I. Kushnirenko, V. S. Lysenko, A. N. Nazarov, Y. Ishikawa, and J. Salonen, "The nature of white luminescence in SiO_2:C layers," *Tech. Phys. Lett.*, vol. 35, no. 6, pp. 559–562, 2009, doi: 10.1134/S1063785009060224.

[47] A. V. Vasin *et al.*, "Study of the Processes of Carbonization and Oxidation of Porous Silicon by Raman and IR Spectroscopy," *Semiconductors*, vol. 45, no. 3, pp. 350–354, 2011, doi: 10.1134/S1063782611030249.

[48] Y. Ding and H. Shirai, "White light emission from silicon oxycarbide films prepared by using atmospheric pressure microplasma jet," *J. Appl. Phys.*, vol. 105, no. 4, 2009, doi: 10.1063/1.3080129.

[49] X. Liu, L. Cao, H. Song, and H. Jiang, "Strong ultraviolet and green photoluminescence from SiC/SiO_2 core-shell nanowires," *Phys. E Low-Dimensional Syst. Nanostructures*, vol. 61, pp. 167–170, 2014, doi: 10.1016/j.physe.2014.03.029.

[50] L. Cao, X. Liu, H. Jiang, H. Song, J. Zhao, and H. Lu, "Photoluminescence studies of SiC/SiO_2 aloetic-shaped nanowires," *J. Nanosci. Nanotechnol.*, vol. 14, no. 5, pp. 3928–3931, 2014, doi: 10.1166/jnn.2014.7949.

[51] Z. Lin *et al.*, "Effect of thermal annealing on the blue luminescence of amorphous silicon oxycarbide films," *J. Non. Cryst. Solids*, vol. 428, pp. 184–188, 2015, doi: 10.1016/j.jnoncrysol.2015.08.022.

[52] Z. Lin *et al.*, "Influence of the oxygen content in obtaining tunable and strong

photoluminescence from low-temperature grown silicon oxycarbide films," *J. Alloys Compd.*, vol. 633, pp. 153–156, 2015, doi: 10.1016/j.jallcom.2015.02.027.

[53] Z. Lin *et al.*, "Dense nanosized europium silicate clusters induced light emission enhancement in Eu-doped silicon oxycarbide films," *J. Alloys Compd.*, vol. 694, pp. 946–951, 2017, doi: 10.1016/j.jallcom.2016.10.132.

[54] J. Zhang, S. Yan, Q. Jia, J. Huang, L. Lin, and S. Zhang, "Preparation of SiC/SiO_2 core-shell nanowires via molten salt mediated carbothermal reduction route," *Phys. E Low-Dimensional Syst. Nanostructures*, vol. 80, pp. 19–24, 2016, doi: 10.1016/j.physe.2016.01.002.

[55] A. V. Vasin *et al.*, "The effect of deposition processing on structural and luminescent properties of a-SiOC:H thin films fabricated by RF-magnetron sputtering," *J. Lumin.*, vol. 191, pp. 102–106, 2017, doi: 10.1016/j.jlumin.2016.10.029.

[56] I. García *et al.*, "Luminescence Enhancement in Silicon Oxycarbide Thin Films Obtained by Catalytic Chemical Vapor Deposition Using Mesoporous Silica Pellets and Tetraethoxysilane," *Thin Solid Films*, vol. 713, no. November 2019, p. 138358, 2020, doi: 10.1016/j.tsf.2020.138358.

[57] A. V. Vasin *et al.*, "Broad band (UV–VIS) photoluminescence from carbonized fumed silica: Emission, excitation and kinetic properties," *J. Lumin.*, vol. 190, no. February, pp. 141–147, 2017, doi: 10.1016/j.jlumin.2017.05.045.

[58] T. Hata and H. Nakayama, "An organic catalytic CVD: Principle, apparatus and applications," *Thin Solid Films*, vol. 516, no. 5, pp. 558–563, 2008, doi: 10.1016/j.tsf.2007.06.093.

[59] S. Yamazaki, K. Wada, and I. Taniguchi, "Silicon Nitride Prepared by the SiH_4 - NH_3 Reaction with Catalysts," *Jpn. J. Appl. Phys.*, vol. 9, no. 12, pp. 1467–1477, 1970, doi: 10.1143/JJAP.9.1467.

[60] H. Wiesmann, A. K. Ghosh, T. McMohan, and M. Strongin, "a-Si : H produced by high-temperature thermal decomposition of silane," *J. Appl. Phys.*, vol. 50, no. 5, pp. 3752–3754, 1979, doi: https://doi.org/10.1063/1.326284.

[61] H. Matsumura and H. Tachibana, "Amorphous silicon produced by a new thermal chemical vapor deposition method using intermediate species SiF_2," *Appl. Phys. Lett.*, vol. 47, no. 8, pp. 833–835, 1985, doi: 10.1063/1.96000.

[62] H. Matsumura, "Catalytic chemical vapor deposition (CTL-CVD) method producing high quality hydrogenated amorphous silicon," *Jpn. J. Appl. Phys.*, vol. 25, no. 12,

pp. L949–L951, 1986, doi: 10.1143/JJAP.25.L949.

[63] J. Doyle, R. Robertson, and G. H. Lin, "Production of high-quality amorphous silicon films by evaporative silane surface decomposition," *J. Appl. Phys.*, vol. 64, no. 6, pp. 3215–3223, 1988, doi: https://doi.org/10.1063/1.341539.

[64] A. H. Mahan, J. Carapella, B. P. Nelson, R. S. Crandall, and I. Balberg, "Deposition of device quality, low H content amorphous silicon," *J. Appl. Phys.*, vol. 69, no. 9, pp. 6728–6730, 1991, doi: 10.1063/1.348897.

[65] H. Matsumura, H. Umemoto, and A. Masuda, "Cat-CVD (hot-wire CVD): How different from PECVD in preparing amorphous silicon," *J. Non. Cryst. Solids*, vol. 338–340, no. 1 SPEC. ISS., pp. 19–26, 2004, doi: 10.1016/j.jnoncrysol.2004.02.014.

[66] R. E. I. Schropp, "Frontiers in HWCVD," *Thin Solid Films*, vol. 517, no. 12, pp. 3415–3419, 2009, doi: 10.1016/j.tsf.2009.01.038.

[67] J. K. Rath, M. de Jong, and R. E. I. Schropp, "Low temperature (< 100 °C) fabrication of thin film silicon solar cells by HWCVD," *Thin Solid Films*, vol. 516, no. 5, pp. 751–754, 2008, doi: 10.1016/j.tsf.2007.06.059.

[68] L. G. Britton, "Combustion hazards of silane and its chlorides," *Plant/operations Prog.*, vol. 9, no. 1, pp. 16–38, 1990, doi: 10.1002/prsb.720090107.

[69] F. Tamanini, J. L. Chaffee, and R. L. Jambor, "Reactivity and Ignition Characteristics of Silane/Air Mixtures," *Process Saf. Prog.*, vol. 17, no. 4, pp. 243–258, 1998, doi: 10.1002/prs.680170405.

[70] E. Eduard and J. Nickl, "Process for the production of extremely pure silicon," 758973, 1962.

[71] E. Mon-Pérez *et al.*, "Experimental and theoretical rationalization of the growth mechanism of silicon quantum dots in non-stoichiometric SiN_x : role of chlorine in plasma enhanced chemical vapour deposition," *Nanotechnology*, vol. 27, no. 455703, pp. 1–12, 2016, doi: 10.1088/0957-4484/27/45/455703.

[72] R. Fan, W. Zhang, Y. Wang, D. Chen, and Y. Zhang, "Metal Material Resistant to Hydrochloric Acid Corrosion," *J. Phys. Conf. Ser.*, vol. 1732, no. 012134, pp. 1–8, 2021, doi: 10.1088/1742-6596/1732/1/012134.

[73] S. H. Mir, L. A. Nagahara, T. Thundat, P. Mokarian-Tabari, H. Furukawa, and A. Khosla, "Review—Organic-Inorganic Hybrid Functional Materials: An Integrated Platform for Applied Technologies," *J. Electrochem. Soc.*, vol. 165, no. 8, pp. B3137–B3156, 2018, doi: 10.1149/2.0191808jes.

[74] U. Díaz and A. Corma, "Organic-Inorganic Hybrid Materials: Multi-functional

Solids for Multi-step Reaction processes," *Chem. - A Eur. J.*, vol. 24, no. 16, pp. 3944–3958, 2018, doi: 10.1002/chem.201704185.

[75] Y. Iwase, T. Fuchigami, Y. Horie, Y. Daiko, S. Honda, and Y. Iwamoto, "Formation and thermal behaviors of ternary silicon oxycarbides derived from silsesquioxane derivatives," *Materials (Basel).*, vol. 12, no. 10, 2019, doi: 10.3390/MA12101721.

[76] S. B. Desu, "Decomposition Chemistry of Tetraethoxysilane," *J. Am. Ceram. Soc.*, vol. 72, no. 9, pp. 1615–1621, 1989.

[77] G. B. Raupp, T. S. Cale, H. P. W. Hey, G. B. Raupp, and T. S. Cale, "The role of oxygen excitation and loss in plasma enhanced deposition of silicon dioxide from tetraethylorthosilicate," *J. Vac. Sci. Technol. B*, vol. 10, no. 1, pp. 37–45, 1992, doi: 10.1116/1.586361.

[78] E. K. Grubbs, J. Moore, and P. A. Bermel, "Photoluminescence Excitation Spectroscopy Characterization of Surface and Bulk Quality for Early-Stage Potential of Material Systems," in *IEEE 46th Photovoltaic Specialists Conference (PVSC), Chicago, IL, USA, 2019*, 2019, pp. 0377–0381, doi: 10.1109/PVSC40753.2019.8980637.

[79] W. K. Metzger, R. K. Ahrenkiel, P. Dippo, J. Geisz, M. W. Wanlass, and S. Kurtz, "Time-resolved photoluminescence and photovoltaics," in *DOE Solar Energy Technologies Program Review Meeting*, 2005, vol. 1, no. January, pp. 1–2, [Online]. Available: http://www.nrel.gov/docs/fy05osti/37028.pdf.

[80] W. Ananda, "External quantum efficiency measurement of solar cell," in *QiR 2017 - 2017 15th International Conference on Quality in Research (QiR): International Symposium on Electrical and Computer Engineering*, 2017, pp. 450–456, doi: 10.1109/QIR.2017.8168528.

CHAPTER 3
SiO_xC_y THIN FILMS DEPOSITED WITH MMS AND VINYL SILANE

3.1. Experimental Details

An organic catalytic chemical vapor deposition (O-Cat-CVD) system was used, as shown in Fig. 2.1 (a), to deposit silicon oxycarbide (SiO_xC_y) thin films. These SiO_xC_y thin films were deposited on polished P-type crystalline silicon substrate with (100) orientation (resistivity 1-10 Ω-cm) by using monomethyl Silane (MMS) and vinyl silane precursor. The substrate was cleaned by using the RCA method [1]. In this method, the substrate was cleaned with Xylan, Acetone, and hydrogen peroxide for 10-10 minutes, respectively, and then kept for 20 seconds in hydrogen fluoride (HF) of 10 % dilution with water. After this process, the substrate was dried using nitrogen gas.

Furthermore, the MMS gas was purchased from Sigma Aldrich Company with a purity of 99.9% while vinyl silane gas was purchased from Gelest Company with a purity of 97-100%, and product code and case Nos. were SIV9096.7 and 7291-09-0, respectively. Oxygen (O_2) and hydrogen (H_2) gases were also used as reactant gases. This O-Cat-CVD system has two vacuum pumps, a primary mechanical type in which vacuum pressures reached in the range of $1x10^{-2}$ torr and a secondary turbo molecular type in which maximum vacuum reached up to $4x10^{-6}$ torr. Control systems for mass flow controller and filament temperature are also presented. Tantalum (T_a) wire with a diameter of 0.5 mm was used as a catalyst with 5 cm distance between the filament and substrate. The substrate (T_s) temperature and filament (T_f) temperature were 200ºC and 1800ºC, respectively. The filament temperature is monitored throughout the process using an infrared camera (Chino Brand Model IR-AHS) through the window of the corresponding chamber.

3.2. Results and discussions

The effect of deposition duration on SiO_xC_y thin films by using MMS and vinyl silane gas as precursors, is discussed in subsequent sections to understand its various properties.

3.2.1. SiO_xC_y thin films deposited by monomethyl silane

In this work, the effect of deposition duration was evaluated, so it was kept as a variable parameter for preparing thin films. The chambers working pressure (Ps) was 0.13 Torr, while the flow rate of MMS, hydrogen and oxygen gases were 4, 20, and 1 sccm, respectively [2].

3.2.1.1. Fourier Transform Infrared (FTIR) Spectroscopy

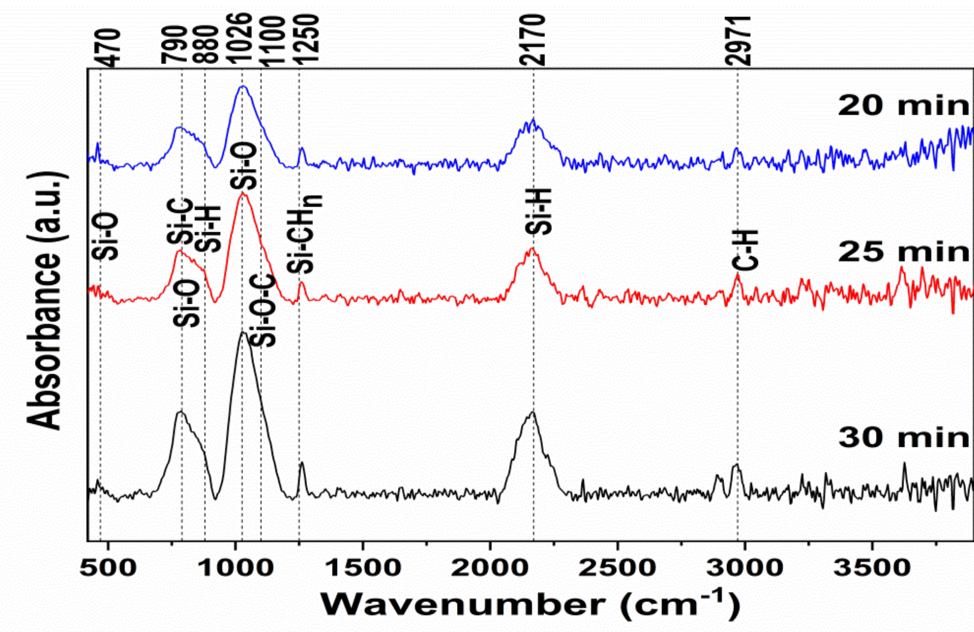

Fig. 3.1 FTIR spectra of deposited samples at various deposition duration by using MMS [2].

The vibrational modes of FTIR absorption bands are illustrated in Fig. 3.1, and their corresponding wavenumbers are also mentioned in Table 3.1 for the deposited thin films. Normally, the rocking, bending, and stretching vibrational modes for the Si-O-Si bonding are observed at 470, 800, and 1080 cm^{-1}, respectively, but the stretching vibrational mode of the Si-O-Si bond is positioned at 1026 cm^{-1} [2]. Hence, deposited thin films show a shift in stretching vibrational mode the Si-O-Si bond from the stoichiometry value (1080 cm^{-1}) [3]. This shift from the stoichiometry value of Si-O-Si bond corresponds to the oxygen deficiency in Si-O-Si bonding, which may give higher possibilities of having one or more silicon or carbon neighboring atoms [3]–[5]. This stoichiometry and/or composition

modifications in the oxide layer allow controlling the Photo-Luminescence (PL) intensity and its spectral composition [6]. An absorption band can also be noticed at 1100 cm^{-1}, which refers to the presence of Si-O-C bonds and confirming the formation of SiO_xC_y thin film [7].

Other absorption bands positioned at 2971, 1250, and 800 cm^{-1} are related to C-H, Si–CH_n, and Si-C bonds, respectively [8]. It can be clearly noticeable in Fig. 3.1 that the intensity of these bonding states is gradually intensifying with an increase in deposition time for the obtained thin films. The proportionally elevated intensity of Si-C mode can be due to the shift in the absorption band of Si-O-Si stretching mode from its stoichiometry value which increase the possibility of having one or more C or Si neighboring atoms [9]. The absorption bands of Si-H_n were observed at 880 and 2170 cm^{-1}, which corresponds to the scissors and stretching vibrational modes, respectively [10]. The 2170 cm^{-1} stretching mode is usually assigned to the clustered Si-H bonds with one or more carbon atoms [11].

From Fig. 3.1, it is also noticeable that the intensities of the absorption bands at 800, 1026, 1250, 2170, and 2971 cm^{-1} bonding states are proportionally elevating with the deposition duration, which indicates that the contribution of carbon related-bondings increased in the thin film [2].

Table 3.1 FTIR infrared absorption bands with their respective wavenumbers [9].

Wavenumber (cm^{-1})	Vibrational mode
470	Si-O-Si rocking band
670	Si-H_n
800	Si-O-Si bending band, Si-C
880	Si-H_n
1080	Si-O-Si stretching band
1100	Si-O-C
1250	Si-H_n
2170	Si-H
2971	C-H

3.2.1.2. X-Ray Photoelectron Spectroscopy (XPS)

The chemical analysis for the 30 min deposited sample were characterized by XPS and it is illustrated in the Fig. 3.2. Si 2p, C 1s and O 1s XPS spectrum peaks are noticeable in Fig. 3.2 (b), (c), and (d), respectively and relative content of the phases are shown in the Table 3.2.

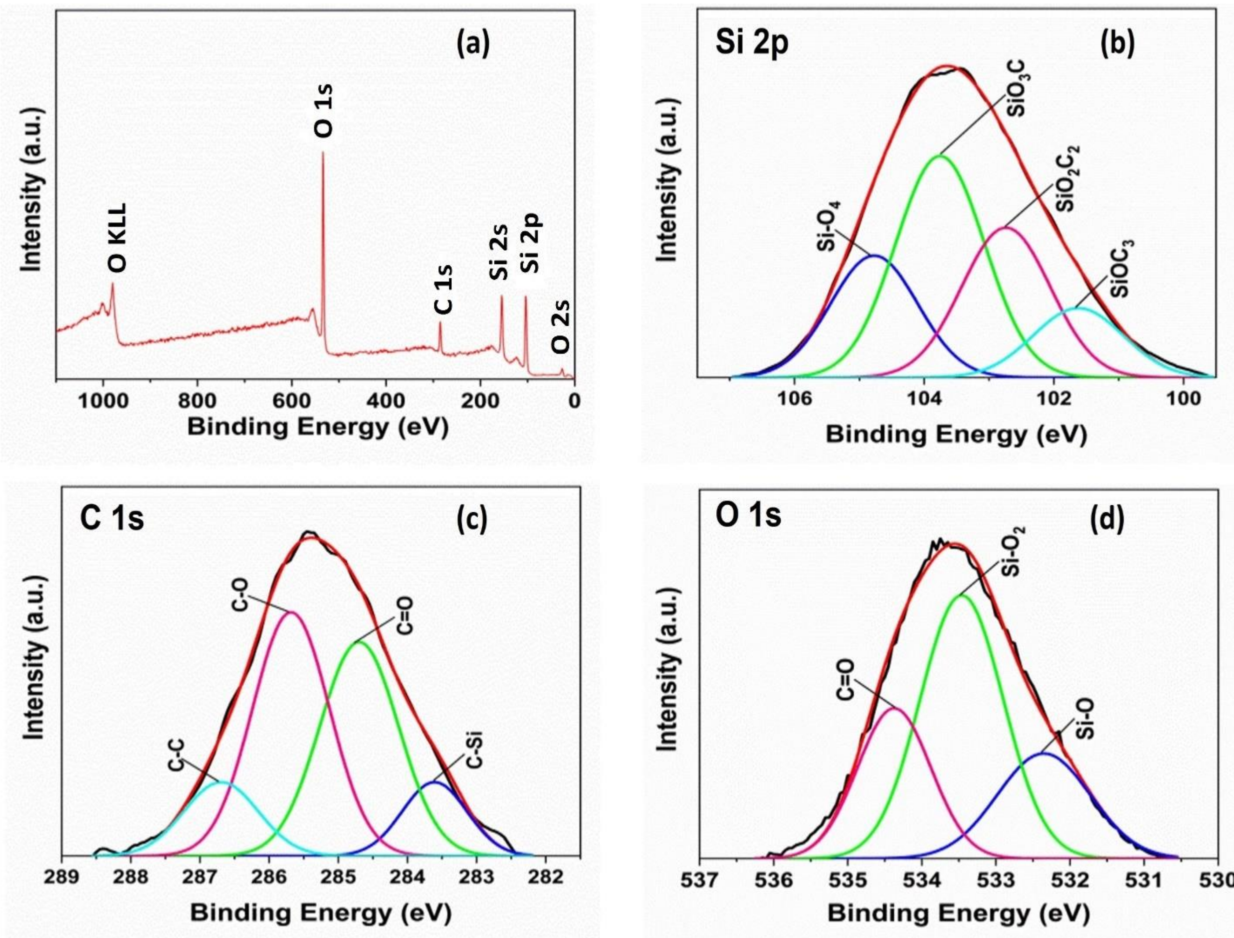

Fig. 3.2 XPS spectra of a) SiOxCy, b) Si 2p, c) C 1s, and d) O 1s for 30 min deposited sample by using MMS.

Table 3.2 The relative content of the phases calculated by the XPS fitted results.

Spectra	Si 2p				C 1s				O 1s		
Bonding	$SiOC_3$	SiO_2C_2	SiO_3C	$Si\text{-}O_4$	C-Si	C-C	C-O	C=O	Si-O	$Si\text{-}O_2$	C=O
BE (eV)	101.5	102.8	103.7	104.9	283.0	284.5	285.8	287.0	532.4	533.4	534.5
Atomic %	12.6	26.6	39.5	21.3	10.4	36.8	40.9	11.9	22.9	51.3	25.8

The high-resolution Si 2p spectra contain $SiOC_3$, SiO_2C_2, SiO_3C, and SiO_4 phases at 101.5 eV, 102.8 eV, 103.7 eV, and 104.9 eV peaks, respectively [12]. The figure shows that the content of $SiOC_3$, SiO_2C_2, SiO_3C, and SiO_4 bond phases are 12.6 %, 26.6 %, 39.5 % and 21.3 atm%, respectively. This analysis justifies the presence of SiO_xC_y bonding in the thin film, including with the SiO_2 bonds.

C 1s spectra contain peaks at 283 eV, 284.5 eV, 285.8, and 287 eV for C-Si, C-C, C-O and C=O bonds, respectively [13]. Here, C-Si bonds show the presence of C in the form of SiC and SiOC, C-C bonds show the presence of C in the form of amorphous C or as graphite and C–O shows the carbon bonded to O, C–O or C=O, in the above mentioned phases, respectively [14].

Here, C-Si bonds have 10.4 atm% content, showing the presence of SiC or SiOC bonds in the thin film. C-C bonds may be identified as amorphous carbon bonds or free carbon. From Fig 3.1, the FTIR spectra also justify the presence of the C-C bond in the thin film. Except this, the spectra also show a quantities of C-O and C=O bondings with 40.9 % and 11.9 atm%, respectively. This can be identified as the formation of carbon dioxide in the thin film.

Besides this, in O 1s spectra, the Si-O, SiO_2, and C=O bond phases were also detected at 532.4 eV, 533.4 eV and 534.5 eV peaks, respectively [12]. Here the Si-O bonds show the presence of oxygen in silicon oxycarbide, SiO_2 shows the presence of oxygen in silicon oxide, while the C=O bond shows the oxygen bonded to carbon [14].

Here the Si-O, SiO_2 and C=O content is 22.9 %, 51.3 % and 25.8 atm%, respectively. These results approve the presence of SiO_xC_y, SiO_2 and CO_2 in the thin film, which also correlates with the results of FTIR.

3.2.1.3. Ellipsometry

Fig. 3.3 illustrates the thickness and the refractive index (RI) of the deposited samples and their corresponding values are mentioned in Table 3.3, respectively. Here, the effect of deposition time was investigated on the thickness and refractive index of thin films. The

refractive index deposited thin films vary from 1.63 to 1.73 while the thickness is proportionally increasing from 154.3 nm to 268.3 nm, respectively, with the increment of deposition time.

Here it is noticeable that the refractive index (RI) of deposited thin films, alters, but it is expected that it should be constant for every thickness in these thin films. The compositional change of thin films can be the reason for this variation of the RI which can be due to the dissociation process of different molecules with time, which may consequently alter the value of the RI [15]. The differences in the bonding states of various thin films are clearly noticeable from FTIR and XPS spectra, which are justified by the variation of deposition time, and the composition modification of the film affects the variation of RI [9].

The substrate temperature may also change due to the hitting of hot electrons in the chamber, which may alter radicals sticking coefficient and surface mobility [16]. This might modify the deposition kinetics, which can also be the cause for the variation of RI [9].

Table 3.3 Refractive index and thickness of samples by ellipsometry.

Deposition Duration	Thickness (nm)	Refractive Index (RI)
20	154.3 ± 0.1	1.70 ± 0.002
25	179.2 ± 0.1	1.63 ± 0.002
30	268.3 ± 0.1	1.73 ± 0.002

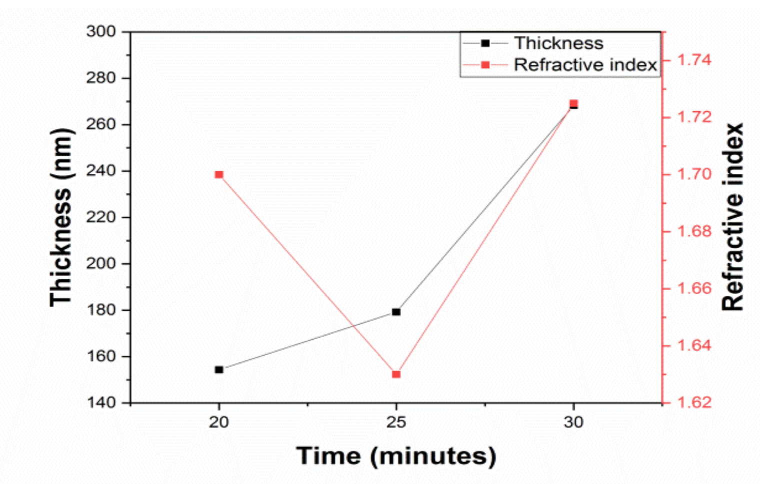

Fig. 3.3 Refractive index and thickness of deposited samples at various deposition times using MMS [2].

3.2.1.4. Photo-Luminescence Spectroscopy

The PL spectra of thin films deposited at different conditions are illustrated in Fig. 3.4. An intense PL spectrum is observed in a wide region of visible spectra with a peak at 574 nm (2.2 eV) for 30 min-deposited samples, while considerably less intense spectra are noticed at 477 nm (2.7 eV) for 25 and 20 min-deposited samples. The cause for this blue shift in the PL spectra from 2.2 to 2.7 eV can be the decrease of Si-C bonding, as illustrated in FTIR spectra (Fig. 3.1). Other articles have also showed this shift from red to blue spectra, but nobody has in the past considered this phenomenon of Si-C bonding [7], [17]–[19]. This phenomenon can be significant in achieving required optoelectronic devices.

The origin of PL emission at 2.2 eV can be due to different reasons, in which the shift in the non-stoichiometry composition [20], as discussed previously from FTIR analysis, can be one possible reason and this may also generate carbon-related defects [21] for PL emission at this band. Carbon-related neutral oxygen vacancy (NOV) defects [18], oxygen deficiency centers or silicon-related NOV can be the possible reasons of PL at 2.7 eV [22]. Quantum Confinement Effect (QCE) can be another probable reason for the PL emission in the visible range [19], [23].

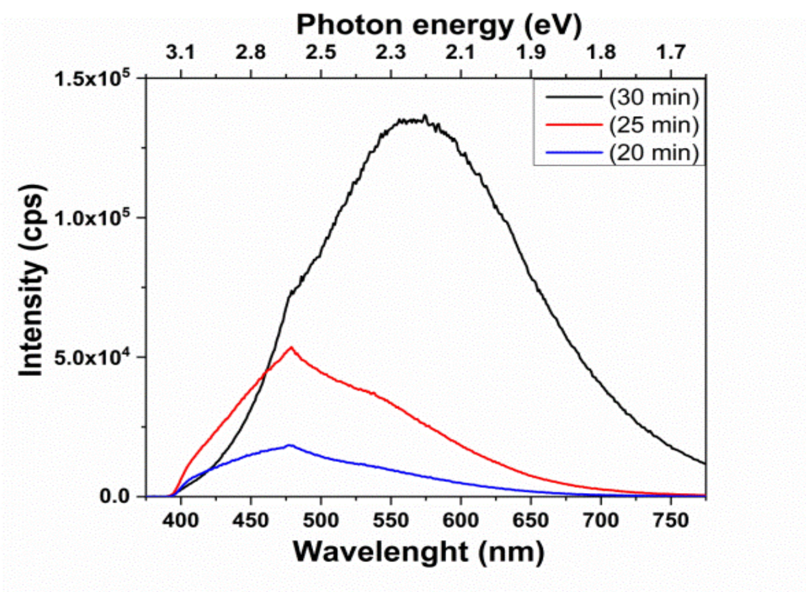

Fig. 3.4 PL spectra of deposited samples at room temperature for various deposition times by using MMS [2].

3.2.2. SiO_xC_y thin films deposited by vinyl silane

In this section, the effect of deposition time was evaluated and kept as a variable parameter for the preparation of thin films. The chambers working pressure (Ps) was 0.11 torr, while the flow rate of vinyl silane, hydrogen and oxygen gases were 7, 20, and 0.5 sccm, respectively.

3.2.2.1. Fourier Transform Infrared (FTIR) Spectroscopy

The FTIR absorption bands of vibrational modes are shown in Fig. 3.5. An absorption band can be observed at 1107 cm^{-1} for the deposited thin films, representing the presence of Si-O-C bonds and confirming the formation of SiO_xC_y thin film [7]. A broad absorption band from 580-800 cm^{-1} and another peak at 2931 cm^{-1} can also be observable, which are getting more intense with the increase of the deposition time. Here, the peak at 2931 cm^{-1} shows the presence of CH bonds which represents the asymmetric stretch vibrations of methyl groups bonded to silicon [24], while the broad absorption band from 580-800 cm^{-1} shows the presence of Si-C bond-related characteristic peaks appears at 609 cm^{-1} and 800 cm^{-1} [25]. The absorption band at 670 cm^{-1} shows the presence of a $Si–H_n$ bond.

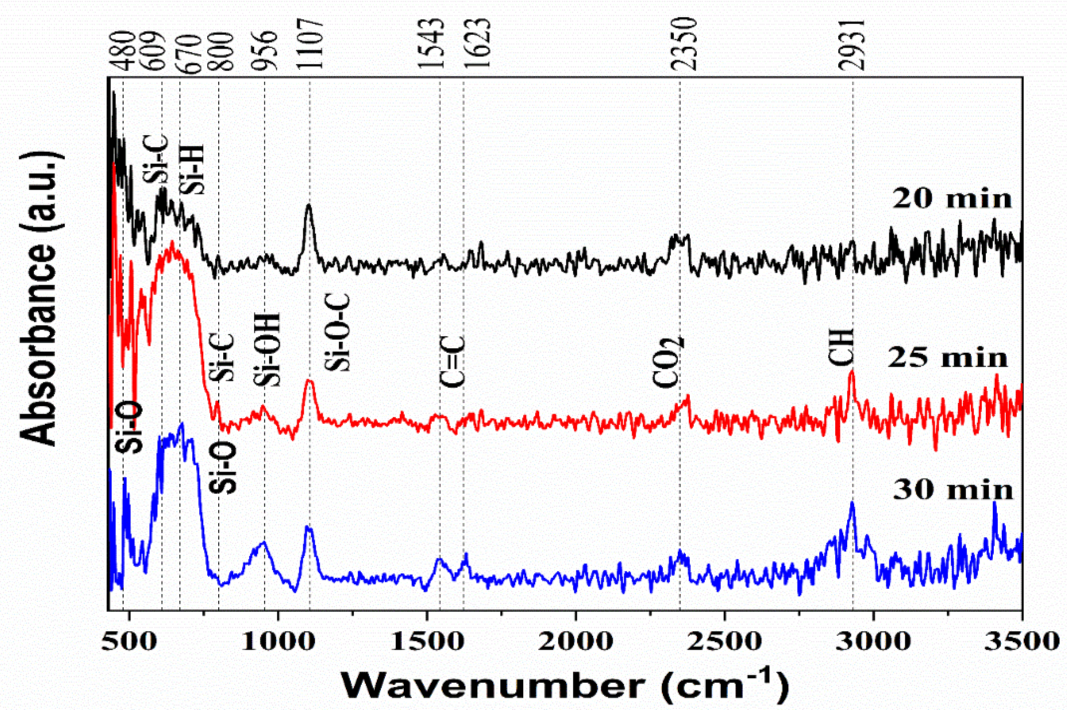

Fig. 3.5 FTIR spectra of deposited samples at various deposition duration by using vinyl silane.

The absorption bands of rocking and bending for the Si-O-Si bonding are at 480 and 800 cm^{-1}, respectively [2], [26]. In addition to these absorption bands, other bands related to Si–OH, C=C, and CO_2 bonds were also observed at 956, 1600, and 2350 cm^{-1}, respectively [27]–[29].

3.2.2.2. Ellipsometry

Fig. 3.6 illustrates the thickness and the refractive index (RI) of the deposited samples, and their corresponding values are mentioned in Table 3.4, respectively. Here, the effect of deposition time was investigated as a function the thickness and refractive index of thin films. The refractive index of the deposited thin films varies from 1.75 to 1.83, while the thickness is proportionally increasing from 90.1 nm to 195.3 nm, respectively, with the increment of deposition time.

Table 3. 4 Refractive index and thickness of samples by ellipsometry.

Deposition Duration	Thickness (nm)	Refractive Index (RI)
20	90.1 ± 0.1	1.78 ± 0.002
25	142.6 ± 0.1	1.83 ± 0.002
30	195.3 ± 0.1	1.75 ± 0.002

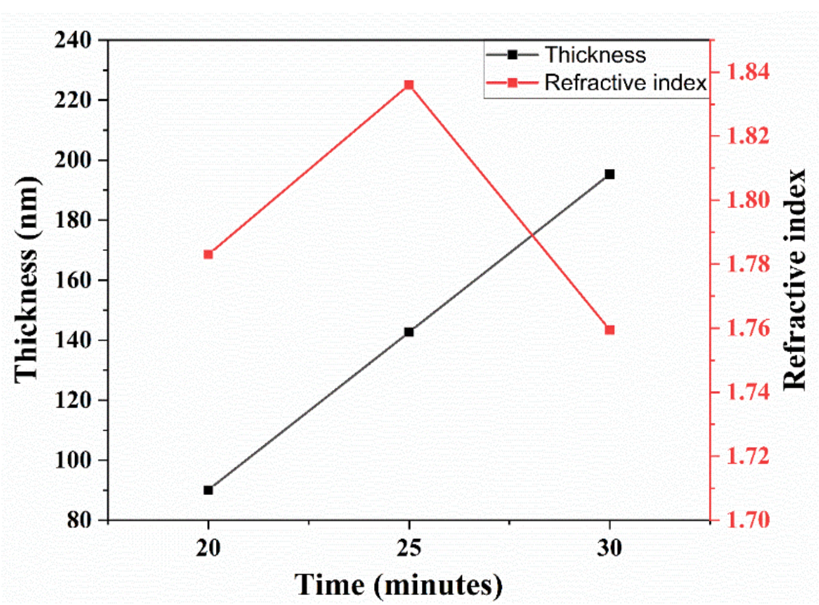

Fig. 3.6 Refractive index and thickness of deposited samples at various deposition times by using vinyl silane.

Here it is noticeable that the refractive index (RI) of deposited thin films is not uniform, when it should be constant for every thickness in these thin films. The compositional change of thin films can be the reason for this variation of the RI, which can be due to the dissociation process of different molecules with time, which may consequently alter the value of the RI [15]. The differences in the bonding states of various thin films are clearly noticeable from FTIR and XPS spectra, which are justified by the variation of deposition time, and the composition modification of the film affects the variation of the RI [9].

Besides, the substrate temperature may also change due to the hitting of hot electrons in the chamber, which may alter radicals sticking coefficient and surface mobility [16]. This might modifies the deposition kinetics, which can also be the cause for the variation of RI [9].

3.2.2.3. Photo-Luminescence Spectroscopy

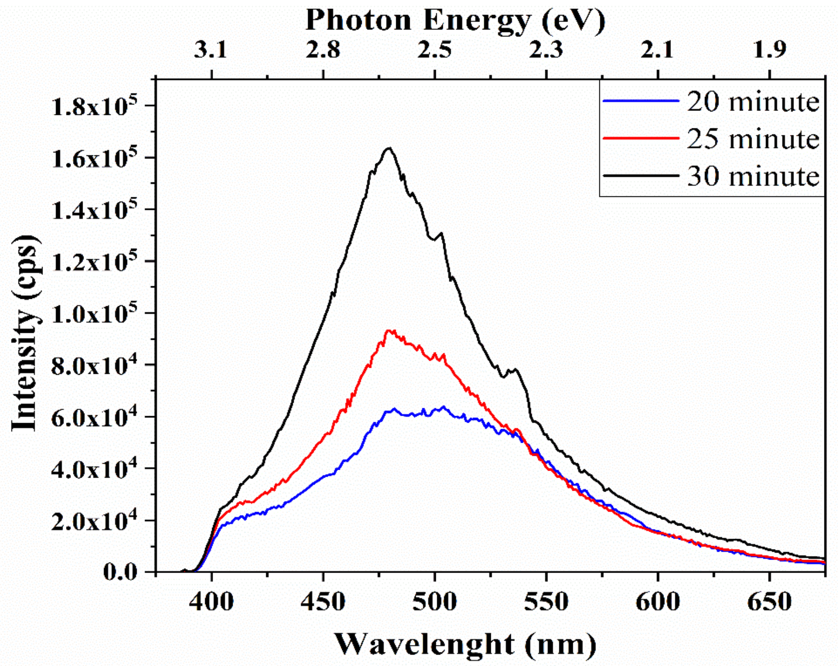

Fig. 3.7 PL spectra of deposited samples at at room temperature for various deposition times by using vinyl silane.

The PL spectra for different deposition conditions are shown in Fig. 3.7. Broad and intense PL spectra are observed, and their peaks are positioned at 480 nm (2.7 eV) for the deposited samples. The intensity of the PL are proportionally dependent on the thickness of

the deposited samples [2]. Tunneling luminescence theory was also used to describe PL at 2.7 eV in amorphous materials, which carries one radiative and two non-radiative recombination centers [30], [31].

PL at 2.7 eV can be described by many other causes such as a triplet–singlet transition of a molecule-like oxygen deficiency center, either the neutral oxygen vacancy (NOV); the twofold coordinated Si atom [32]; ion implantation of Si^{+} and C^{+} or SiC nanocluster [9], [17], [21].

Some previous works had mentioned Quantum Confinement Effect (QCE) as one of the potential reasons for the origin of PL emission [9], [23], [33]. The study of PLE spectra and TRPL can assist in identifying additional information about the PL emission, e.g., the origin of Photo-Luminescence.

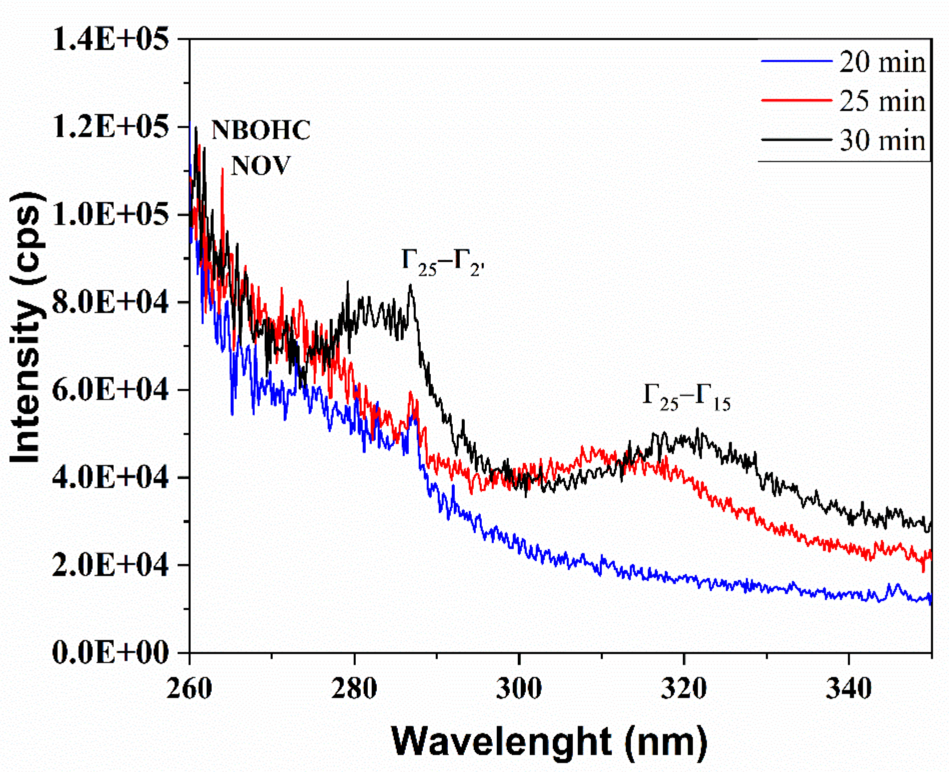

Fig. 3.8 PLE spectra of as deposited thin films by using vinyl silane.

PLE spectra is shown in Fig. 3.8 for deposited samples at different times. The excitation energy was selected according to the peak of PL emission spectra. Hence, 480 nm or 2.65 eV was tuned as excitation energy for obtaining PLE spectra. Different excitation bands

can be observed in PLE spectra from 260 nm to 350 nm. The excitation band at 265 nm of PLE spectra is referred to as the Non-Bridging Oxygen Hole Center (NBOHC) and Oxygen-Deficiency Centers (ODC)-related defects. Here, it is notable that neutral oxygen vacancy (NOV) related defect centers, whose PL emission bands around 630 and 460 nm on PL spectra, respectively [7], [34], [35], are shown. Other excitation bands, such as 285 and 320 nm, show direct optical transitions and these bands are represented by the absorption transition (Γ_{25}- $\Gamma_{2'}$) and (Γ_{25}- Γ_{15}), respectively [36], [37]. These transitions and observed shifts usually correspond either to aSi-NCs or Si-NCs in the SiO_xC_y matrix [36].

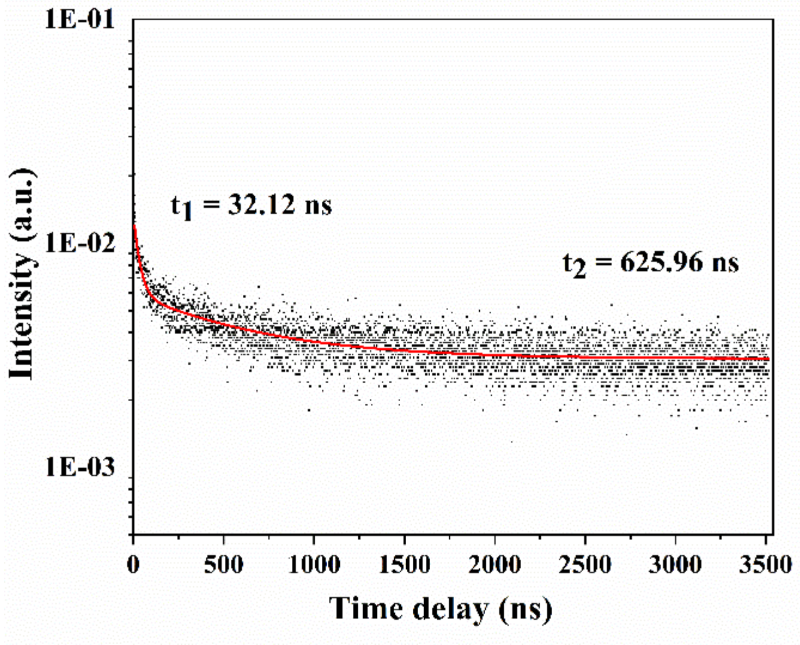

Fig. 3.9 PL lifetime decay measurements (TRPL) for a 30 min. deposited sample by using vinyl silane.

Time-resolved PL (TRPL) measurements were also performed to elucidate and understand the origin of PL emissions. Measurements were made in the same PL system using a pulsed beam with a wavelength of 250 nm, with pulses 1ns wide, and a power of 1-2 pJ / pulse. Fig. 3.9 illustrates the TRPL measurements for the sample deposited during 30 min. Different lifetimes were obtained after using an exponential function in the following adjustment curve:

$$y = y_0 + A_1 e^{-x/t_1} + A_2 e^{-x/t_2} \quad \text{.......................} \quad (3.1)$$

After using the above equation (3.1), different components in lifetimes can be distinguished, i.e., short lifetimes in the order of a few nanoseconds (32 ns) and long lifetimes in the order of microseconds (626 ns). Here, the lifetime near the few ns (32 ns) corresponds to the presence of different defects in the SiOC matrix, mainly oxygen deficient centers, particularly NOV and E'_{δ} centers [38]. Furthermore, carbon-related NOV-type defects have also been shown to have a lifetime in this range which may contribute to emissions in the blue region [18]. Moreover, another lifetime (626 ns) corresponds to a quantum confinement effect in silicon nanocrystals [39], [40].

3.3. General Discussion

The practicability of SiO_xC_y thin film formation has been discussed using the O-Cat CVD technique with safer silicon based organometallic precursors, i.e., MMS and vinyl silane. In the case of MMS deposited thin films, The Si-O-Si stretching bonds showed a shift from its stoichiometry value in FTIR analysis, which may control the composition and intensity of PL emission spectra, while the formation of the SiO_xC_y matrix was corroborated by XPS analysis. An intense PL spectrum was noticed in a wide range of visible spectra with a blue shift which can be due to the decrease of Si-C bondings in the thin films. On the other hand, the presence of SiO_xC_y matrix was also confirmed in the case of vinyl silane deposited thin films by FTIR analysis. This matrix also showed the PL emission which was comparatively lower than MMS deposited thin films. The potential reasons for the origin of PL emission were also discussed for the thin films deposited with both precursors, i.e., MMS and vinyl silane, but additional research could provide more details to confirm the origin of the PL mechanism. This work could be important for some possible applications based on low-cost Si-based optoelectronic devices with a safer precursor [2].

References

[1] W. Kern and D. A. Puotinen, "Cleaning solutions based on hydrogen peroxide for use in silicon semiconductor technology," in *RCA Review*, vol. 31, no. 2, J. A. Amick, Ed. 1970, pp. 187–206.

[2] M. Jain, J. R. Ramos-serrano, A. Dutt, and Y. Matsumoto, "The influence of deposition time on the photoluminescent properties of SiO_xC_y thin films obtained by Cat-CVD from monomethyl silane precursor," *Mater. Lett.*, vol. 291, p. 129547, 2021, doi: 10.1016/j.matlet.2021.129547.

[3] P. G. Pai, S. S. Chao, Y. Takagi, and G. Lucovsky, "Infrared spectroscopic study of SiO_x films produced by plasma enhanced chemical vapor deposition," *J. Vac. Sci. Technol. A Vacuum, Surfaces, Film.*, vol. 4, no. 3, pp. 689–694, 1986, doi: 10.1116/1.573833.

[4] W. Kaiser, P. H. Keck, and C. F. Lange, "Infrared absorption and oxygen content in silicon and germanium," *Phys. Rev.*, vol. 101, no. 4, pp. 1264–1268, 1956, doi: 10.1103/PhysRev.101.1264.

[5] A. V. Vasin *et al.*, "The effect of deposition processing on structural and luminescent properties of a-SiOC:H thin films fabricated by RF-magnetron sputtering," *J. Lumin.*, vol. 191, pp. 102–106, 2017, doi: 10.1016/j.jlumin.2016.10.029.

[6] A. P. Baraban, S. N. Samarin, V. A. Prokofiev, V. A. Dmitriev, A. A. Selivanov, and Y. Petrov, "Luminescence of SiO_2 layers on silicon at various types of excitation," *J. Lumin.*, vol. 205, pp. 102–108, 2019, doi: 10.1016/j.jlumin.2018.09.009.

[7] J. R. Ramos-Serrano, Y. Matsumoto, A. Méndez-Blas, A. Dutt, C. Morales, and A. I. Oliva, "Luminescent silicon oxycarbide thin films obtained with monomethyl-silane by hot-wire chemical vapor deposition," *J. Alloys Compd.*, vol. 780, pp. 341–346, 2019, doi: 10.1016/j.jallcom.2018.11.353.

[8] C. Y. Kim, H. S. Lee, C. K. Choi, and Y. H. Yu, "Method of sealing pores in porous low-k SiOC(-H) films fabricated using plasma-assisted atomic layer deposition," *J. Korean Phys. Soc.*, vol. 62, no. 8, pp. 1143–1149, 2013, doi: 10.3938/jkps.62.1143.

[9] M. Jain, J. R. Ramos-Serrano, A. Dutt, and Y. Matsumoto, "Photoluminescence properties of thin-film SiO_xC_y deposited by O-Cat CVD technique using MMS and

TEOS," in *2020 17th International Conference on Electrical Engineering, Computing Science and Automatic Control (CCE). Mexico City, Mexico. November 11-13*, 2020, pp. 1–6, doi: 10.1109/cce50788.2020.9299113.

[10] A. A. Langford, M. L. Fleet, B. P. Nelson, W. A. Lanford, and N. Maley, "Infrared absorption strength and hydrogen content of hydrogenated amorphous silicon," *Phys. Rev. B*, vol. 45, no. 23, pp. 13367–13377, 1992.

[11] H. Wieder, M. Cardona, and C. R. Guarnieri, "Vibrational spectrum of hydrogenated amorphous Si-C films," *Phys. Status Solidi*, vol. 92, no. 1, pp. 99–112, 1979, doi: 10.1002/pssb.2220920112.

[12] J. Huang *et al.*, "An interfacial crosslinking strategy to fabricate an ultrathin two-dimensional composite of silicon oxycarbide-enwrapped silicon nanoparticles for high-performance lithium storage," *J. Mater. Chem. A*, vol. 7, no. 40, pp. 22950–22957, 2019, doi: 10.1039/c9ta07738c.

[13] H. Xu *et al.*, "In situ preparation of C-SiC_xO_y coatings with controllable composition on continuous oxygen-enriched SiC fibres," *RSC Adv.*, vol. 9, no. 3, pp. 1319–1326, 2019, doi: 10.1039/c8ra09095e.

[14] A. Avila, I. Montero, L. Galán, J. M. Ripalda, and R. Levy, "Behavior of oxygen doped SiC thin films: An x-ray photoelectron spectroscopy study," *J. Appl. Phys.*, vol. 89, no. 1, pp. 212–216, 2001, doi: 10.1063/1.1332796.

[15] R. T. Holm, S. W. McKnight, E. D. Palik, and W. Lukosz, "Interference effects in luminescence studies of thin films," *Appl. Opt.*, vol. 21, no. 14, p. 2512, 1982, doi: 10.1364/ao.21.002512.

[16] B. P. Swain and R. O. Dusane, "Effect of substrate temperature on HWCVD deposited a-SiC:H film," *Mater. Lett.*, vol. 61, no. 25, pp. 4731–4734, 2007, doi: 10.1016/j.matlet.2007.03.029.

[17] L. Rebohle, T. Gebel, H. Fröb, H. Reuther, and W. Skorupa, "Ion beam processing for Si/C-rich thermally grown SiO_2 layers: Photoluminescence and microstructure," *Appl. Surf. Sci.*, vol. 184, pp. 156–160, 2001, doi: 10.1016/S0169-4332(01)00490-1.

[18] V. Nikas *et al.*, "The origin of white luminescence from silicon oxycarbide thin films," *Appl. Phys. Lett.*, vol. 061906, no. 104, pp. 1–5, 2014, doi: 10.1063/1.4865100.

[19] A. Dutt, Y. Matsumoto, S. Godavarthi, G. Santana-Rodríguez, J. Santoyo-Salazar, and A. Escobosa, "White bright luminescence at room temperature from TEOS-based thin films via catalytic chemical vapor deposition," *Mater. Lett.*, vol. 131, pp.

295–297, 2014, doi: 10.1016/j.matlet.2014.05.206.

[20] I. Hinić, G. Staniŝić, and Z. Popović, "Influence of the synthesis conditions on the photoluminescence of silica gels," *J.Serb.Chem.Soc.*, vol. 68, no. 12, pp. 953–959, 2003, doi: https://doi.org/10.2298/JSC0312953H.

[21] A. V. Vasin *et al.*, "The effect of deposition processing on structural and luminescent properties of a-SiOC:H thin films fabricated by RF-magnetron sputtering," *J. Lumin.*, vol. 191, pp. 102–106, 2017, doi: 10.1016/j.jlumin.2016.10.029.

[22] L. Skuja, "Optically active oxygen-deficiency-related centers in amorphous silicon dioxide," *J. Non. Cryst. Solids*, vol. 239, no. 1–3, pp. 16–48, 1998, doi: 10.1016/s0022-3093(98)00720-0.

[23] Y. Matsumoto *et al.*, "Luminescence study of Si/SiC Nano-particles embedded in SiO_xC_y matrix deposited using O-Cat-CVD," *Phys. E Low-dimensional Syst. Nanostructures*, vol. 111, no. March, pp. 179–184, 2019, doi: 10.1016/j.physe.2019.03.024.

[24] A. Kleinová, J. Huran, V. Sasinková, M. Perný, V. Šály, and J. Packa, "FTIR spectroscopy of silicon carbide thin films prepared by PECVD technology for solar cell application," *Reliab. Photovolt. Cells, Modul. Components, Syst. VIII*, vol. 9563, no. 95630U, pp. 1–8, 2015, doi: 10.1117/12.2186748.

[25] Z. G. Sun, S. J. Wang, X. J. Qiao, Y. Li, W. H. Zheng, and P. Y. Bai, "Synthesis and microwave absorbing properties of SiC nanowires," *Appl. Phys. A Mater. Sci. Process.*, vol. 124, no. 12, pp. 1–8, 2018, doi: 10.1007/s00339-018-2202-4.

[26] J. R. Ramos, C. Morales, and Y. Matsumoto, "Oxygen concentration effect on properties of SiOC thin films obtained by HWCVD," *2017 14th Int. Conf. Electr. Eng. Comput. Sci. Autom. Control. CCE 2017*, pp. 1–4, 2017, doi: 10.1109/ICEEE.2017.8108846.

[27] F. Rubio, J. Rubio, and J. L. Oteo, "A FT-IR study of the hydrolysis of Tetraethylorthoselicate (TEOS)," *Spectrosc. Lett.*, vol. 31, no. 1, pp. 199–219, 1998, doi: 10.1080/00387019808006772.

[28] S. Park, B. Parida, and K. Kim, "Thin film solar cells with Si nanocrystallites embedded in amorphous intrinsic layers by hot-wire chemical vapor deposition," *J. Nanosci. Nanotechnol.*, vol. 13, no. 5, pp. 3397–3402, 2013, doi: 10.1166/jnn.2013.7312.

[29] H. Yamada and W. B. Person, "Absolute Infrared Intensities of the Fundamental

Absorption Bands in Solid CO_2 and N_2O," *J. Chem. Phys.*, vol. 41, no. 8, pp. 2478–2487, 1964, doi: 10.1063/1.1726291.

[30] S. Sato, H. Ono, S. Nozaki, and H. Morisaki, "Photoluminescence study on Oxygen-containing silicon nanostructures," *Nanostructured Mater.*, vol. 5, no. 5, pp. 589–598, 1995, doi: 10.1016/0965-9773(95)00269-K.

[31] R. A. Street, "Luminescence in amorphous semiconductors," *Adv. Phys.*, vol. 25, no. 4, pp. 397–453, 1976, doi: http://dx.doi.org/10.1080/00018737600101412.

[32] L. Rebohle, J. Von Borany, H. Fröb, and W. Skorupa, "Blue photo- and electroluminescence of silicon dioxide layers ion-implanted with group IV elements," *Appl. Phys. B Lasers Opt.*, vol. 71, no. 2, pp. 131–151, 2000.

[33] J. R. Ramos-Serrano, Y. Matsumoto, and C. Morales, "Luminescent Silicon Oxycarbide Thin Films via Hot-wire CVD using Tetraethyl Orthosilicate: Role of the Chamber Pressure and Post-deposition Annealing," *2018 15th Int. Conf. Electr. Eng. Comput. Sci. Autom. Control. CCE 2018*, pp. 1–4, 2018, doi: 10.1109/ICEEE.2018.8533970.

[34] A. Podhorodecki, G. Zatryb, L. W. Golacki, J. Misiewicz, J. Wojcik, and P. Mascher, "On the origin of emission and thermal quenching of SRSO:Er^{3+} films grown by ECR-PECVD," *Nanoscale Res. Lett.*, vol. 8, no. 98, pp. 1–12, 2013, doi: https://doi.org/10.1186/1556-276X-8-98.

[35] L. Palacios-Huerta, S. A. Cabañas-Tay, M. A. Cardona-Castro, M. Aceves-Mijares, C. Domínguez-Horna, and A. Morales-Sánchez, "Structural and optical properties of silicon rich oxide films in graded-stoichiometric multilayers for optoelectronic devices," *Appl. Phys. Lett.*, vol. 109, no. 3, 2016, doi: 10.1063/1.4959080.

[36] A. Podhorodecki, J. Misiewicz, F. Gourbilleau, and R. Rizk, "Absorption mechanisms of silicon nanocrystals in cosputtered silicon-rich-silicon oxide films," *Electrochem. Solid-State Lett.*, vol. 11, no. 3, pp. 60–62, 2008, doi: 10.1149/1.2828207.

[37] J. P. Wilcoxon and G. A. Samara, "Tailorable , visible light emission from silicon nanocrystals," *Appl. Phys. Lett.*, vol. 74, no. 21, pp. 3164–3166, 1999.

[38] G. R. Lin, C. J. Lin, and K. C. Yu, "Time-resolved photoluminescence and capacitance-voltage analysis of the neutral vacancy defect in silicon implanted SiO_2 on silicon substrate," *J. Appl. Phys.*, vol. 96, no. 5, pp. 3025–3027, 2004, doi: 10.1063/1.1775041.

[39] C. Bulutay and S. Ossicini, *Electronic and Optical Properties of Silicon*

Nanocrystals. 2010.

[40] J. Joo *et al.*, "Enhanced quantum yield of photoluminescent porous silicon prepared by supercritical drying," *Appl. Phys. Lett.*, vol. 108, no. 153111, pp. 1–5, 2016, doi: 10.1063/1.4947084.

CHAPTER 4
SiO_xC_y THIN FILMS DEPOSITED WITH TEOS

4.1. Experimental Details

An organic catalytic chemical vapor deposition (O-Cat-CVD) system was used as shown in Fig. 2.1 (b) to deposit silicon oxycarbide (SiO_xC_y) thin films. These SiO_xC_y thin films were deposited on polished P-type crystalline silicon substrate with (100) orientation (resistivity 1-10 Ω-cm) by using Tetraethyl orthosilicate [TEOS; ($Si(OC_2H_5)_4$)] precursor. The substrate was cleaned using the RCA method as explained in chapter 3 [1]. Furthermore, TEOS liquid precursor was purchased from Sigma-Aldrich Company with a purity of 98%, and the product code and case Nos. are 131903 and 78-10-4, respectively. Moreover, argon gas was also used as a reactant gas. This O-Cat-CVD system has one mechanical vacuum pump where the initial pressure of the chamber reaches up to 0.08 torr.

In this work, the effect of argon flow and deposition time were evaluated separately, so these parameters, i.e., the flow of argon and deposition time, were kept as variable parameters for preparing thin films, respectively [2], [3]. Moreover, the effect of the deposition time was also observed for the monocrystalline silicon solar cells. During all the depositions, the chamber's working pressure (Ps) was constant at 0.30 Torr. Furthermore, mass flow controllers and filament temperature control systems are also presented. A Tungsten (W) wire (0.75 mm diameter) was used as a catalyst with a distance between the substrate and the filament of 5 cm. The substrate (T_s) and filament (T_f) temperatures were 200ºC and 1800ºC, respectively. The filament temperature is monitored throughout the process using an infrared camera (Chinese Brand Model IR-AHS) through the window of the corresponding chamber.

4.2. Results and discussions

Three sections are used to understand the properties of SiO_xC_y thin films deposited by TEOS precursor. The effect of argon flow will be explained in the first section, while the

second section is dedicated to understanding the effect of deposition duration on SiO_xC_y thin films. Finally, the third section is dedicated to understanding the effect of SiO_xC_y thin films on solar cells with the variation in deposition time and the downshifting effect.

4.2.1. Effect of the argon flow on SiO_xC_y thin films

In this work, the effect of the argon flow was observed on the Photo-Luminescence (PL) properties of the SiO_xC_y thin films. The argon flow was variable from 20-60 sccm for the constant deposition time of 30 minutes.

4.2.1.1. Fourier Transform Infrared (FTIR) Spectroscopy

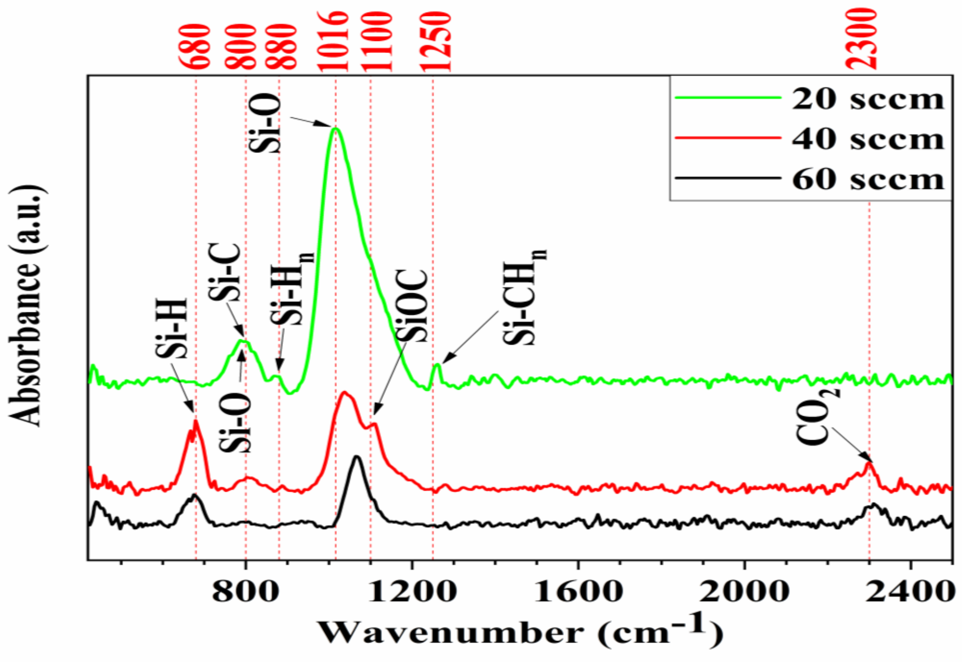

Fig. 4.1 FTIR spectra of the as-deposited samples at various argon flows by using TEOS [3].

The FTIR spectra of SiO_xC_y thin films with the variation of argon flow is shown in Fig. 4.1, where the influence of argon flow is noticeable on the absorption bands. Normally, the rocking, bending, and stretching vibrational modes for the Si-O-Si bonding are noticed at 470, 800, and 1080 cm^{-1}, respectively, but the stretching vibrational mode of the Si-O-Si bond is observed with a shift from its stoichiometry value for different argon flow [4], [5]. This shift from the stoichiometry value of Si-O-Si bond corresponds to the oxygen deficiency in Si-O-Si bonding, which may cause a higher possibilities of having one or more silicon or carbon neighboring atoms [5]–[7]. This stoichiometry and/or composition

modifications in the oxide layer allow controlling the Photo-Luminescence (PL) intensity and its spectral composition [8].

The intensity of the Si-O stretching bond demonstrates an anti-proportional phenomenon with the variation of argon flow. This phenomenon can be associated with the Brownian motion of argon atoms, which changes the kinetics of the CVD process [3], [9]. An absorption band can also be noticed at 1100 cm^{-1}, which refers to the presence of Si-O-C bonds and confirming the formation of SiO_xC_y thin film [10].

Furthermore, the absorption bands at 680, 800, 880, 1250, and 2300 cm^{-1} refer to the Si-H, Si-C, Si-H_n, Si-CH_n, and CO_2 bondings, respectively. It can be easily observable in Fig. 4.1 that the intensity of Si-bound carbon and hydrogen bondings are abating with the increase of argon flow. This behavior can be due to the existence of a higher flow of inert argon, which firstly decomposes the ethyl radical coupled with the outer part of the TEOS molecule [2], [3], [11], [12].

4.2.1.2. X-Ray Photoelectron Spectroscopy (XPS)

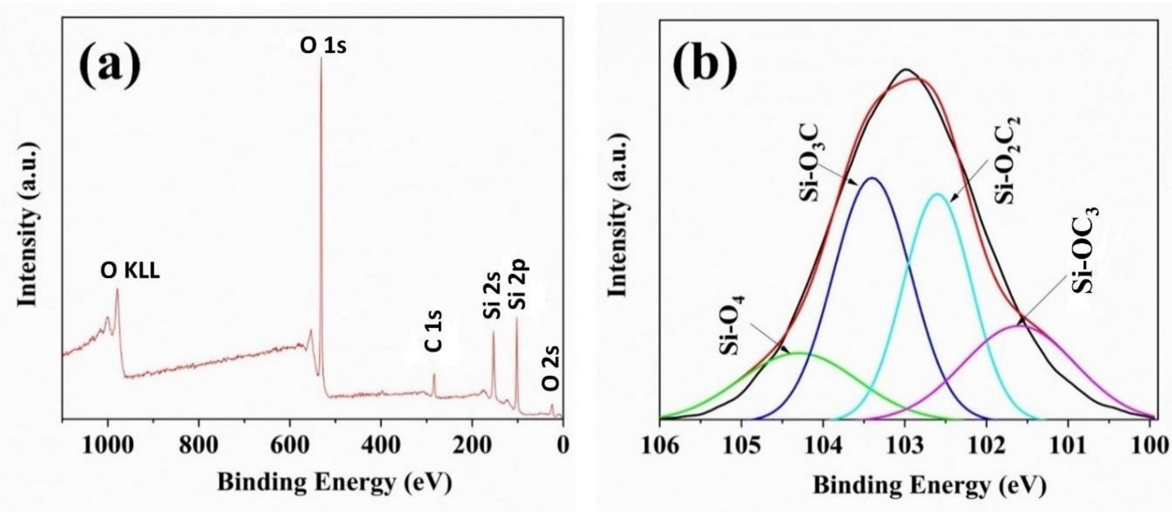

Fig. 4.2 a) XPS Spectrum b) Si 2p XPS fitted spectrum for the deposited sample at 20 sccm argon flow by using TEOS [3].

The chemical analysis of the deposited sample for 20 sccm argon flow is characterized by XPS and illustrated in the above Fig. 4.2. This analysis facilitates understanding the shifting of Si-O stretching bond and their high intensity through different SiO_xC_y phases

for this thin film. Different elemental peaks such as Si 2p, C 1s, and O 1s peaks are noticeable in Fig. 4.2 (a). At the same time, four types of gaussian deconvoluted bonding phases as SiC_3O, SiC_2O_2, $SiCO_3$, and SiO_4 of Si 2p Spectra are illustrated in Fig. 4.2 (b) and mentioned in Table 4.1 for binding energy at 101.6 eV, 102.6 eV, 103.4 eV and 104.3 eV, respectively [13] and the full width at half maximum (FWHM) of these bonding phases were 1.62, 1, 1.12 and 1.71, respectively. The high presence of SiC_3O, SiC_2O_2 and $SiCO_3$ bonding phases confirms the SiO_xC_y content in the thin film. These XPS results also relate with the FTIR results, where the bonding of carbon and/or silicon atoms were explained with Si-O stretching bonds [3].

Table 4.1 The relative content of the different bonding phases of si 2p spectra calculated by the XPS fitted results [3], [13].

Bonding	BE (eV)	Atomic %
SiC_3O	101.60	20.1
SiC_2O_2	102.60	29.0
$SiCO_3$	103.40	35.6
SiO_4	104.30	15.2

4.2.1.3. Ellipsometry

Fig. 4.3 illustrates the thickness and the RI of the deposited samples and their corresponding values are mentioned in Table 4.2, respectively. Here, the dependence of thickness and RI on argon gas flow is analyzed. The RI of deposited thin films is near 1.45 to 1.46 while the thickness increases anti-proportionally with the flow of argon from 68.7 nm to 152.8 nm, respectively. Here, it is noticeable that the variation of the argon gas flow affects the refractive index and the thickness of the deposited thin films, because it influences the growth rate and structure of the thin film. It is worth mentioning that argon gas cannot ionize in O-Cat CVD because the ionization energy of argon gas is very high (15.8 eV), due to which inert argon gas has a large electron collision cross-section. This phenomenon instantly cools down the produced electrons by the hot tungsten filament, which causes the decrease of the dissociation of molecules at the filament, and this is the cause for the decline in the thickness of thin film with the elevation of argon gas [3], [14], [15].

Here, it is also noticeable that the RI of deposited films is altered, when it is expected to be constant for every thickness in these thin films. This variation of the RI can be due to the compositional change of thin films due to the different molecule dissociation processes with the presence of argon gas in the chamber, which may subsequently alter the RI [16]. The variation in the bonding states of different thin films is clearly noticeable from the FTIR and XPS spectra. This justifies the variation of argon flow, and the composition variation of the film causes the change of RI [2].

Table 4.2 Refractive index and thickness of samples by ellipsometry.

Argon Flow (sccm)	Thickness (nm)	Refractive Index (RI)
20	152.8 ± 0.1	1.45 ± 0.002
40	91.3 ± 0.1	1.46 ± 0.002
60	68.7 ± 0.1	1.45 ± 0.002

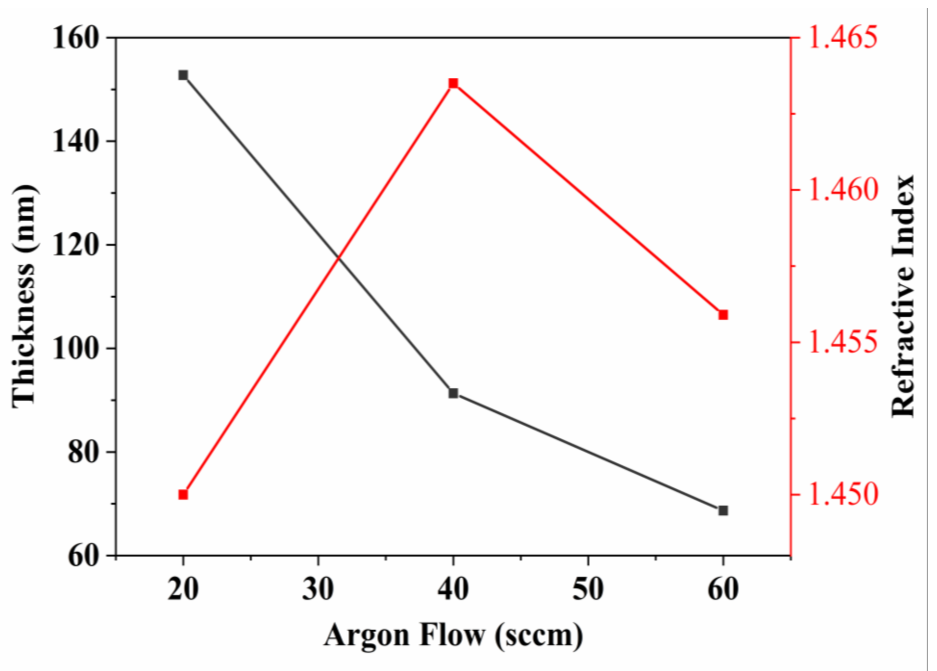

Fig. 4.3 Thickness and refractive index of as-deposited samples at various argon flow by using TEOS [3].

4.2.1.4. Photo-Luminescence Spectroscopy

The PL spectra for different deposition conditions are shown in Fig. 4.4. A broad and intense PL spectra is observed from 385 to 700 nm in the visible region, and the PL peak is

noticeable at 477 nm (2.7 eV) at various flows of argon. Furthermore, a PL shoulder is also observed at 550 nm for the deposited films at 40 and 60 sccm flow of argon.

The intensity of PL is directly proportional to the thickness of the deposited film [4], and the thickness of the thin film grows with the abatement of argon flow, as shown in Table 4.2. Therefore, the high intensity of PL is achieved when the presence of argon is less in the chamber environment during deposition [3].

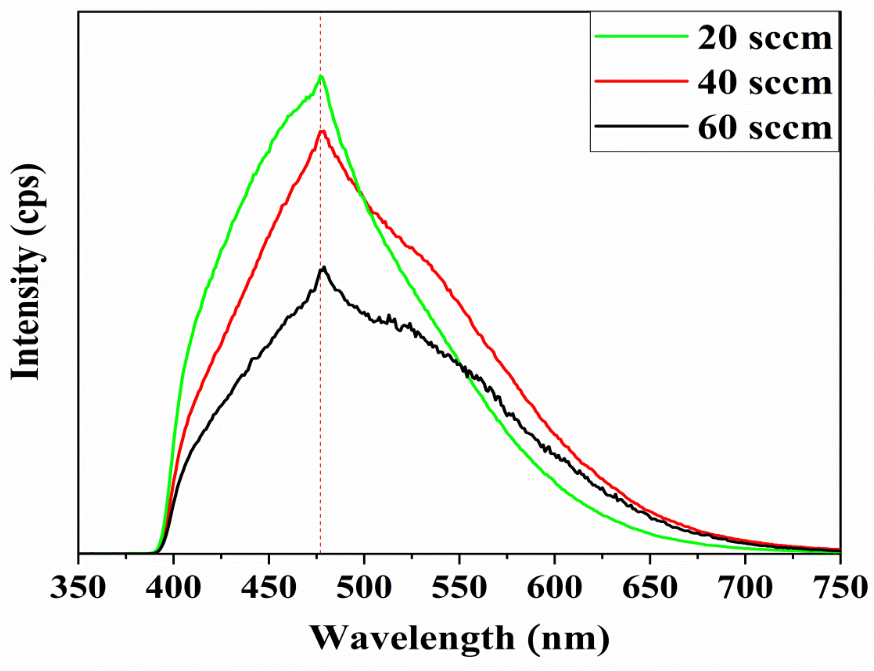

Fig. 4.4 PL spectra of samples obtained at at room temperature for different argon flows by using TEOS [3].

Furthermore, the origin of Photo-Luminescence at 477 nm or 2.7 eV at the spectra is explained in various ways, including the tunneling luminescence theory in amorphous materials, which holds one radiative and two non-radiative recombination centers [17], [18]. Additionally, ion implantation of Si^{+} and C^{+} or SiC nanocluster and the presence of defects related to C or Si due to non-stoichiometric composition, can also be the further causes for the PL emission at 2.7 eV of the spectra [4], [19]–[22]. Besides, carbon-related neutral oxygen vacancy (NOV) defects, oxygen deficiency centers, Si-related NOV, or non-bridging oxygen hole center (NBOHC) can also be probable reasons for the PL emission in the visible region [23], [24]. Here, It is noteworthy that the NOV defect density and crystallinity of thin film are a function of argon gas [12], and consequently the

presence of an argon environment during the deposition impacts the PL emission properties as well [3]. Besides it, a PL emission at 550 nm can be related to the presence of carbon-related bonding in the deposited thin films [4].

However, these previously mentioned PL emission processes may not be the only cause for the emission of the PL spectra. Quantum Confinement Effect (QCE) can be another probable reason for the PL emission in the visible range [19], [25]. These phenomena can play a vital role to achieve the required optoelectronic devices.

4.2.2. Effect of the deposition time on SiO_xC_y thin films

In this section, the effect of deposition time was evaluated on the Photo-Luminescence (PL) properties of the SiO_xC_y thin films. The deposition time was variable from 20 to 30 minutes for the constant deposition argon flow of 40 sccm.

4.2.2.1. Fourier Transform Infrared (FTIR) Spectroscopy

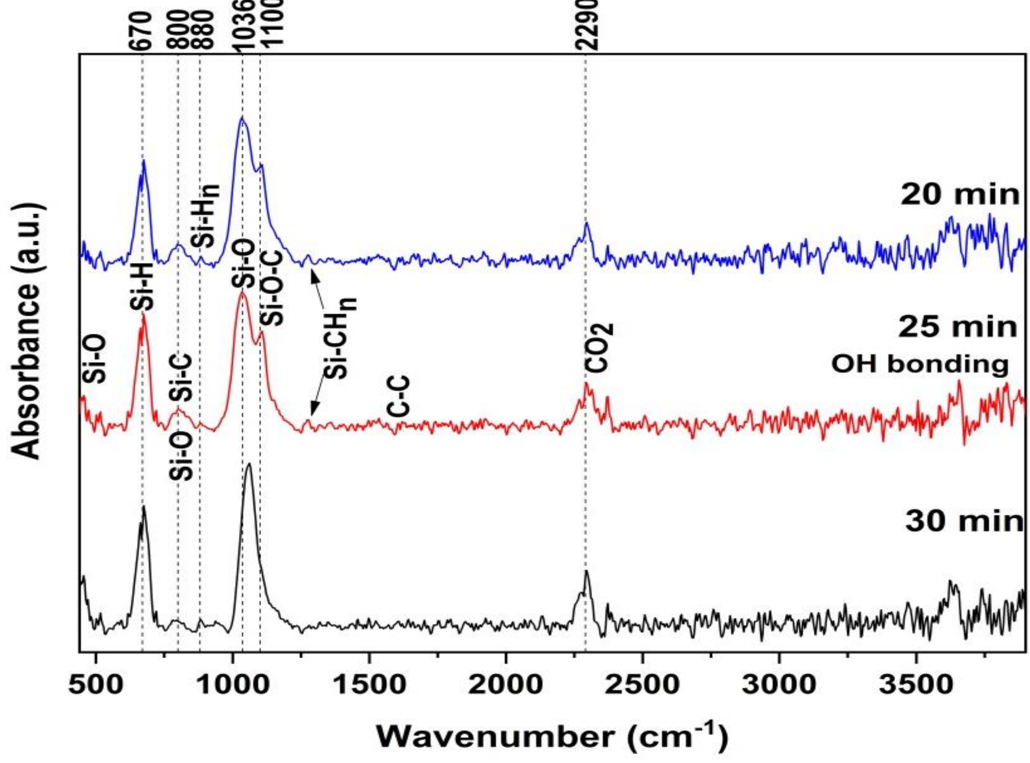

Fig. 4.5 FTIR spectra of deposited samples at various deposition times by using TEOS [2].

The FTIR spectra are shown in Fig. 4.5, where the influence of deposition time is noticeable on the absorption bands. Normally, the rocking, bending, and stretching vibrational modes for the Si-O-Si bonding are observed at 470, 800, and 1080 cm^{-1}, respectively, but the stretching vibrational mode of the Si-O-Si bond is positioned at 1036 cm^{-1} [4]. Hence, deposited films show a shift from the stoichiometry value of the Si-O-Si (1080 cm^{-1}) absorption band [5]. As it was discussed already, this shift from the stoichiometry value of Si-O-Si bond corresponds to the oxygen deficiency in Si-O-Si bonding, which may cause a higher possibilities of having one or more silicon or carbon neighboring atoms [5]–[7]. This stoichiometry and/or composition modifications in the oxide layer allow controlling the Photo-Luminescence (PL) intensity and its spectral composition [8]. An absorption band can additionally be noticed at 1100 cm^{-1}, which refers to the presence of Si-O-C bonds and confirming the formation of SiO_xC_y thin film [10]. It is also noticeable that the absorption band at 1100 cm^{-1} tends to disappear with the increment of deposition time in these thin films and Si-O-Si stretching mode is also shifting from 1036 to 1060 cm^{-1}. This phenomenon shows that the nature of TEOS-deposited thin films is similar to SiO_x films with the increment of deposition time [2].

The reason for this shift in the Si-O-Si stretching bonds can be associated with the molecular structure of TEOS. A molecular structure of TEOS is shown in Fig. 2.3 (c) and there it can be seen that the four oxygen atoms of a TEOS molecule are innately bounded by silicon atoms and the ethyl radicals are attached in the outer part of the molecule. These ethyl radicals got dissociated, first from the TEOS molecule during the dissociation process, due to which much of the carbon is transported out of the reaction zone as a by-product with the increment of deposition time [2], [26], [27]. Additionally, the effect of dissociation of ethyl radicals can also be observable on the Si–C bonds absorption band, which is situated at 800 cm^{-1}. The intensity of these bonds is slightly reduced for the deposited films with higher deposition time.

In addition to these absorption bands, other absorption bands can also be observable in Fig. 4.5. Here, $Si–H_n$, Si–H, and $Si–CH_n$ bonds are also noticed at 670, 880, and 1250 cm^{-1}, respectively, while the absorption band associated to C=C, CO_2, and OH bonds are additionally noticeable at 1600, 2290, and 3600 cm^{-1}, respectively [2], [28]–[30].

4.2.2.2. X-Ray Photoelectron Spectroscopy (XPS)

The chemical analysis for a 30 min. deposited sample was characterized by XPS, and it is illustrated in Fig. 4.6. Si 2p, C 1s and O 1s XPS spectrum peaks are observable in Fig. 4.6 (a), which confirm the Si, C and O content in the thin film. Furthermore, relative contents of the different phases of the Si 2p spectra are shown in Fig. 4.6 (b) and Table 4.3. Here, the high-resolution Si 2p spectra contain $SiOC_3$, SiO_2C_2, SiO_3C, and SiO_4 phases at 101.5 eV, 102.8 eV, 103.7 eV, and 104.9 eV peaks, respectively [31]. The figure and table show that the content of $SiOC_3$, SiO_2C_2, SiO_3C and SiO_4 bond phases is 4.8 %, 19.2 %, 39.6 % and 36.4 atm%, respectively. So, this analysis justifies the presence of SiO_xC_y bondings in the thin film. Moreover, the high presence of SiO_2 bonds also confirms and correlates with the results and discussion of FTIR spectra.

Table 4.3 The relative content of the different bonding phases of si 2p spectra calculated by the XPS fitted results [2], [31].

Bonding	BE (eV)	Atomic %
SiC_3O	101.50	4.8
SiC_2O_2	102.80	19.2
$SiCO_3$	103.70	39.6
SiO_4	104.90	36.4

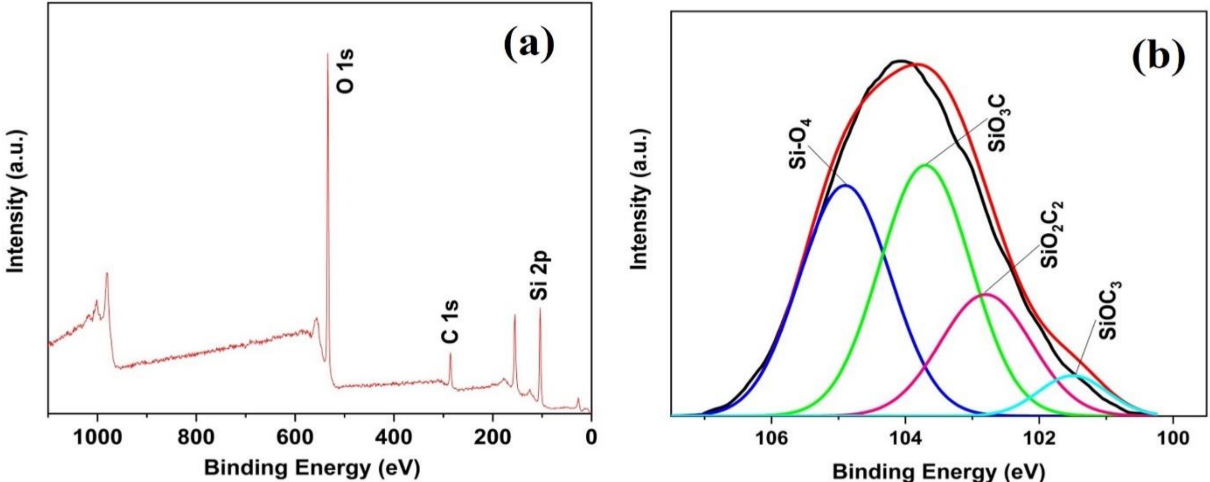

Fig. 4.6 XPS Spectrum b) Si 2p XPS for 30 min. deposited sample with TEOS precursor [2].

4.2.2.3. Ellipsometry

Fig. 4.7 illustrates the thickness and the refractive index (RI) of the deposited samples, and their corresponding values are mentioned in Table 4.4, respectively. Here, the dependence of RI and thickness on the deposition time is analyzed. The RI of deposited thin films varies from 1.39 to 1.57 while the thickness is proportionally increasing from 69.8 nm to 160 nm, respectively with the increment of deposition time.

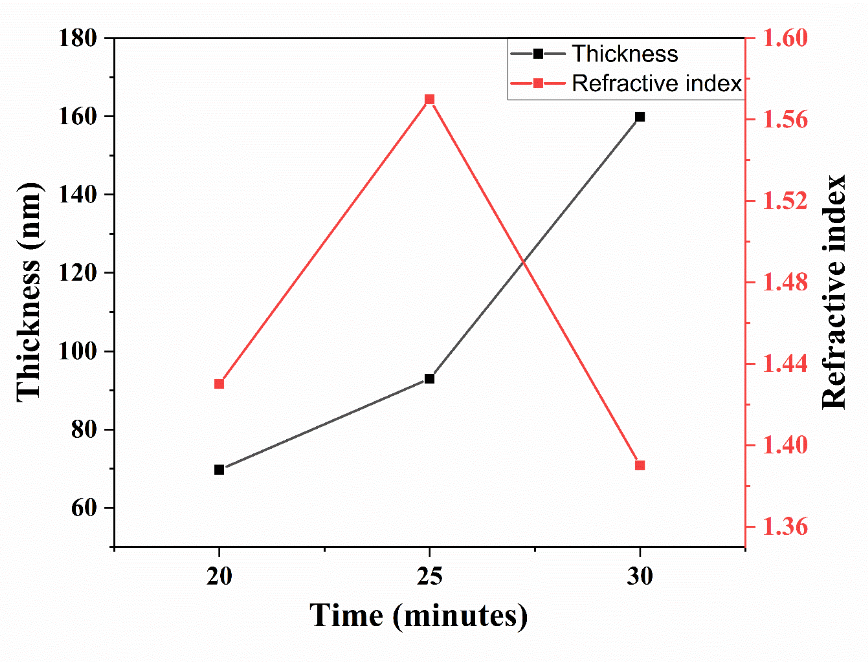

Fig. 4.7 Refractive index and thickness of deposited samples at various deposition times by using TEOS [2].

Table 4.4 Refractive index and thickness of samples by ellipsometry [2].

Deposition Duration	Thickness (nm)	Refractive Index (RI)
20	69.8 ± 0.1	1.43 ± 0.002
25	93 ± 0.1	1.57 ± 0.002
30	160 ± 0.1	1.39 ± 0.002

Here, it is noticeable that the refractive index (RI) of deposited thin films alters, when it is expected to be constant for every thickness in these thin films. The compositional change of thin films can be the reason for this variation of the RI which can be due to the dissociation process of different molecules with time, which may consequently alter the value of the RI [16]. The differences in the bonding states of various thin films are clearly

noticeable from FTIR and XPS spectra, which justify the variation with deposition time, and the composition modification of the film affects the value of RI [2].

The substrate temperature may also change due to the hitting of hot electrons in the chamber, which may alter radicals sticking coefficient and surface mobility of radicals [32]. This might modify the deposition kinetics, which can also be the cause for the refractive index variation [2].

4.2.2.4. Photo-Luminescence Spectroscopy

The PL spectra for various deposition conditions are illustrated in Fig. 4.8. A broad and intense PL spectra are observed in the visible region and the PL peak is noticeable at 477 nm (2.7 eV) at various deposition times. Furthermore, a PL shoulder is also observed at 550 nm for the deposited films.

The intensity of PL is directly proportional to the thickness of the deposited film [4], and the thickness of the thin film increases with the addition of deposition time.

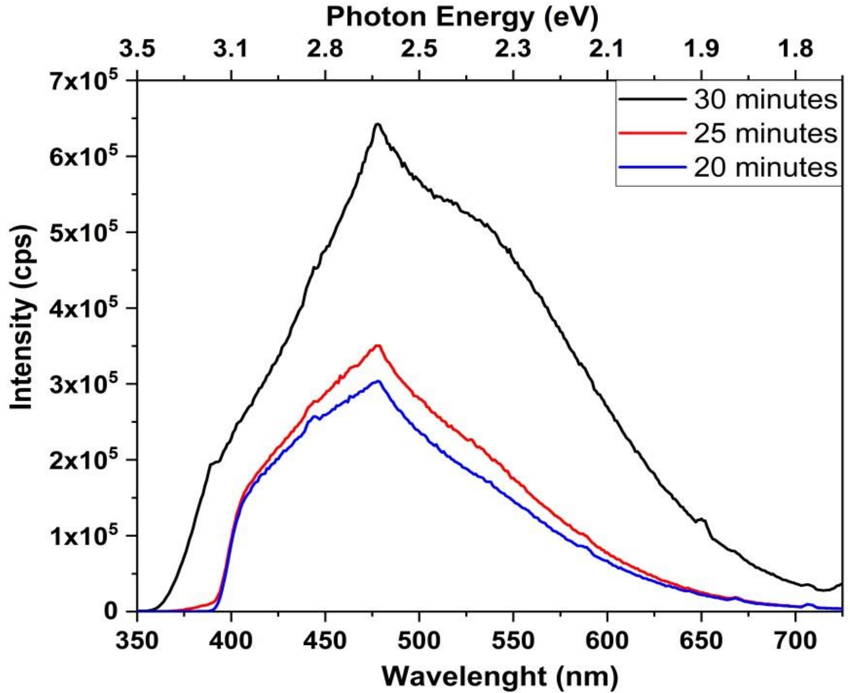

Fig. 4.8 PL spectra of deposited samples at at room temperature for various deposition times by using TEOS [2].

The origin of Photo-Luminescence at 477 nm or 2.7 eV at the spectra is explained in various ways, including the tunneling luminescence theory in amorphous materials, which holds one radiative and two non-radiative recombination centers [17], [18]. Additionally, ion implantation of Si^+ and C^+ or SiC nanoclusters and the presence of defects related to carbon or silicon due to non-stoichiometric composition can also be the other reasons for the PL emission at 2.7 eV of the spectra [4], [19]–[22]. Moreover, h carbon-related neutral oxygen vacancy (NOV) defects, oxygen deficiency centers, Si-related NOV, or non-bridging oxygen hole center (NBOHC) can also be probable reasons for the PL emission in the visible region [23], [24]. Besides, a PL emission at 550 nm can be related to carbon-related bondings in the deposited thin films [4]. Quantum Confinement Effect (QCE) can be another probable reason for the PL emission in the visible range [2], [19], [33]. The study of PLE spectra and TRPL can assist in identifying additional information about the PL emission, e.g., the origin of Photo-Luminescence.

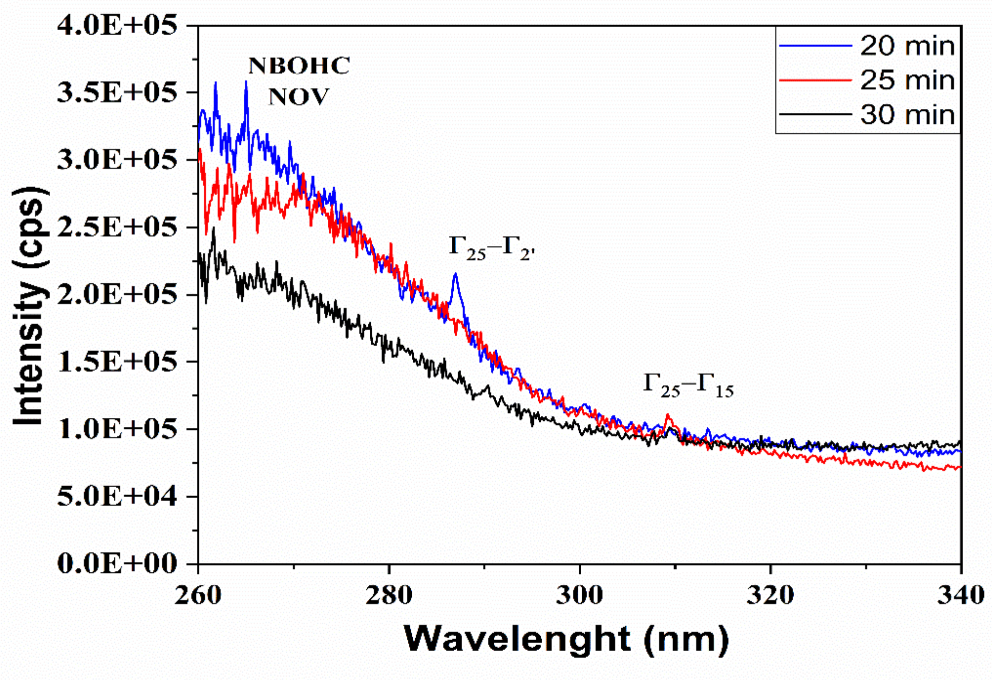

Fig. 4.9 PLE spectra of as-deposited thin films by using TEOS.

PLE spectra are shown in Fig. 4.9 for deposited samples at different times. The excitation energy was selected according to the peak of PL emission spectra. Hence, 477 nm or 2.7 eV was tuned as excitation energy for obtaining PLE spectra. Different excitation bands can be observed from 260 nm to 340 nm in PLE spectra. The excitation band at 265 nm is

referred to as the NBOHC and ODC-related defects, particularly NOV defect centers which show their PL emission bands around 630 and 460 nm, respectively [10], [34], [35]. Moreover, other excitation bands, such as 285 and 310 nm show direct optical transitions, and these bands are represented by the absorption transition (Γ_{25}- $\Gamma_{2'}$) and (Γ_{25}- Γ_{15}), respectively [36], [37]. These transitions and observed shifts usually correspond to aSi-NCs or Si-NCs in the SiO_xC_y matrix [36].

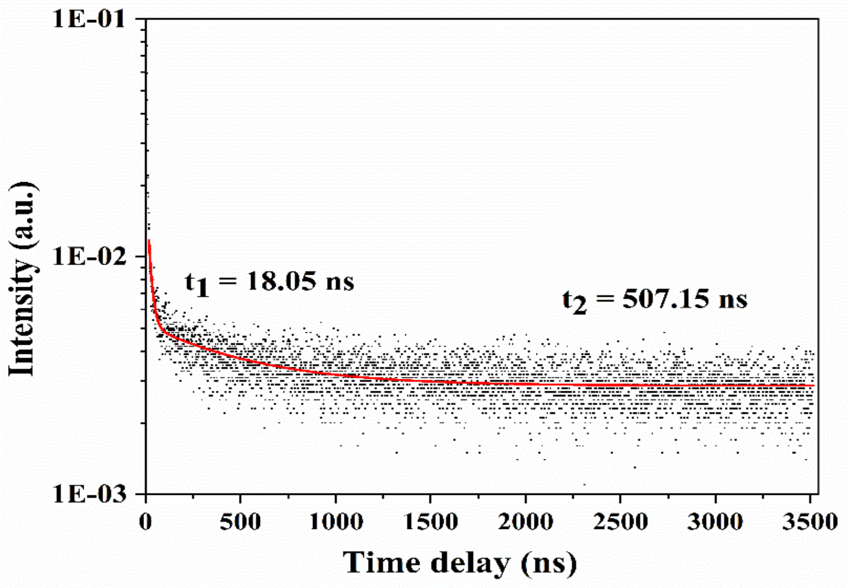

Fig. 4.10 PL lifetime decay measurements (TRPL) for 30 min. deposited sample by using TEOS.

Time-resolved PL (TRPL) measurements were also performed to elucidate and understand the origin of PL emissions. Measurements were made in the same PL system using a pulsed beam with a wavelength of 250 nm, with pulses 1ns wide, and a power of 1-2 pJ / pulse. Fig. 4.10 illustrates the TRPL measurements for the sample deposited for 30 min. Different lifetimes were obtained after using an exponential function in the adjustment curve:

$$y = y_0 + A_1 e^{-x/t_1} + A_2 e^{-x/t_2} \quad \text{......................... (4.1)}$$

After using the above equation (4.1), different components in lifetimes can be distinguished, i.e., short lifetimes in the order of a few nanoseconds (18 ns) and long lifetimes in the order of near to microseconds (507 ns) were obtained. Here, the lifetime near the few ns (18 ns) corresponds to the presence of different defects in the SiOC matrix, mainly oxygen deficient centers, particularly NOV and E'$_\delta$ centers [38]. Furthermore,

carbon-related NOV-type defects have also been shown to have a lifetime in this range which may contribute to emissions in the blue region [23]. Moreover, another lifetime (507 ns) corresponds to quantum confinement effects in silicon nanocrystals [39], [40].

4.2.2.5 High-Resolution Transmission Electron Microscopy (HR-TEM)

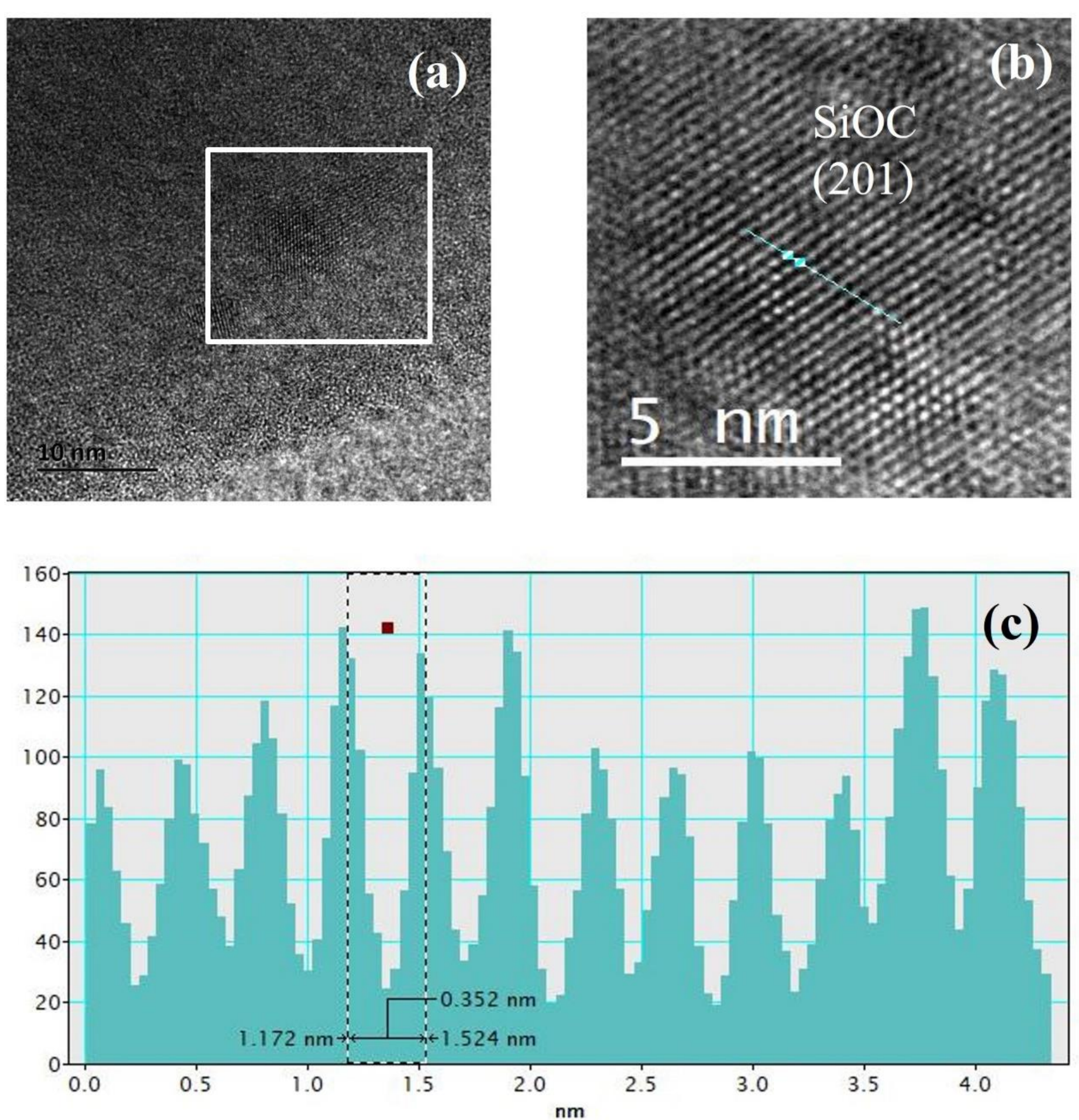

Fig. 4.11 HRTEM images of SiO_xC_y films obtained at 30 min deposition by using TEOS [41].

To elucidate the PLE and TRPL results of deposited thin films, as discussed in the previous section, high resolution transmission electron microscopy (HRTEM) is performed to investigate the possibility of nanostructures existence in the deposited thin films. The morphological and crystallization property of the deposited sample is shown in Fig. 4.11 for the SiO_xC_y films obtained during 30 min. The crystalline nature of the nanoparticles is

clearly noticeable in Fig. 4.11 (a) and (b). Moreover, Gatan digital micrograph software was used to determine the interplanar distance (d) between the crystals, as shown in Fig. 4.11 (b) and (c). A particular zone was selected in the sample where an interplanar distance of 0.352 nm was obtained. This value represents {2 0 1} plane spacing of SiOC with tetragonal crystal structure according to the JCPDS card no. 96-900-8245 [41].

Theoretically, the quantum confinement effect (QCE) of silicon and silicon carbide can be explained by using equations (4.2) and (4.3) [19], [42], [43], which assist the relationship between calculated PL peak energy emission and the size of the nanoparticles, as shown in Table 4.5.

$$E = 0.925 + \frac{3.73}{d^{1.39}} + \frac{0.881}{d} \quad \ldots\ldots\ldots\ldots\ldots\ldots\ldots\ldots \text{(4.2)}$$

$$E = 1.24 + \frac{2.18}{d^{0.850}} \quad \ldots\ldots\ldots\ldots\ldots\ldots\ldots\ldots\ldots\ldots \text{(4.3)}$$

Table 4.5 The effect of Si and SiC nanoparticles size on PL peak energy by using eq. (4.2) and (4.3) [19].

Size (nm)	PL energy (eV) (eq. 4.2)	PL energy (eV) (eq. 4.3)
1	5.77	3.42
2	3.46	2.45
3	2.85	2.09
4	2.58	1.91
5	2.43	1.79

The above-mentioned relation between the size of nanoparticles and PL peak energy may help identify nanoparticles' nature. Moreover, some previous results have also shown the relationship between TRPL and HRTEM results where the presence of longer lifetime decay correlated with the presence of silicon or silicon carbide nanocrystals in the matrix [19], [44]–[46].

4.2.3. Effect of the SiO_xC_y thin films on solar cells

In this work, the effects of thin films on solar cells were investigated at different deposition times. This work motivates us to achieve the downshifting of solar cells by using silicon-based photoluminescent thin films.

4.2.3.1. UV-Vis Spectroscopy

UV-Vis spectroscopy is a fundamental technique for understanding the optical properties such as transmittance, reflectance, and absorbance of materials. In this work, transmittance (T) was studied, which provides information about the opaque nature of the material or how much light can pass through the material on a particular wavelength of light. This can be defined as the ratio of incident light to the resulting light that emerged after passing through the material.

$$T = \frac{I}{I_0} \text{.....................} (4.4)$$

Here in equation (4.4), I_0 is referred to as the intensity of light incident on the sample, while I is referred to the intensity of light after passing through the other side of the sample. The unit of light intensity is Lux.

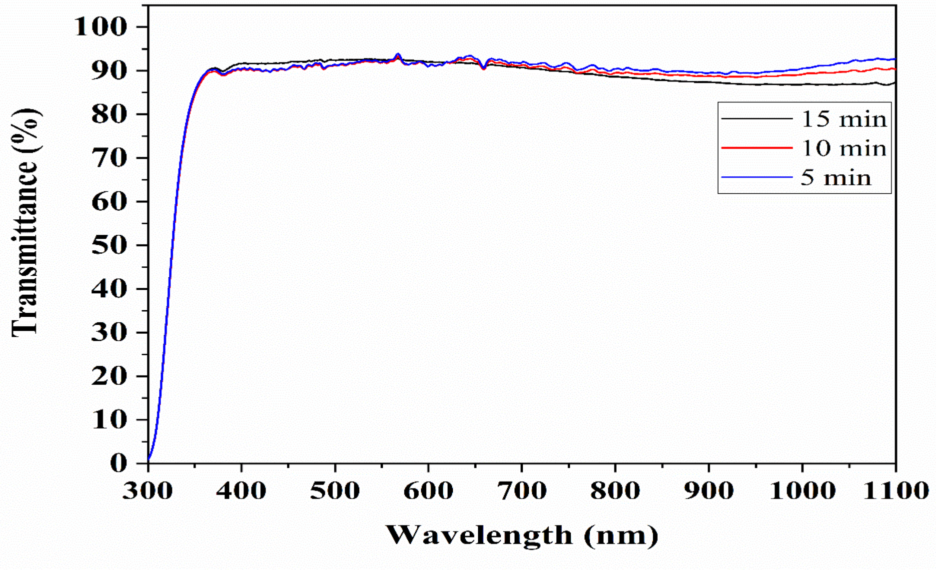

Fig. 4.12 UV-Vis transmittance spectra at various deposition times with TEOS precursor-based SiO_xC_y thin films.

The study of transmittance is crucial for understanding silicon solar cells' optical properties. In this work, a higher transmittance is required so that light can transmit through the material, e.g., SiO_xC_y thin films and create the electron-hole pairs in the solar cell. For the desired higher transmittance, the thickness (*d*) (nm) of the thin film should be equal to or less than the theoretical formula as given [47]:

$$d = \frac{\lambda}{4n} \quad \text{......................} \quad (4.5)$$

Here in equation (4.5), *n* represents the refractive index (unitless) and λ (nm) represents the highest transmittance wavelength from the spectra.

Fig. 4.12 shows the transmittance spectra of SiO_xC_y thin films deposited on Corning glass at various deposition times. A high transmittance % (~ 90%) shows the transparent nature of SiO_xC_y thin films. This helps the maximum light to energize the minority carriers of the solar cell.

4.2.3.2. Current density-Voltage (J-V) measurement

Current density-Voltage (J-V) measurement is illustrated in Fig. 4.13 for solar cells with deposited SiOxCy thin films at various deposition durations. Table 4.6 represents the characteristics of the solar cell previous and after the deposition of SiO_xC_y thin films.

Table 4.6 Characteristics of monochromatic solar cells with and without the presence of deposited SiO_xC_y thin films.

Deposition duration	V_{oc} initial (V)	V_{oc} after (V)	J_{sc} Initial (mA/cm^2)	J_{sc} After (mA/cm^2)	FF initial (%)	FF after (%)	η initial (%)	η After (%)
15 minutes	0.609	0.618	38.09	39.56	52.54	52.28	12.19	12.78
10 minutes	0.622	0.632	38.74	38.81	55.25	55.30	13.31	13.56
5 minutes	0.624	0.634	38.99	39.24	53.04	53.88	12.90	13.40

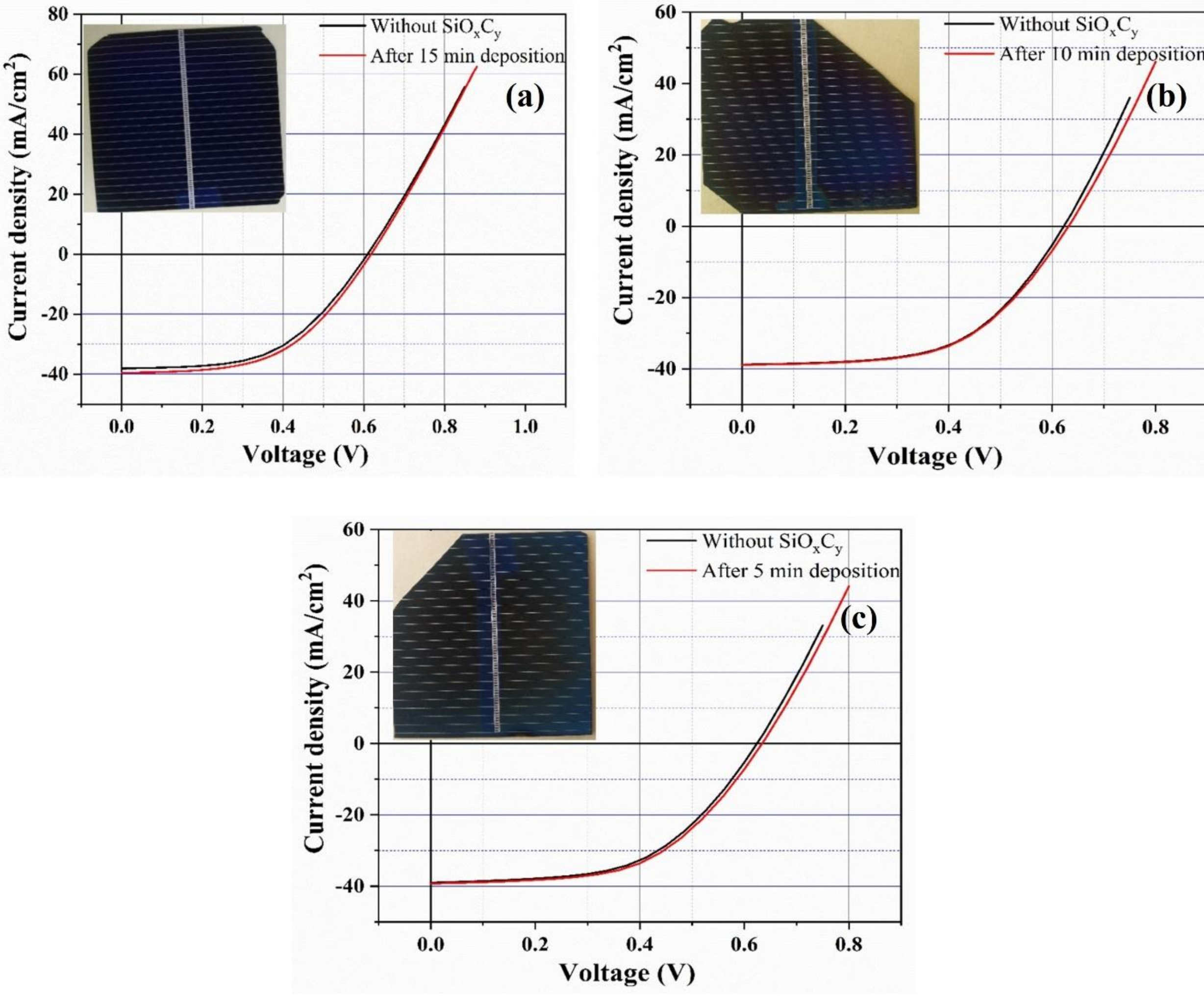

Fig. 4.13 J-V characteristics of solar cells at various deposition times with TEOS precursor based SiO_xC_y thin films.

The solar cell characteristics, i.e., open circuit voltage (V_{oc}), short circuit current density (J_{sc}), fill factor (FF), and efficiency (η) were studied by using the obtained J-V graphs. The improved characteristics of solar cell can be observable in the table, which shows the efficiency of solar cells were improved after the deposition of SiO_xC_y thin film at various deposition times. The efficiency of solar cells modified from 12.19 to 12.78 %, 13.31 to 13.56 % and 12.90 to 13.40 % after the deposition of thin films for 15 min, 10 min and 5 min deposited samples, respectively. This investigation confirms that the SiO_xC_y thin films improve the efficiency of solar cells by 4.84 %, 1.72 %, and 3.87 % for 15 min, 10 min, and 5 min deposited samples, respectively. The reason for improvement in efficiency can be an either downshifting or anti-reflection coating (ARC) effects. Here, it is also observable that the current density of solar cells is improving, which shows that more photons are participating in generating the current [48]. Essentially, the Photo-

Luminescence process converts a high-energy photon into a lower-energy photon which permits easy absorption by the solar cell [48]. Here, the downshifting process can't be confirmed alone by using the J-V measurement. Hence, the study of external quantum efficiency can help to establish the explanation behind the improved efficiency of the solar cell.

4.2.3.3. External Quantum Efficiency (EQE) measurement

The normalized EQE graph is illustrated in Fig. 4.14 for solar cells with SiOxCy thin films deposited at various deposition durations. The improved EQE up to 470 nm confirms that the photons of the UV-Blue region contributed more in comparison to the solar cell without the deposition of thin films. This correlates with the results of J-V measurements and confirms the presence of a downshifting process in the solar cell. Hence, these results demonstrate that silicon-based photoluminescent thin film can improve solar cells' efficiency. However, a decay in EQE can be seen in the spectrum from 470 nm to 800 nm. This can be due to the deposited SiO_xC_y matrix in the finger (side contacts) of solar cells which reduced its conductivity.

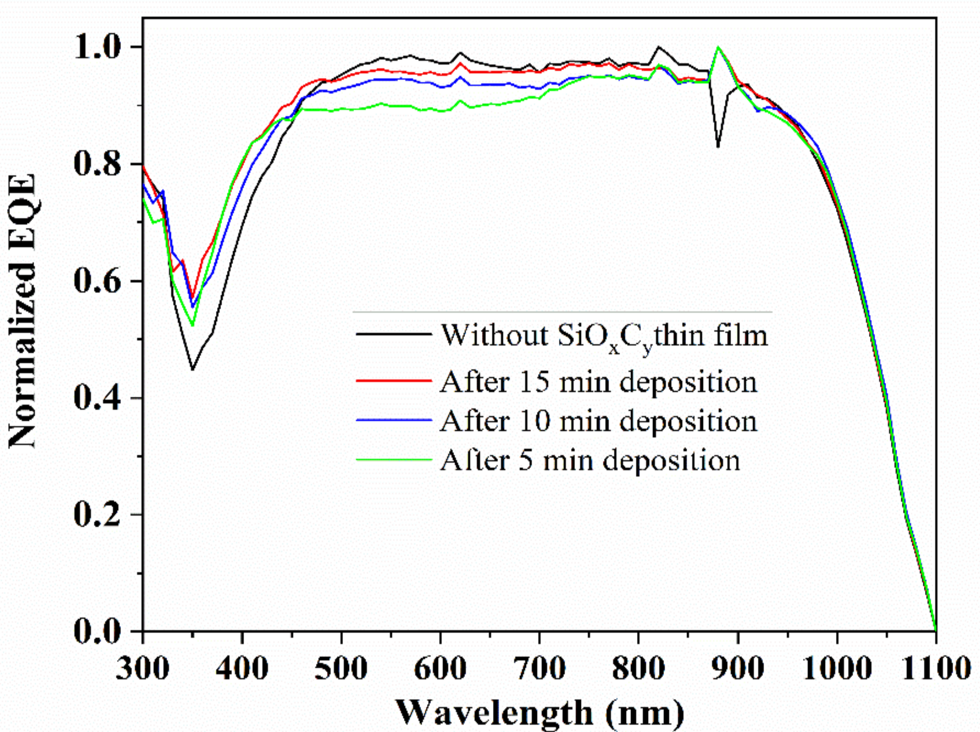

Fig. 4.14 EQE characteristics of solar cells at various deposition duration of SiO_xC_y thin films.

4.3. General Discussion

The effect of argon flow and deposition time was discussed on deposited SiO_xC_y thin films by using organometallic precursor, i.e., TEOS. The effect of SiO_xC_y thin films on Solar cells was analyzed. FTIR and XPS analysis were used to confirm the presence of the SiO_xC_y matrix. Furthermore, using ellipsometry measurements, the nature of TEOS-based SiO_xC_y thin films was noticed near to SiO_x thin films. Broad PL emission was observed in the visible region of the spectra, where different mechanisms for the PL emissions were discussed by using PLE and TRPL analysis. The possible reasons for the origin of PL emission were obtained due to both nanocrystals and defects-related mechanisms such as NBOHC and NOV, etc. The study of HRTEM confirms that the presence of nanostructures and quantum confinement effect (QCE) can also be one reason for PL emission. Moreover, the study of deposited SiO_xC_y thin films on solar cells showed improved J-V characteristics, confirming that these thin films improve the efficiency of solar cells. Furthermore, the external quantum efficiency (EQE) of solar cells confirms the presence of the downshifting process as one of the main reasons for improved solar cell efficiency. This work has confirmed that efficient solar cells can be obtained by using low-cost Si-based organometallic precursors through a downshifting process.

Reference

[1] W. Kern and D. A. Puotinen, "Cleaning solutions based on hydrogen peroxide for use in silicon semiconductor technology," in *RCA Review*, vol. 31, no. 2, J. A. Amick, Ed. 1970, pp. 187–206.

[2] M. Jain, J. R. Ramos-Serrano, A. Dutt, and Y. Matsumoto, "Photoluminescence properties of thin-film SiO_xC_y deposited by O-Cat CVD technique using MMS and TEOS," in *2020 17th International Conference on Electrical Engineering, Computing Science and Automatic Control (CCE). Mexico City, Mexico. November 11-13*, 2020, pp. 1–6, doi: 10.1109/cce50788.2020.9299113.

[3] M. Jain, A. Galdamez-Martinez, A. Dutt, and Y. Matsumoto, "Photoluminescence properties of SiO_xC_y-films deposited under argon atmosphere and Si-based organometallic precursor by O-Cat-CVD," in *CCE 2021 - 2021 18th International Conference on Electrical Engineering, Computing Science and Automatic Control*, 2021, pp. 1–4, doi: 10.1109/CCE53527.2021.9633067.

[4] M. Jain, J. R. Ramos-serrano, A. Dutt, and Y. Matsumoto, "The influence of deposition time on the photoluminescent properties of SiO_xC_y thin films obtained by Cat-CVD from monomethyl silane precursor," *Mater. Lett.*, vol. 291, p. 129547, 2021, doi: 10.1016/j.matlet.2021.129547.

[5] P. G. Pai, S. S. Chao, Y. Takagi, and G. Lucovsky, "Infrared spectroscopic study of SiO_x films produced by plasma enhanced chemical vapor deposition," *J. Vac. Sci. Technol. A Vacuum, Surfaces, Film.*, vol. 4, no. 3, pp. 689–694, 1986, doi: 10.1116/1.573833.

[6] W. Kaiser, P. H. Keck, and C. F. Lange, "Infrared absorption and oxygen content in silicon and germanium," *Phys. Rev.*, vol. 101, no. 4, pp. 1264–1268, 1956, doi: 10.1103/PhysRev.101.1264.

[7] A. V. Vasin *et al.*, "The effect of deposition processing on structural and luminescent properties of a-SiOC:H thin films fabricated by RF-magnetron sputtering," *J. Lumin.*, vol. 191, pp. 102–106, 2017, doi: 10.1016/j.jlumin.2016.10.029.

[8] A. P. Baraban, S. N. Samarin, V. A. Prokofiev, V. A. Dmitriev, A. A. Selivanov, and Y. Petrov, "Luminescence of SiO_2 layers on silicon at various types of excitation," *J. Lumin.*, vol. 205, pp. 102–108, 2019, doi:

10.1016/j.jlumin.2018.09.009.

[9] V. Baranauskas, A. C. Peterlevitz, H. J. Ceragioli, and S. F. Durrant, “Micro-crystalline diamond and nano-carbon structures produced using a high argon concentration in hot-filament chemical vapor deposition,” *J. Vac. Sci. Technol. A Vacuum, Surfaces, Film.*, vol. 19, no. 4, pp. 1057–1062, 2001, doi: 10.1116/1.1366701.

[10] J. R. Ramos-Serrano, Y. Matsumoto, A. Méndez-Blas, A. Dutt, C. Morales, and A. I. Oliva, “Luminescent silicon oxycarbide thin films obtained with monomethyl-silane by hot-wire chemical vapor deposition,” *J. Alloys Compd.*, vol. 780, pp. 341–346, 2019, doi: 10.1016/j.jallcom.2018.11.353.

[11] K. Benzhour, J. Szatkowski, F. Rozploch, and K. Stec, “The influence of argon on the deposition and structure of polycrystalline diamond films,” *Acta Phys. Pol. A*, vol. 118, no. 3, pp. 447–449, 2010, doi: 10.12693/APhysPolA.118.447.

[12] Y. Ding and H. Shirai, “White light emission from silicon oxycarbide films prepared by using atmospheric pressure microplasma jet,” *J. Appl. Phys.*, vol. 105, no. 4, 2009, doi: 10.1063/1.3080129.

[13] H. Xu *et al.*, “In situ preparation of C-SiC_xO_y coatings with controllable composition on continuous oxygen-enriched SiC fibres,” *RSC Adv.*, vol. 9, no. 3, pp. 1319–1326, 2019, doi: 10.1039/c8ra09095e.

[14] S. G. Ansari, T. L. Anh, H. K. Seo, K. G. Sung, D. Mushtaq, and H. S. Shin, “Growth kinetics of diamond film with bias enhanced nucleation and $H_2/CH_4/Ar$ mixture in a hot-filament chemical vapor deposition system,” *J. Cryst. Growth*, vol. 265, pp. 563–570, 2004, doi: 10.1016/j.jcrysgro.2004.02.098.

[15] N. A. Bakr *et al.*, “Role of argon in hot wire chemical vapor deposition of hydrogenated nanocrystalline silicon thin films,” *Thin Solid Films*, vol. 519, no. 11, pp. 3501–3508, 2011, doi: 10.1016/j.tsf.2011.01.105.

[16] B. P. Swain and R. O. Dusane, “Effect of substrate temperature on HWCVD deposited a-SiC:H film,” Mater. Lett., vol. 61, no. 25, pp. 4731–4734, 2007, doi: 10.1016/j.matlet.2007.03.029.

[17] R. A. Street, “Luminescence in amorphous semiconductors,” *Adv. Phys.*, vol. 25, no. 4, pp. 397–453, 1976, doi: http://dx.doi.org/10.1080/00018737600101412.

[18] S. Sato, H. Ono, S. Nozaki, and H. Morisaki, “Photoluminescence study on Oxygen-containing silicon nanostructures,” *Nanostructured Mater.*, vol. 5, no. 5, pp. 589–598, 1995, doi: 10.1016/0965-9773(95)00269-K.

[19] Y. Matsumoto *et al.*, "Luminescence study of Si/SiC Nanoparticles embedded in SiO_xC_y matrix deposited using O-Cat-CVD," *Phys. E Low-dimensional Syst. Nanostructures*, vol. 111, no. March, pp. 179–184, 2019, doi: 10.1016/j.physe.2019.03.024.

[20] F. Gamiz *et al.*, "The effect of deposition processing on structural and luminescent properties of a-SiOC:H thin films fabricated by RF-magnetron sputtering," *J. Lumin.*, vol. 45, no. 3, pp. 559–562, 2017, doi: 10.1016/j.jlumin.2016.10.029.

[21] A. V. Vasin *et al.*, "The effect of deposition processing on structural and luminescent properties of a-SiOC:H thin films fabricated by RF-magnetron sputtering," *J. Lumin.*, vol. 191, pp. 102–106, 2017, doi: 10.1016/j.jlumin.2016.10.029.

[22] I. Hinić, G. Staniŝić, and Z. Popović, "Influence of the synthesis conditions on the photoluminescence of silica gels," *J.Serb.Chem.Soc.*, vol. 68, no. 12, pp. 953–959, 2003, doi: https://doi.org/10.2298/JSC0312953H.

[23] V. Nikas *et al.*, "The origin of white luminescence from silicon oxycarbide thin films," *Appl. Phys. Lett.*, vol. 061906, no. 104, pp. 1–5, 2014, doi: 10.1063/1.4865100.

[24] Y. D. Glinka, S. Lin, and Y. Chen, "Two-photon-excited luminescence and defect formation in SiO_2 nanoparticles induced by 6.4-eV ArF laser light," *Phys. Rev. B*, vol. 62, no. 7, pp. 4733–4743, 2000, doi: https://doi.org/10.1103/PhysRevB.62.4733.

[25] A. Dutt, Y. Matsumoto, S. Godavarthi, G. Santana-Rodríguez, J. Santoyo-Salazar, and A. Escobosa, "White bright luminescence at room temperature from TEOS-based thin films via catalytic chemical vapor deposition," *Mater. Lett.*, vol. 131, pp. 295–297, 2014, doi: 10.1016/j.matlet.2014.05.206.

[26] G. B. Raupp, T. S. Cale, H. P. W. Hey, G. B. Raupp, and T. S. Cale, "The role of oxygen excitation and loss in plasma enhanced deposition of silicon dioxide from tetraethylorthosilicate," *J. Vac. Sci. Technol. B*, vol. 10, no. 1, pp. 37–45, 1992, doi: 10.1116/1.586361.

[27] S. B. Desu, "Decomposition Chemistry of Tetraethoxysilane," *J. Am. Ceram. Soc.*, vol. 72, no. 9, pp. 1615–1621, 1989.

[28] F. Rubio, J. Rubio, and J. L. Oteo, "A FT-IR study of the hydrolysis of Tetraethylorthoselicate (TEOS)," *Spectrosc. Lett.*, vol. 31, no. 1, pp. 199–219, 1998, doi: 10.1080/00387019808006772.

[29] H. Yamada and W. B. Person, “Absolute Infrared Intensities of the Fundamental Absorption Bands in Solid CO_2 and N_2O,” *J. Chem. Phys.*, vol. 41, no. 8, pp. 2478–2487, 1964, doi: 10.1063/1.1726291.

[30] S. Park, B. Parida, and K. Kim, “Thin film solar cells with Si nanocrystallites embedded in amorphous intrinsic layers by hot-wire chemical vapor deposition,” *J. Nanosci. Nanotechnol.*, vol. 13, no. 5, pp. 3397–3402, 2013, doi: 10.1166/jnn.2013.7312.

[31] J. Huang *et al.*, “An interfacial crosslinking strategy to fabricate an ultrathin two-dimensional composite of silicon oxycarbide-enwrapped silicon nanoparticles for high-performance lithium storage,” *J. Mater. Chem. A*, vol. 7, no. 40, pp. 22950–22957, 2019, doi: 10.1039/c9ta07738c.

[32] B. P. Swain and R. O. Dusane, “Effect of substrate temperature on HWCVD deposited a-SiC:H film,” *Mater. Lett.*, vol. 61, no. 25, pp. 4731–4734, 2007, doi: 10.1016/j.matlet.2007.03.029.

[33] J. R. Ramos-Serrano, Y. Matsumoto, and C. Morales, “Luminescent Silicon Oxycarbide Thin Films via Hot-wire CVD using Tetraethyl Orthosilicate: Role of the Chamber Pressure and Post-deposition Annealing,” *2018 15th Int. Conf. Electr. Eng. Comput. Sci. Autom. Control. CCE 2018*, pp. 1–4, 2018, doi: 10.1109/ICEEE.2018.8533970.

[34] A. Podhorodecki, G. Zatryb, L. W. Golacki, J. Misiewicz, J. Wojcik, and P. Mascher, “On the origin of emission and thermal quenching of SRSO:Er^{3+} films grown by ECR-PECVD,” *Nanoscale Res. Lett.*, vol. 8, no. 98, pp. 1–12, 2013, doi: https://doi.org/10.1186/1556-276X-8-98.

[35] L. Palacios-Huerta, S. A. Cabañas-Tay, M. A. Cardona-Castro, M. Aceves-Mijares, C. Domínguez-Horna, and A. Morales-Sánchez, “Structural and optical properties of silicon rich oxide films in graded-stoichiometric multilayers for optoelectronic devices,” *Appl. Phys. Lett.*, vol. 109, no. 3, 2016, doi: 10.1063/1.4959080.

[36] A. Podhorodecki, J. Misiewicz, F. Gourbilleau, and R. Rizk, “Absorption mechanisms of silicon nanocrystals in cosputtered silicon-rich-silicon oxide films,” *Electrochem. Solid-State Lett.*, vol. 11, no. 3, pp. 60–62, 2008, doi: 10.1149/1.2828207.

[37] J. P. Wilcoxon and G. A. Samara, “Tailorable , visible light emission from silicon nanocrystals,” *Appl. Phys. Lett.*, vol. 74, no. 21, pp. 3164–3166, 1999, doi: https://doi.org/10.1063/1.124096.

[38] G. R. Lin, C. J. Lin, and K. C. Yu, "Time-resolved photoluminescence and capacitance-voltage analysis of the neutral vacancy defect in silicon implanted SiO_2 on silicon substrate," *J. Appl. Phys.*, vol. 96, no. 5, pp. 3025–3027, 2004, doi: 10.1063/1.1775041.

[39] C. Bulutay and S. Ossicini, *Electronic and Optical Properties of Silicon Nanocrystals*. 2010.

[40] J. Joo *et al.*, "Enhanced quantum yield of photoluminescent porous silicon prepared by supercritical drying," *Appl. Phys. Lett.*, vol. 108, no. 153111, pp. 1–5, 2016, doi: 10.1063/1.4947084.

[41] V. B. Kamenar and M. Bruvo, "Die Kristallstruktur des Siliciura(IV)-acetats," *Zeitschrift für Krist.*, vol. 141, pp. 97–103, 1975.

[42] S. Wang, C. Zhang, Z. Wang, and X. Zu, "Quantum confinement effect in silicon carbide nanostructures: A first principles study," *Optoelectron. Adv. Mater. Rapid Commun.*, vol. 4, no. 6, pp. 771–773, 2010.

[43] G. Ledoux *et al.*, "Photoluminescence properties of silicon nanocrystals as a function of their size," *Phys. Rev. B*, vol. 62, no. 23, pp. 15942–15951, Dec. 2000, doi: 10.1103/PhysRevB.62.15942.

[44] R. Huang *et al.*, "Growth of nearly one nanometer large silicon particles in silicon carbide and their quantum-confined photoluminescence features," *Nanotechnology*, vol. 18, no. 44, pp. 1–5, 2007, doi: 10.1088/0957-4484/18/44/445605.

[45] A. A. Prokofiev *et al.*, "Direct bandgap optical transitions in Si nanocrystals," *J. Exp. Theor. Phys. Lett.*, vol. 90, no. 12, pp. 758–762, 2010, doi: 10.1134/S0021364009240059.

[46] S. J. Xu, M. B. Yu, Rusli, S. F. Yoon, and C. M. Che, "Time-resolved photoluminescence spectra of strong visible light-emitting SiC nanocrystalline films on Si deposited by electron-cyclotron-resonance chemical-vapor deposition," *Appl. Phys. Lett.*, vol. 76, no. 18, pp. 2550–2552, 2000, doi: 10.1063/1.126382.

[47] J. Hofstetter, C. Del Cañizo, S. Ponce-Alcántara, and A. Luque, "Optimisation of SiN_x:H anti-reflection coatings for silicon solar cells," in *2007 Spanish Conference on Electron Devices, Proceedings*, 2007, pp. 131–134, doi: 10.1109/SCED.2007.383961.

[48] C. Strümple *et al.*, "Modifying the solar spectrum to enhance silicon solar cell efficiency — An overview of available materials," *Sol. Energy Mater. Sol. Cells*, vol. 91, pp. 238–249, 2007, doi: 10.1016/j.solmat.2006.09.003.

CHAPTER 5
CONCLUSIONS AND FUTURE SCOPES

A Silicon solar cell is one of the most manufactured and distributed semiconducting devices in the world. The main objective of this thesis was to obtain silicon-based photoluminescent thin films, i.e., SiO_xC_y thin films, by using organo-metallic precursors with the O-Cat-CVD technique. MMS, vinyl silane and TEOS were used as precursors which are also safer alternatives to using silane gas. The various properties of these thin films such as optical, morphological, and structural were also explored. Subsequently, TEOS based SiO_xC_y matrix was used to explore its application for improving the efficiency of solar cells by Photo-Luminescence downshifting (PLDS) process.

In this work, different characterization techniques were used to understand the nature and properties of the deposited thin films. Fourier Transform Infrared (FTIR) and X-ray Photoelectron Spectroscopy (XPS) characterization techniques were used to explain the presence of different bonds and chemical states of the thin films, respectively, which confirmed the presence of the SiO_xC_y matrix in thin films. The thickness and refractive index of the thin films were measured by ellipsometry. These characterizations also showed that the nature of TEOS-deposited thin films was closer to the silicon oxide (SiO_x) composition, while the nature of thin films deposited with MMS and vinyl silane were more similar to the silicon carbide (SiC). Furthermore, the Photo-Luminescence (PL) technique was used to understand the optoelectronic properties of thin films, where an intense PL emission was observed over a wide range of the visible spectrum. Here, a redshift was observed in the MMS-deposited thin films compared to the TEOS and vinyl silane-deposited thin films.

Time-Resolved Photo-Luminescence (TRPL), Photo-Luminescence Excitation (PLE), and High-Resolution Transmission Electron Microscopy (HRTEM) techniques were used to confirm the origin of PL emission. PLE and TRPL confirmed the PL emission due to the presence of defect-related mechanisms and nanocrystals. Here, NBOHC and ODC-related

defects, particularly NOV defect centers, are the more common defect centers. Moreover, HRTEM confirms the presence of nanocrystals which also validates the contribution of the quantum confinement effect (QCE) for the PL emission. Furthermore, the effect of the Si-O-Si stretching bond's stoichiometry value shift was also discussed for the PL emission (Intensity and spectral composition) because this shift generates a higher probability of having one or more silicon or carbon neighboring atoms due to the deficiency of oxygen in Si-O-Si bonding.

UV-Vis, current density-voltage (J-V), and external quantum efficiency (EQE) measurements were also performed to understand SiO_xC_y thin films effect on solar cells. The current density-voltage (J-V) characteristics of solar cells with the SiO_xC_y thin films confirm the improvement in the efficiency of the solar cells, while the EQE graph confirms the improved quantum efficiency in the UV-Blue region. Hence, the improved solar cell efficiency was concluded due to by Photo-Luminescence downshifting (PLDS) process. This work is promising for developing low-cost Si-based optoelectronic devices compatible with current technologies, including crystalline Si solar cells with PL downshifting thin films.

Future works

The following recommendations can be considered for possible future investigation and study:

- To analyze the effects of the Plasma/heat treatment of various gases (H_2/O_2/Ar) at different times/flows/temperatures on the SiO_xC_y matrix.
- To analyze the electroluminescence (EL) properties of SiO_xC_y thin films for possible EL device development.
- To analyze the PL downshifting (PLDS) effect on perovskite, or another compound solar cells by using SiO_xC_y thin films.

Appendix

A. Publications

1. **M. Jain,** J. R. Ramos-Serrano, A. Galdamez, A. Méndez-Blas, G. Santana, A. Dutt, Y. Matsumoto· Effect of deposition duration on the Photo-Luminescence properties of SiO_xC_y thin films deposited by organometallic Si precursor, **The Journal of Materials Science: Materials in Electronics**, (in communication)
2. A. Dutt, Rafael A Salinas, Shirlley E. Martínez Tolibia, J.R.Ramos-Serrano, **M. Jain** et. al., Silicon compound nanosystems: Exploring emission mechanisms and photobiological applications, **Advanced Photonics Research** (Accepted). 10.1002/adpr.202300054
3. A. Galdámez-Martínez, A. Dutt, **M. Jain**, Lourdes Bazán-Díaz, G. Santana, A. Méndez-Blas, O. de Melo, Decay emission study of ZnO nanostructures obtained by low-pressure vapor transport technique, **Applied Surface Science Advances**, 12 (2022) 100334. https://doi.org/10.1016/j.apsadv.2022.100334
4. **M. Jain,** A. Galdámez-Martínez, A. Dutt, Y. Matsumoto, Photo-Luminescence properties of SiO_xC_y-films deposited under argon atmosphere and Si-based organometallic precursor by O-Cat-CVD, in: 2022 **18th Int. Conf. Electr. Eng. Comput. Sci. Autom. Control (CCE).** Mex. City, Mex. Novemb. 10-12, 2021. https://doi.org/10.1109/CCE53527.2021.9633067.
5. **M. Jain,** S. Juneja, K. Lodhi, C. Kant, S. Kumar, M. Jain, A. Dutt, Y. Matsumoto, Effect of argon plasma treatment on electronic properties of doped hydrogenated Silicon thin films for photovoltaic applications, in: 2022 **18th Int. Conf. Electr. Eng. Comput. Sci. Autom. Control (CCE).** Mex. City, Mex. Novemb. 10-12, 2021. https://doi.org/10.1109/CCE53527.2021.9633065.
6. **M. Jain,** J.R. Ramos-serrano, A. Dutt, Y. Matsumoto, The influence of deposition time on the photoluminescent properties of SiO_xC_y thin films obtained by Cat-CVD from monomethyl silane precursor, **Mater. Lett.** 291 (2021) 129547. https://doi.org/10.1016/j.matlet.2021.129547.
7. **M. Jain**, J.R. Ramos-Serrano, A. Dutt, Y. Matsumoto, Photo-Luminescence properties of thin-film SiO_xC_y deposited by O-Cat CVD technique using MMS and

TEOS, in: 2020 **17th Int. Conf. Electr. Eng. Comput. Sci. Autom. Control (CCE).** Mex. City, Mex. Novemb. 11-13, 2020: pp. 1–6. https://doi.org/10.1109/cce50788.2020.9299113.

8. **M. Jain**, J.R. Ramos-Serrano, A. Dutt, Y. Matsumoto, Estudio de fotoluminiscencia de películas delgadas de SiO_xC_y depositadas mediante precursores de Si orgánicos, **Materiales Avanzados,** número 33, 2021, pp 66-69. https://www.iim.unam.mx/MA/33/#page/66

B. Conference Activities

1. **Oral and poster presentation** in XXX International Materials Research Congress (IMRC) held in Cancun, Mexico from August 14th to 19th, 2022.
2. **Oral presentation** in 19th Cat-CVD Study Group Lecture, AIST Kyushu Center, Tosu city (Saga), Japan. July 14th to 15th, 2022.
3. **Oral presentation** in 18th International Conference on Electrical Engineering, Computing Science and Automatic Control (CCE). Mexico City, Mexico. November 10th to 12th, 2021.
4. **Poster presentation** in XXIX International Materials Research Congress (IMRC) held in Cancun, Mexico from August 15th to 20th, 2021.
5. **Oral and poster presentation** in 9th Annual Student Symposium at the Institute of Materials Research of the Universidad Nacional Autónoma de México, Autónoma de México, Mexico City, Mexico. May 4th to 7th, 2021.
6. **Poster presentation** in 4th Symposium of interdisciplinary materials organized by student chapter of CINVESTAV-Zacatenco, Mexico City, Mexico. May 5th to 6th, 2021.
7. **Oral presentation** in 17th International Conference on Electrical Engineering, Computing Science and Automatic Control (CCE). Mexico City, Mexico. November 11th to 13th, 2020.
8. **Oral presentation** in 8th Annual Student Symposium at the Institute of Materials Research of the Universidad Nacional Autónoma de México, November 10th to 13th, 2020, Mexico City, Mexico.

9. **Poster presentation** in 2020 Express Conference on the Physics of Materials and Their Applications in Energy Harvesting, an online event held from August 17th to 19th, 2020.